The Effect of Model Predictive Control on the Interplay between Electromagnetic and Wave-Induced Instability in Hyperloop Systems

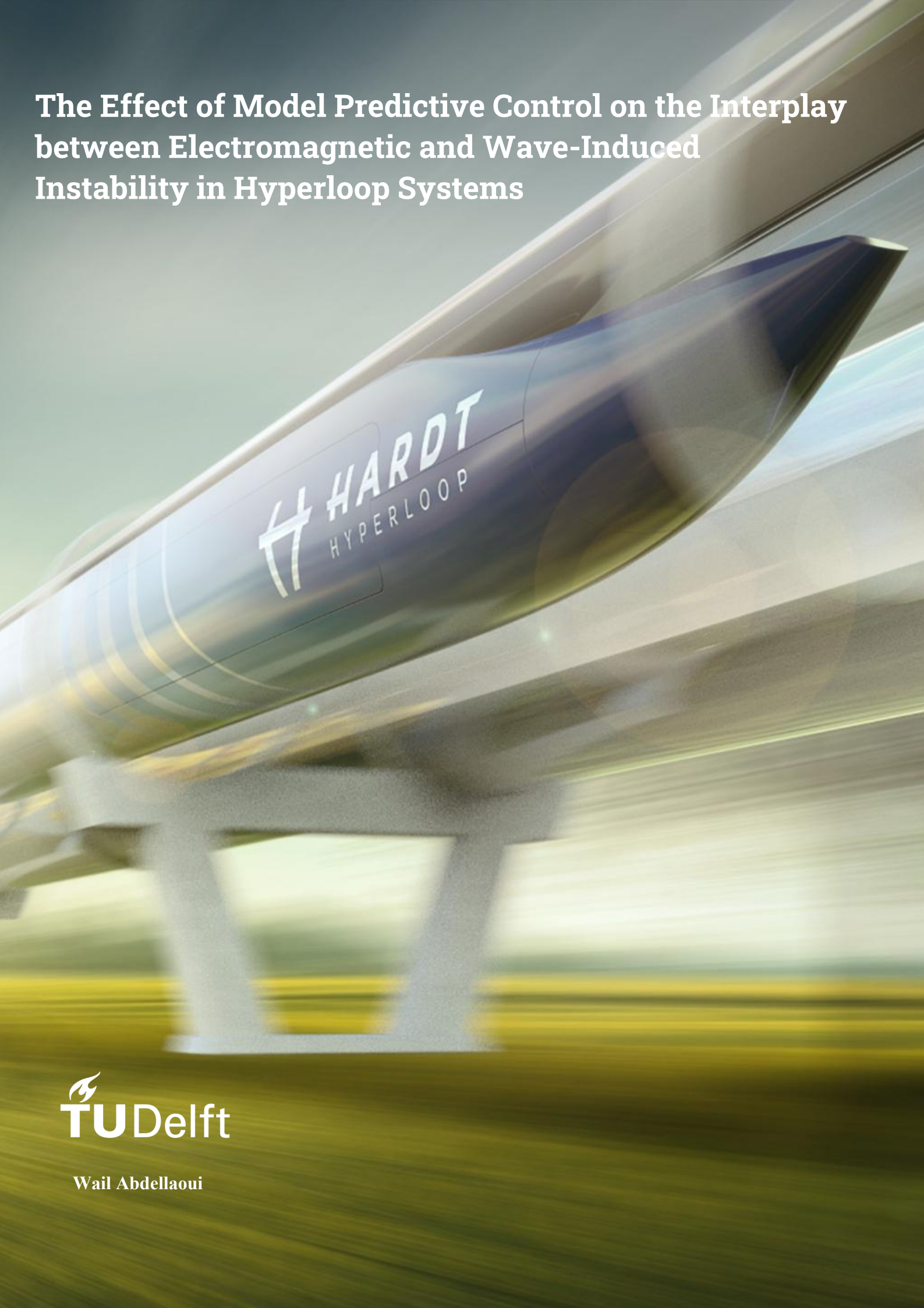

TU Delft

Wail Abdellaoui

The effect of model predictive control on the interplay between electromagnetic and wave-induced instability in hyperloop systems

Modelling and understanding the dynamic behaviour of the hyperloop system

By

Wail Abdellaoui

in partial fulfilment of the requirements for the degree of

Master of Science
in Civil Engineering

at the Delft University of Technology,
to be defended publicly on Monday April 20th, 2026 at 14:00.

Student number: 5130654
Thesis committee:

Dr. ir. K. N. Van Dalen,	TU Delft, supervising chair
Dr. ir. A. B. Fărăgău,	TU Delft, weekly supervisor
ir. F. Cordiano	TU Delft, weekly supervisor
Dr.ir. P.C. Meijers	TU Delft, external assessor

(An electronic version of this thesis is available at http://repository.tudelft.nl/.)

TU Delft

Acknowledgements

This thesis is submitted in partial fulfilment of the requirements for the Master's degree in Civil Engineering, with a specialisation in Structural Engineering. This thesis may be of interest to those working on moving load problems and to control engineers involved in designing controllers for dynamic systems.

After completing my Bachelor's degree in Civil Engineering, I continued with the Master's programme in Civil Engineering, choosing the Structural Engineering track. I developed an interest in moving load problems and structural dynamics in this period, partly thanks to the interesting and engaging lectures within the programme. Throughout my studies, I tried to broaden my knowledge, for which this master programme offered many opportunities through the many electives. During one of these electives, called Control System Design, I was introduced to the fundamental of control theory. Therefore, the topic of this thesis felt as a logical choice, as it allowed me to combine my background in structural engineering with control theory and apply the concepts I had learned to an innovative concept. I am grateful to have had the opportunity to work on this project.

I would like to sincerely thank Andrei for his great continuous support and guidance throughout this process. I would also like to thank Francesco for his ideas, insights, and valuable feedback. In addition, I would like to thank Karel van Dalen for his practical input and helpful suggestions.
I would also like to thank my fellow students and friends for their support, motivation, and the many enjoyable moments throughout my studies.
Finally, I would like to thank my family for their unconditional support and encouragement throughout my studies.

Wail Abdellaoui
Arnhem, April 2026

Abstract

Hyperloop has emerged as a promising mode of transportation and has attracted strong interest from student teams and startups. Its potential lies in enabling faster and more sustainable transport. However, the characteristics of the hyperloop system may also lead to different instability mechanisms. This study focuses on two of these, namely electromagnetic instability and wave-induced instability. Previous studies have generally considered either a conventional control strategy or simplified models of the vehicle-guideway dynamics. This study contributes by investigating the effect of an advanced control strategy, Model Predictive Control (MPC), on both sources of instability. MPC is applied because of its predictive nature and its ability of handling constraints.

The analysis first considers a simplified 1.5-degree-of-freedom (DOF) system to see the effect of MPC on electromagnetic instability. An eigenvalue analysis of the MPC parameters was conducted. It is found that linear MPC does not achieve stabilization. Therefore, a nonlinear MPC is designed and compared with a PD controller, showing improved control performance.

To capture the influence of vehicle velocity on system stability, an infinite guideway with coupled vehicle-beam interaction is considered, allowing anomalous Doppler waves to arise at high velocities. In the supercritical velocity regime, where wave-induced instability becomes dominant, numerical simulations show that MPC can maintain stability for suitably tuned controller parameters over a wider range of longitudinal vehicle velocities. Compared with the PD controller, MPC appears better able to achieve fast convergence while also suppressing wave-induced instability.

Overall, MPC showed improved control performance compared with the PD controller and appears to be a promising control strategy. However, more research is needed to make real-time implementation feasible. A more formal and comprehensive study stability analysis is also needed.

Contents

Abstract iv
1. Introduction 1
1.1 Background 1
1.2 Problem statement 1
1.3 Objectives 2
1.4 Research questions 2
1.5 Outline 2
2. Literature review/theoretical background 3
2.1 Stability 3
2.1.1 Electromagnetic instability 3
2.1.2 Wave-induced instability 4
2.2 Control 6
2.3 Introduction MPC 8
3. System modelling 13
4. Control of the 1.5-DOF system 17
4.1 Linear MPC 17
4.1.1 Eigenvalue analysis 21
4.1.2 Results 28
4.2 LQR 29
4.3 Nonlinear MPC 32
4.4 PD 41
4.5 Comparative analysis 43
5. Control of the continuous guideway model 46
5.1 Method 46
5.2 Results 48
6. Conclusion 54
7. Discussion 55
Bibliography 56

1. Introduction

1.1 Background

Between 2020 and 2050, passenger and freight transport demand are predicted to grow significantly by 196% and 200%, respectively (Tjandra et al., 2024). This trend could lead to a further rise of greenhouse gas emissions. Given the climate change issues and the increasing demand of transport, the future calls for a more sustainable transport sector (Tjandra et al., 2024). The hyperloop is emerging as an alternative mode of transportation that potentially requires a relatively low amount of energy compared to other transportation systems and it could significantly reduce travel time. In 2013, entrepreneur Elon Musk proposed the concept of a hyperloop as a transportation system (Musk, 2013). Similar concepts of the hyperloop, based on related principles, had been proposed earlier. An overview of these concepts is provided by Özbek and Çodur (2021). However, Musk's Hyperloop Alpha design stands out due to its more detailed system description. Moreover, his proposal introduced the use of air-bearing levitation (Chaidez et al., 2019).

This transportation system is a high-speed transport concept in which passenger capsules move through a low-pressure tube. The design aims to minimise two primary sources of resistance. First, it eliminates rolling friction between the vehicle and the track through levitation. Second, the use of a low-pressure tube significantly reduces the aerodynamic drag (Chaidez et al., 2019). In the concept proposed by Musk, levitation is achieved using air bearings, and propulsion is provided by track-integrated electromagnetic coils (Noland, 2021). Since the initial proposal in 2013, the hyperloop concept has been evolved into numerous variations by different parties. The public sector, along with industry and research institutes are collaborating on the realisation of the hyperloop. They are all working on an own concept of the hyperloop, which will differ from the original concept proposed by Musk. The company Hardt Hyperloop, located in the Netherlands is one of them working on the development of the hyperloop. The concept developed by Hardt Hyperloop serves as the basis for this thesis.

Although the Hyperloop has great potential to become a successful and new mode of transport, numerous challenges must still be addressed before commercial implementation can be realised. Among the issues are tube depressurisation, managing aerodynamic effects such as air resistance, choked flow around the capsule, and ensuring passenger safety in a sealed high-speed system. Also critical is the development of a reliable levitation system that can operate effectively at the proposed velocities (Noland, 2021).
This research focuses on the latter challenge by contributing to the design of a robust levitation controller for electromagnetic suspension systems. By addressing this aspect, the work aims to bring the hyperloop one step closer to industrial application.

1.2 Problem statement

The hyperloop designed by Hardt, is based on an electromagnetic suspension (EMS). However, this levitation method is inherently unstable, as confirmed by Mas Soldevilla (2022), who demonstrated that the EMS-based system applied at Hardt Hyperloop cannot maintain stable equilibrium without active control. This instability stems from a fundamental physical limitation described by Earnshaw's theorem (1848), which states that it is impossible to achieve stable equilibrium using only electrostatic or magnetostatic forces that follow an inverse-square law. This shows the need for a closed loop feedback control. The control strategy aims to modify the inversely proportional relation, such that the electromagnetic attraction force is proportional to the distance (Han & Kim, 2016).

The Hyperloop primarily aims to develop a high-speed transportation system capable of reaching velocities up to 700 km/h. As the vehicle approaches these high speeds, additional sources of instability can arise, one of which is wave-induced instability. This phenomenon is caused by the occurrence of anomalous Doppler waves (Denisov et al., 1985). The explanation of this instability was firstly provided by Metrikine and Popp (1999).

Various studies have discussed topics such as EMS and control strategies to address the electromagnetic instability (Zhu et al., 2024). Also, studies on the appearance and nature of the dynamic instability in systems involving a moving mass on a continuous guideway have been reviewed. Research applying

different control strategies that allow the guideway to deform, by modelling the guideway as a mass-spring-damper system, showed promising results of MPC (Oppeneiger et al., 2024). However, in this research, wave propagation was not possible, thus the wave-induced instability was not captured.
The conducted literature review revealed a research gap. A study addressing both wave-induced instability and electromagnetic instability with a more complex control strategy is currently missing. The dynamic type of instability is typically not considered in studies focused on designing control strategies to address electromagnetic instability. The interplay between electromagnetic and wave-induced instability has been studied by Faragau et al. (2023). But in their work a simplified PD control strategy was applied. Whereas companies developing the hyperloop are using a more complex or advanced control architecture capable of meeting industrial demands. One example is the use of cascaded PD controllers by Hardt, this approach eliminates the nonlinear relation in the electromagnetic force.

The effect of these advanced control strategies on the interplay between two fundamentally different instability mechanisms is currently missing and will therefore be studied. To address this gap, the controller will be designed, and stability analysis will be performed. Other sources of instability, like aerodynamic instability, are not considered.

1.3 Objectives
The objective of this research project is to investigate the effect of model predictive control on the interplay between electromagnetic instability and wave-induced instability, and to compare the effect of this strategy with alternative control strategies.

1.4 Research questions
The main question can be formulated as: “What is the effect of implementing a realistic control strategy on the interplay between electromagnetic instability and wave-induced instability?”

To answer the main question, the following tasks will be addressed:

1. Evaluate the control strategy:
    a) Identify the requirements for the control strategy.
    b) Select and analyse the feedback controller to be used.
    c) Design and implement the controller.

2. Analyse the influence of the control strategy on the system:
    a) Analyse the effect on electromagnetic instability.
    b) Analyse the effect on wave-induced instability?
    c) Analyse the effect on the interplay between these two types of instability.

3. Evaluate the effect on the stability domain compared to other control strategies:
    a) Identify the stable regimes, specifying for which velocities and at which gains.
    b) Compare the stability of the PD and MPC controller.

1.5 Outline
The context of research is provided in chapter 1. Chapter 2 discusses the relevant theory, reviews different control methods, and then introduces the concept of MPC as the control strategy that meets the objectives. Chapter 3 presents a detailed description of the inherently unstable system for which the MPC control will be designed. In Chapter 4, the MPC controller is designed in a simplified configuration, focusing on the electromagnetic instability. Chapter 5 expands the system to include wave-induced instability. Chapter 6 points out the differences of the MPC control with a PD-control and gives a conclusion. Finally, chapter 7 discusses the results and presents recommendations for future work.

2. Literature review/theoretical background

This chapter provides a review of the relevant literature and outlines the theoretical concepts forming the basis of this thesis. It begins by presenting the stability theory. Next, the two sources of instability are discussed: the first one related to the applied levitation method and the second source related to the moving load problem. Subsequently, existing control strategies applied to address instability are reviewed and evaluated. Based on the literature review, MPC emerged as a suitable control strategy for stabilising such systems. The fundamental principles of MPC are then discussed in more detail, as they form the foundation for the control design developed in this thesis. Finally, several additional theoretical concepts relevant to the problem formulation and control strategy are introduced.

It was chosen not to include an extensive discussion of stability theory and electromagnet fundamentals in this thesis. For a detailed treatment of these topics, the reader is referred to J.Mas Soldevilla (2022). The theoretical concepts directly relevant to the methodology and results of this thesis are presented in this chapter.

2.1 Stability

2.1.1 Electromagnetic instability

To eliminate the friction resistance of the vehicle, the vehicle is levitated and kept at a certain distance from the rail. The three main methods for achieving vehicle levitation are air bearing suspension, electrodynamic suspension (EDS) and electromagnetic suspension (EMS).

The initial hyperloop concept proposed the use of a thin air cushion to levitate the object. In this approach, the vehicle is levitated at the distance of micrometres from the surface to maintain feasible flowrates. Among the drawbacks of this levitation method is the high maintenance cost and the increased pod weight resulting from the air-bearing infrastructure. Another crucial issue is maintaining dynamic stability when moving at high speeds. Due to these limitations, more research is focused on employing magnetic levitation as an alternative (Mitropoulos et al., 2021).

EMS and EDS are different ways to achieve magnetic levitation. In EMS, the electromagnet is attached to the vehicle and levitates it using attractive magnetic forces, maintaining an airgap of around 1 cm from the conductive track. EMS relies on a feedback loop to change the magnetic field of the electromagnet. This active control mechanism is required, because inherent to this levitation method is the occurrence of electromagnetic instability. When assuming no control, so a constant current, the magnetic force will increase as the airgap decreases, and the force decreases as the airgap increases. This follows from the inverse relationship: $F \propto (i(t)/z(t))^2$. Therefore, the closed loop feedback should make sure that the airgap and attraction force are proportional rather than inversely proportional (Han & Kim, 2016). The same EMS-system can also be used for vehicle guidance. By actively controlling the electromagnets, both the levitation cap and the lateral motion of the pod can be regulated. This enables lane switching without large mechanical components, unlike EDS systems, as demonstrated by Hardt Hyperloop.

The EDS configuration, in contrast to an EMS system, is inherently stable. When the magnets on the vehicle move over the passive coils in the guideway, they induce an opposing magnetic field in the track. Therefore, EDS-systems need a certain minimum speed to generate the repulsive force, so landing wheels are needed for at low speeds. However, EMS systems also typically include landing wheels as a safety measure to maintain support in case of suspension failure. This configuration keeps the vehicle at a larger distance from the guideway, usually a few centimetres, compared to EMS.
There are different EDS designs, the most well-known being Inductrack, which is based on permanent magnets mounted on the vehicle (Chaidez et al., 2019). Other designs are based on the use of superconducting magnets on the vehicle. These require more complex onboard infrastructure, needed for cooling of the superconducting coil used to generate the magnetic field.

This study will focus on the hyperloop concept as developed by Hardt Hyperloop, which uses an EMS (Hardt Hyperloop, 2023). A permanent magnet performs the heavy lifting, and the electromagnet stabilizes

around the target airgap, thereby reducing the energy consumption. The levitation design is depicted in figure 2.1, where the vehicle is suspended from above.

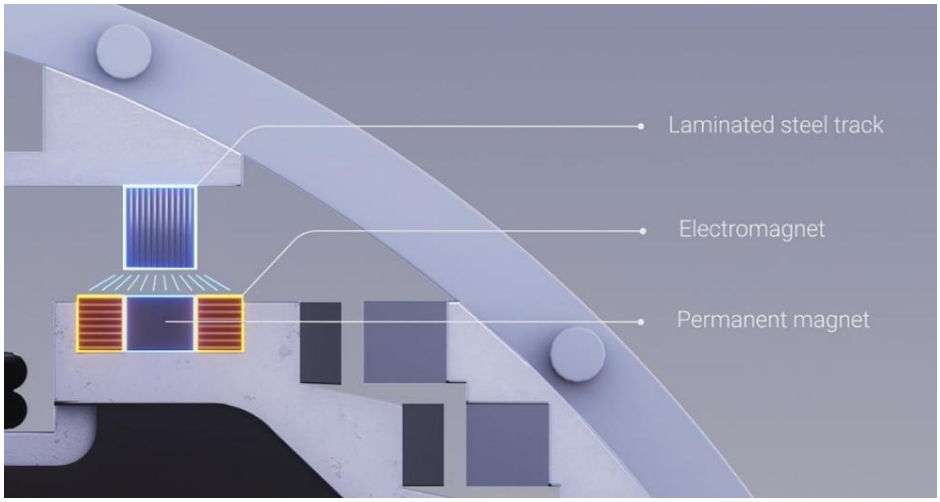

Figure 2.1: Schematic representation of Hardt's suspension system (Hardt Hyperloop, 2025).

2.1.2 Wave-induced instability

In literature, various models have been applied to describe the hyperloop system, each focusing on specific parts of its behaviour. For describing the moving vehicle, two principal approaches to the moving load problem can be found (Veritchev, 2002). In the first, the moving load is modelled with a fixed magnitude. This formulation is capable of capturing only the structural resonance.
The second method provides a more accurate representation of the moving load problem by introducing an additional internal degree of freedom for the vehicle, thereby accounting for the interaction of the load and structure. This approach gives rise to an instability phenomenon, which occurs when the vehicle speed exceeds the minimum phase velocity of the medium. Thereby leading to destabilisation of the vehicle vibrations. As hyperloop vehicles may operate near or beyond this critical velocity, potentially causing wave-induced instability, this more realistic approach is used in this research.

It is important to note the difference between instability and resonance. Resonance only happens at a specific velocity, while instability can be found for a range of velocities. Another distinction lies in how these phenomena can be mitigated. Resonance can be effectively damped. In contrast, instability results in an exponential growth of the vibration amplitude, even in the presence of damping. Damping only shifts the boundaries within which instability occurs; therefore, instability is viewed as more dangerous compared to resonance (Veritchev, 2002).

The explanation of wave-induced instability was firstly provided by Metrikine and Popp (1999), who stated that when velocity of an object passes the speed of minimum phase velocity (c_{ph}^{min}), radiated waves are created in the beam. These radiated anomalous doppler waves, contrary to the radiation condition, would inject energy into the object rather than extracting it. This energy transfer leads to the instability of the moving object and structure.

According to the radiation condition, waves should carry energy away from the load. So, waves propagating in front of the moving load should have a group velocity c_{gr} larger than the load velocity (v), and the waves behind should have c_{gr} smaller than the load velocity:

$$c_{\mathrm{ph}} = \frac{\omega}{k}$$
$$c_{\mathrm{gr}} = \frac{\partial \omega}{\partial k}. \tag{2.1}$$

To better demonstrate the theory, an infinite Euler-Bernoulli beam with a uniformly moving one-mass oscillator is considered. The explanation here starts from the algebraic equations obtained by applying a solution method to the equations of motion. These algebraic equations are shown below, the expression in

the first line is the dispersion equation, which describes the possible waves that may propagate in the system. The relation on the second line is referred to as the kinematic invariant and represents all $\omega - k$ combinations excited by the moving load. Dependent on how the structure and load are modelled these relations differ:

$$\begin{aligned} \Delta(\omega, k) &= \alpha^2 k^4 - \omega^2, \\ \omega &= kv + \Omega. \end{aligned} \tag{2.2}$$

Substituting the kinematic invariant into the dispersion equation and equating to zero ($\Delta(\omega, k, v) = 0$) gives the frequencies of the waves excited by the moving load. These waves correspond to the intersection points in figure 2.2. The graph shows a realization of the kinematic invariant for a certain speed of the moving load, being the tangent of kinematic invariant.
Changes in speed influences not only the quantitative behaviour, but also the qualitative behaviour of the system. When no intersections can be found between the kinematic invariant and dispersion curve, evanescent waves are excited. Evanescent waves do not carry energy away, and cause only localized disturbance, known as an eigenfield. For a range of load velocities, the two functions intersect, corresponding to the excitation of propagating waves that carry energy.

For the moving load problem described in the previous paragraph, the radiated waves are graphically shown in the figure below. The two propagating waves (waves 1 and 2, indicated by green dots) in the upper half of the graph, are normal doppler waves. The other two waves are in the lower half of the graph and represent the anomalous Doppler waves, which increase the energy of oscillation of the load.

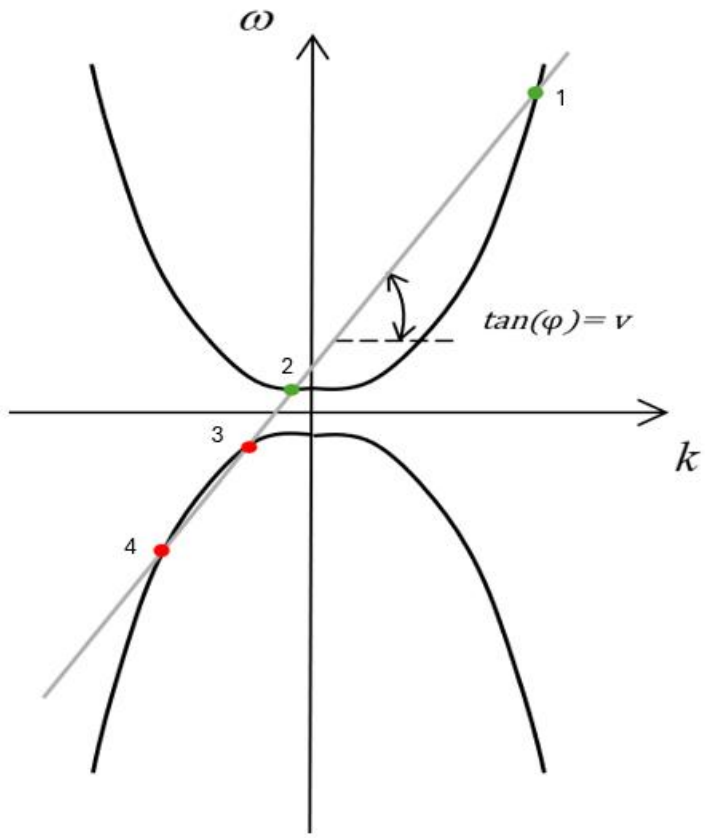

Figure 2.2 Graphical representation of the kinematic invariant and dispersion equation, illustrating the emergence of the normal and anomalous Doppler waves.

2.2 Control

As the need for control is evident in order to achieve stable levitation, the search for an appropriate closed loop feedback-controllers that meets the objectives is required.

Therefore, we start with an explanation of the structure of a feedback controller in the context of the plant studied in this thesis. The plant is the physical system whose dynamics are being manipulated by the controller. In this case, it refers to the hyperloop. A sensor measures the system's state behaviour. These measurements are sent to the controller, where they are compared to a desired reference. The difference between the signal and reference is called the control error. Based on this error and the dynamics of the plant, the controller calculates the input. This controller output, which serves being the input to system, is then sent to the actuator, which in this plant is the electromagnet. The actuator converts the electrical input into a physical effect by generating a magnetic field. This magnetic field creates an electromagnetic force. As a result, the plant dynamics change. The new states are then again measured and the process is repeated, closing the feedback loop. The system is normally also subject to external disturbances and measurement noise, which can affect the plant dynamics and the accuracy of the measured error.

The type of controller described above, constantly measures the mismatch between the desired reference and measured system output, it closes the control loop by feeding back this signal to calculate the control input. This the essential difference from an open-loop feedback system, which doesn't use any measurement information to adjust the control input.

The literature review conducted on the existing control strategies applied to EMS-systems revealed a variety of algorithms, which are classified into three groups in a review paper by Li et al. (2023): linear controllers, nonlinear controllers and intelligent control algorithms.

Linear

This group uses a linear control law, where the input is linearly related to the system states, in contrast to the next group of nonlinear controllers where the input is a nonlinear function of the states. Most of the controllers used in industry are based on the PID controller. This technique is a simple control law and relatively easy to implement (Song et al., 2013). Controller gains are determined after linearizing the system; therefore, the system may become unstable further away from the equilibrium. Another disadvantage is that the gain cannot be adjusted while running the system. This group of control method performs poorly when operating further from equilibrium and is less robust.

Nonlinear

Better performance on robustness and stability can be reached by applying nonlinear control methods: like sliding mode control (SMC) and MPC. MPC can handle nonlinear systems and is able to handle constraints on state and input variables, thereby preventing saturation. The method is also able to deal with multivariable problems. However, MPC is relatively computational expensive. In Ulbig et al. (2008) the nonlinear dynamics of the system is approximated by applying a set of piecewise affine systems, this system accurately captures the nonlinear dynamics of the system. Furthermore, the controller is designed to enable fast implementation by using an explicit formulation of the problem, avoiding the need for online optimisation. Another nonlinear method, sliding method control (SMC), works well for fast systems as its computational cost is low. This method has proven effective in controlling vehicle-railway coupled vibration problems (Li et al., 2023). This control approach is also capable of suppressing external disturbances. The trade-off for its robustness is that it can cause high-frequency oscillations in the control input when operating close to the sliding surface. In addition, SMC cannot explicitly handle constraints.
In general, by accounting for the system's nonlinear dynamics, the nonlinear approach achieves better robustness.

Intelligent control

With the development of artificial intelligence, the concepts of AI have been integrated in control techniques. No accurate model is thereby needed, instead, the self-learning is used to address uncertainty and external disturbance. Hower AI-based levitation control methods lack theoretical analysis due to their black-box nature. Moreover, they may perform poorly in unseen scenarios, making them impractical for

real applications, as significant parameter changes often require re-learning of control rules. The application of this approach is still limited, and more research is needed (Li et al., 2023).

After reviewing the existing control strategies, Model Predictive Control (MPC) was identified as the approach for addressing the control problem considered in this thesis. The hyperloop system is strongly nonlinear, involves multiple variables, is subject to external disturbances, and operates under physical constraints. MPC is therefore expected to be effective in stabilizing such a system, as its main advantage over other controllers lies in its predictive capability and its ability to explicitly handle both input and state constraints (Schwenzer et al., 2021). In addition, MPC can effectively handle coupling between states and inputs, making it suitable for controlling multivariable processes. MPC has also proven to perform well for systems that include non-minimum phase behaviour, large time delays and unstable dynamics.

A known drawback of MPC is its dependence on an accurate model to describe the process, which can be challenging for certain systems. In this study, however, the system equations are given, and a perfect model is assumed. Another limitation is the computational effort required to solve the optimal control problem online at each time step. Nevertheless, nowadays the solvers are very fast, making MPC implementable even for systems with very fast dynamics. These properties make MPC suitable for stabilising the system studied in this thesis.

2.3 Introduction MPC

This chapter aims to introduce the concept of MPC and provide the theoretical foundation required for the development and implementation of the MPC controller in the upcoming chapters.

Concept
MPC is an optimization-based control methodology applied to constrained control problems. It has been introduced in 1970 to slow chemical processes. The principles of MPC were already used in the 1960s. In the beginning, this method was mainly applied to slow industrial processes with large sampling time. Over the last few decades, however, MPC has become increasingly popular due to advances in computational power and developments in optimization algorithms.

This control strategy determines the control action by solving in real-time a finite-horizon optimal control problem at each sampling instant. This optimization yields a finite sequence of control inputs, of which only the first is applied to the plant The rest of the computed control sequence is discarded, and the process is repeated at the next time step using the state measurement as initial condition at every sampling instant. Figure 2.3 illustrates the methodology of an MPC controller. In this figure, the control and prediction horizons were chosen to be equal, however, this can vary depending on the tuning of these parameters.

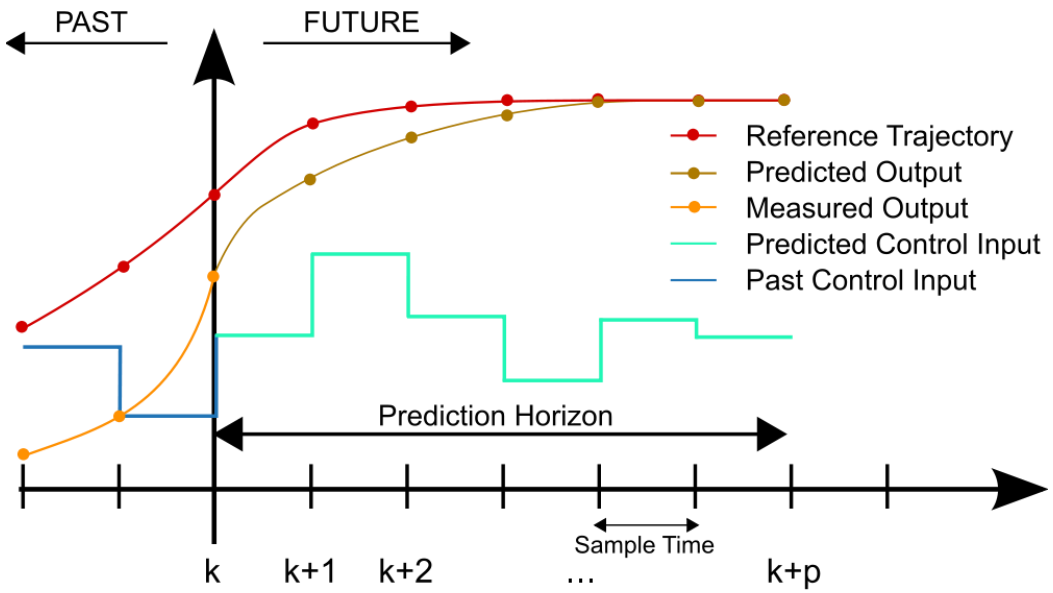

Figure 2.3: MPC concept (Maurice Heemels, 2013).

The method of shifting the horizon at every time step and solving the optimization problem using updated information is known as the receding horizon principle. This feedback principle makes sure that predictions made are based on the latest measurements. Thereby minimizing the effect of unmeasurable disturbances and model-plant inaccuracy, so making it a more robust controller (Morari & Lee, 1999) (Schwenzer et al., 2021).
MPC relies on the availability of a prediction model, which can be derived by means of physical laws or using system identification techniques using measured data. The prediction model is used to forecast the future evolution of the system states over a finite horizon. The predicted system behaviour is incorporated into an objective function, which is then minimised subject to system constraints to determine the optimal control action. This optimisation problem is solved at each sampling instant as part of the receding horizon strategy.
This approach eliminates the need to analytically derive an explicit control law. Instead, MPC computes the control actions automatically through model-based optimisation. This distinguishes MPC from other alternative control methods, which rely on a priori defined control law.

MPC is more a family of control strategies that appear in many forms. MPC variants may differ in the type of objective function, the constraints applied, the optimization algorithm used and the formulation of the prediction model.

In literature, several prediction model formulations are commonly encountered: impulse response models, step response models, and polynomial models. MPC is now commonly formulated in state-space, since it allows for an easier expression of stability as applied in the calculation of the open-loop eigenvalues. It also facilitates their generalization to more complex cases such as multivariable processes.
Predictions obtained at every time instance in this thesis, are based on the dynamics given in the state-space representation (Van Den Boom, 2020).

Since the control strategy involves solving an optimization problem at each sampling instant, it is more practical to use a discrete-time model instead of a continuous one. The model represents the dynamic behaviour of the real system and serves as the basis for prediction and control.

Consider a nonlinear, discrete-time formulation of the process:

$$x(k+1) = f\big(x(k), u(k)\big) \tag{2.3}$$

where $x_k \in \mathbb{R}^n$ represents the states and $u_k \in \mathbb{R}^m$ are the control input at time k.
Ater linearisation, the linear system to be controlled is described by a linear discrete time model:

$$\begin{aligned} x(k+1) &= Ax(k) + Bu(k) \\ y(k) &= Cx(k). \end{aligned} \tag{2.4}$$

In multiple-input multiple-output (MIMO) models, the $x(k) \in \mathbb{R}^n$ represents the state of the system at time k and $u(k) \in \mathbb{R}^m$ is a vector of manipulated variables.
The $A \in \mathbb{R}^{n\times n}$ captures the underlying internal dynamics, while $B \in \mathbb{R}^{n\times m}$ relates the input to the system variables. The measured output $y \in \mathbb{R}^q$ is related to the states by the matrix $C \in \mathbb{R}^{q\times n}$. The C-matrix represents a vector that selects a set of states that you can measure.

In this thesis, both linear MPC and nonlinear MPC (NMPC) approaches are used. The distinction lies in the type of prediction model and type of constraints imposed on the inputs and states. When a linear prediction model is combined with linear constraints, the formulation corresponds to a linear MPC scheme. However, even in this case with a linear model, the resulting closed-loop dynamics may be nonlinear due to the constraints that result in a nonlinear control law with respect to x (Findeisen et al., 2003).

Discretisation
Since the problem initially involves continuous dynamics, the objective function corresponds to a continuous, infinite-dimensional Optimal Control Problem (OCP), which is not directly represented by the finite dimensional expression given in Eq. (2.5). To obtain this expression, the OCP must first be converted to enable numerical solution. This requires the use of methods that numerically solve continuous OCP. In general, three main approaches exist: dynamic programming, the indirect method, and the direct method.
The dynamic programming approach is based on the principle of optimality and derives a control law using the Hamilton-Jacobi-Bellman (HJB) equation.
The indirect method derives a boundary value problem (BVP) by applying the first-order optimality conditions from Pontryagin's Maximum Principle (PMP). This approach is often referred to as "optimize-then-discretize."

In contrast, direct methods are often described as "discretize-then-optimize", as they reformulate the original infinite-dimensional OCP as a finite-dimensional nonlinear programming (NLP) problem, which can then be solved using numerical optimization techniques. The direct method can be further divided into different classes: single shooting (sequential), and multiple shooting and collocation (simultaneous). In all direct methods, the control trajectories are parameterized as finite-dimensional, but they differ in how the

state trajectories are computed. In the sequential approach, the dynamics are integrated in the cost function, and the control is the only optimization variable. Conversely, in the simultaneous approach, both states and inputs are decision variables. The dynamics are included as constraints in the optimization problem.

A key advantage of direct methods lies in their ability to handle inequality constraints. This makes them particularly well suited for MPC problems. On the other hand, a known limitation is that performance may deteriorate when the system dynamics are unstable, since the entire state trajectory depends on forward integration from a single initial condition.

Among all methods to address an OCP, direct methods are widely used in the context of MPC to make the problem suitable to numerical optimization algorithms. Therefore, this thesis will apply this class of methods, despite the known drawback that the underlying system is unstable. Direct NMPC will be employed, where the objective function incorporating a nonlinear system is optimized at each step (Zietkiewicz & Owczarkowski, 2017). To be more precise the direct single shooting method, in which the input is the only optimization variable and the state trajectory is computed through simulation (Diehl et al., 2007).

Objective function:
When dealing with a time-invariant function and cost function, the optimization problem doesn't explicitly depend on time step k, but only on the initial condition x_0 . for ease of notation, $\mathbb{P}_N(x_0, k) = \mathbb{P}_N(x_0, 0) = \mathbb{P}_N(x_0)$. A typical formulation of the optimization problem $\mathbb{P}_N(x_0)$ in MPC after using the simultaneous transcription method leads to the formulation of the optimization problem as follows:

$$\begin{aligned} \underset{\mathbf{x},\mathbf{u}}{\text{minimize}} \quad & \sum_{k=0}^{N-1} \ell\big(x(k), u(k)\big) + V_f\big(x(N)\big) \\ \text{subject to} \quad & x(0) = x_0 \\ & x(k+1) = f\big(x(k), u(k)\big), k = 0,1, \dots, N-1 \\ & u(k) \in \mathbb{U}, k = 0,1, \dots, N-1 \\ & x(k) \in \mathbb{X}, , k = 0,1, \dots, N \\ & x(N) \in \mathbb{X}_f \end{aligned} \tag{2.5}$$

Where $\ell(x,u) = x^T Q x + u^T R u$ is the stage cost and the terminal cost function is: $V_f(x) = x^T P x$.
The cost function includes a terminal weight $P \in \mathbb{R}^{n\times n}$, state penalties $Q \in \mathbb{R}^{n\times n}$, and input penalties $R \in \mathbb{R}^{m\times m}$, horizon length N. Here, it is assumed that $Q \geq 0$ and $R > 0$.

The control horizon here is taken equal to prediction horizon. When $N = \infty$, this is referred to as the infinite horizon problem; when N is finite, it becomes the finite horizon version. The optimization problem is subject to the initial condition x_0, the system dynamics, a set of allowed inputs $\mathbb{U} \subset \mathbb{R}^m$ and states $\mathbb{X} \subset \mathbb{R}^n$ and a terminal region $(\mathbb{X}_f)$ constraint.
An appropriate optimization algorithm should be selected based on the type of problem.
Note that a formulation of the problem is presented in Eq. (2.5), which employs a simultaneous transcription method as indicated by decision variables being both u and x. Later in this thesis, a direct single shooting method will be used, as motivated previously.

For linear MPC these Here it is assumed that prediction horizon equals control horizon will differ, the optimization problem of the linear MPC will then be formulated as follows (Morari & Lee, 1999).:

$$\begin{aligned} J_{(N_p,N_c)}(x_0) = \min_{u(\cdot)} \Bigg[& x^T\big(N_p\big) P x\big(N_p\big) + \sum_{i=0}^{N_{p-1}} x^T(i) Q x(i) \\ & + \sum_{i=1}^{N_c} u^T(i) R u(i) \Bigg] \end{aligned} \tag{2.6}$$

Where N_p is the prediction horizon length, over which the objective function is calculated and minimized. The control horizon N_c is the horizon over which the input is allowed to change. Often N_p is taken larger than N_c, in that case, the last optimized input value remains constant for all timesteps beyond the control horizon: $u^0(N_c - 1) = u^0(N_c) = \cdots = u^0(N_p)$,
Solving this yields an optimal sequence of control, $\mathbf{u}^0(x) = (u^0(0), u^0(1), \ldots, u^0(N_c - 1))$, as well as the optimal state trajectory $\mathbf{x}^0(x) = (x^0(0), x^0(1), \ldots, x^0(N_p))$, which minimizes the cost given the current state $x(k)$.
Constraints are not imposed on the states for computational reasons. However, in practice a physical constraint is that the airgap is larger than zero and stays within a range around the desired airgap.
In contrast, a constraint on the control input is applied. This reflects the fact that the power supply system actuator can only operate within a limited voltage range.

Stability
In a nominal setting, if the MPC problem could be solved over an infinite horizon, the optimal input sequence found at the initial time step, could be applied at all future time steps. In that case, MPC inherently guarantees stability. However, optimization over an infinite horizon is computational intractable when constraints are present or a nonlinear model is used.

That is why, in practice, MPC is implemented with a finite horizon. In finite horizon optimal control problem, there is a difference between predicted and the closed trajectory, even if no model plant mismatch and no disturbance are present (Allgöwer et al., 1999). As a result, the optimal MPC input doesn't inherently guarantee stability, as demonstrated by Bitmead et al. (1990). Moreover, the problem may initially be feasible, meaning there exists a control sequence that satisfies all the constraints, but feasibility at each timestep of the closed-loop system requires additional assumptions.

That is why much work has been focused on ensuring schemes with closed-loop stability and feasibility in finite-horizon MPC. Stability is typically addressed according to a Lyapunov condition in MPC problems, by enforcing conditions such that the optimal value function acts as a Lyapunov function for the closed-loop system. The key idea is to ensure that function J_N acts as a Lyapunov function, where J_N is the optimal finite-horizon cost with length N.

A Lyapunov function is a continuously differentiable scalar function $V(x)$: $\mathbb{R}^n \to \mathbb{R}$. It is positive definite and does not increase over time (Schwenzer et al., 2021):

$$V(0) = 0, V(x) > 0, \forall x \neq 0, \quad \dot{V}(x) \leq 0, \forall x \neq 0. \tag{2.7}$$

Stability is proven, if it can be shown that the right-hand side of Eq. (2.8) is positive. Ensuring the value function behaves like a Lyapunov function, such that $J_N(x(k)) - J_N(x(k+1)) > 0$ for $x \neq 0$. Where $x(k+1) = f(x(k), u^0(0))$, herein $u^0(0)$ is the first control input resulting from the optimal MPC sequence. Rewriting $J_N(x(k)) - J_N(x(k+1))$ using that $J_N(x(k)) = x^T(0)Qx(0) + u^0(0)^T Ru^0(0) + J_{N-1}(x(k+1))$ and using that the optimal-cost-to-go $J_{N-1}(x(k+1))$ itself is optimal for the remaining horizon, follows from the optimality principle, leads to:.

$$\begin{aligned} &J_N(x(k)) - J_N(x(k+1)) \\ &= [x^T(k)Qx(k) + u^0(0)^T Ru^0(0)] \\ &+ [J_{N-1}(x(k+1)) - J_N(x(k+1))]. \end{aligned} \tag{2.8}$$

When $Q > 0$, the stage cost of first step $[x^T(k)Qx(k) + u_N^*(0 \mid x(k))Ru_N^*(0 \mid x(k))]$ is positive (Morari & Lee, 1999). However, without additional assumptions, it cannot be assumed that the second term is positive.

Ensuring that the cost acts as a Lyapunov function and thereby achieving stability can be done through various techniques. One way of achieving stability is by picking a finite horizon large enough N, such that

the first term dominates over the second term. The most used method is to modify the problem by introducing terminal constraints and a terminal cost 0(Mayne, 2014). The terminal constraint drives the state to a steady-state value or a region at the end of the prediction horizon. The terminal cost is added to approximate the infinite-horizon value function (Mayne et al., 2000). Although terminal ingredients or modifications as described can provide formal stability guarantees, the resulting constraints are often restrictive and do not always lead to better practical control performance. As highlighted by Köhler et al. (2023), the feasible set of initial conditions from which the optimisation problem remains solvable becomes smaller. This reduces the size of the region of attraction, excluding states from which closed-loop stability could still have been achieved without enforcing such stability guarantee.

In many cases, a longer prediction horizon provides sufficient stability without terminal conditions. Therefore, this study omits terminal cost and constraints, but stability is achieved through careful tuning, a common practice in industry to avoid unnecessary complexity (Schmid et al., 2019).

3. System modelling

This chapter presents the system model used for analysis and control design. The model is introduced first, followed by the underlying assumptions, after which the governing equations are presented.

A fundamental part of modelling the hyperloop infrastructure is the electromagnetic suspension (EMS). What distinguishes the suspension system employed by Hardt Hyperloop from other hyperloop concepts is the placement of the guideway at the top inside the tube, as can be seen in the cross-section of the vehicle in figure 3.1.

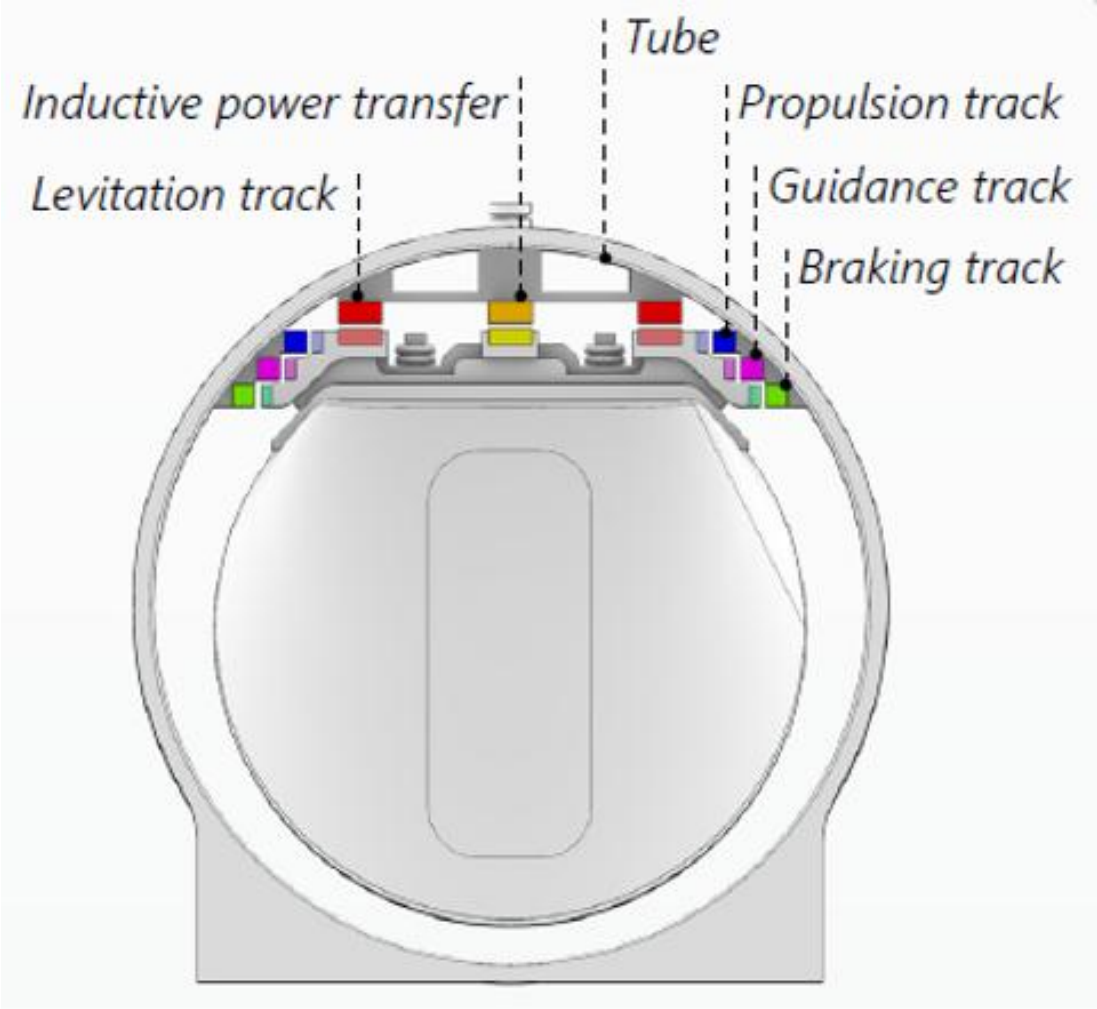

Figure 3.1: Cross-section of the hyperloop concept developed by Hardt Hyperloop (Hardt, 2024).

To reduce the model complexity of the hyperloop system without compromising the accuracy significantly, a few assumptions are made to mathematically describe the system. The length of the tube is significantly larger than its diameters, therefore the effect of shear deformation is neglected. Another assumption is that, since the length of the vehicle is much smaller than the length of the tube, the vehicle can be treated as a point mass. Although the hyperloop tube is periodically supported by piers, the structure is modelled as being continuous supported using springs and dashpots. The stiffness and the mass of the hyperloop infrastructure are captured by the parameters listed in table 3.1.

The hyperloop is modelled as an infinite Euler-Bernoulli beam continuously supported by a viscoelastic foundation subject to a moving point mass (Faragau et al., 2023). This provides a representative way of modelling the tube, pod and guideway considering the problem definition. By modelling the vehicle-guideway interaction in the way as in figure 3.2, propagation of the so-called anomalous Doppler-waves are made possible.

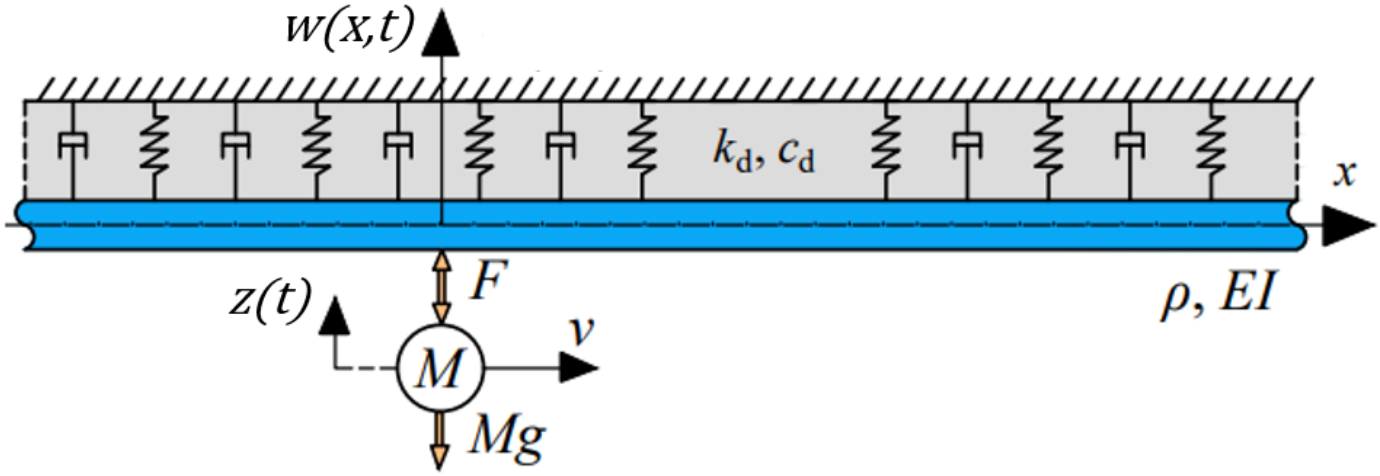

Figure 3.2: Modelling of the vehicle-guideway coupled system (Faragau et al., 2023)

The continuous beam has a mass per unit length of ρ and is supported by a viscoelastic foundation with stiffness k_d and damping c_d, subject to a mass M travelling with a velocity of v. The vehicle and guideway are connected trough the magnetic attraction force F, which is assumed to be constant with respect to the horizontal vehicle velocity and ignores the drag component.

The airgap is studied in a moving reference frame, introducing variables at spatial coordinate $\xi = x - vt$ and temporal coordinate $\tau = t$. Variable w and z are the displacements in vertical direction of the beam and point mass M respectively. The feedback system is monitoring $w(\xi = 0, \tau) = w_0$, being the beam displacement at the location of moving load. In the moving reference frame (ξ, τ), the governing equations are:

$$\begin{gathered} EIw'''' + \rho(\ddot{w} - 2v\dot{w}' + v^2 w'') + c_\mathrm{d}(\dot{w} - vw') + k_\mathrm{d} w = -F(t)\delta(\xi), \\ M\ddot{z} = F(t) - Mg, \\ F(t) = C\frac{I^2}{(w_0 - z)^2}, \\ \dot{I} = \frac{w_0 - z}{2C}\left(U - IR + 2C\frac{I}{(w_0 - z)^2}(\dot{w}_0 - \dot{z})\right), \\ U_{MPC} = \kappa_{MPC}. \end{gathered} \tag{3.1}$$

Where $\delta(\xi)$ locates the moving vehicle, g is the acceleration of gravity and R denotes the electrical resistance. The constant $C = \mu_0 N^2 A_m/4$ includes the parameters related to the electromagnet: permeability of air μ_0 , N is the number of coil turns, A_m is the surface area of the electromagnet. These equations are derived from the Newton's second law and the Kirchoff's law.

Since this system is inherently unstable, a controller is developed. The controller should levitate the vehicle at a specific altitude of δ_0. Herein is U the manipulated variable, being the voltage calculated by the control system. The equation U_{MPC} describes the voltage related to the MPC-control. For the PD controller, this is an explicit function. While for a MPC controller, the control policy κ_{MPC} will follow from an optimization problem and hence lack an explicit description when studying constrained problems or nonlinear systems. The magnitude of control input will follow from optimization of the objective function, which is presented in the next chapter. The input voltage affects the magnetic force through its contribution to the electric current I applied to the coil. When the measured airgap is greater than the desired airgap, the voltage will be adjusted to increase the magnetic force reducing the gap. In later parts of this study, a constraint will be imposed on the input to take physical limits of the actuator into account, formulated as $u_{min} < u < u_{max}$. The magnetic force, however, remains attractive, even when the applied voltage is negative. Allowing negative voltage can still be very useful, as it increases the rate at which the coil current decreases, leading to a faster reduction in the electromagnetic attraction force.

1.5-DOF system

In order to design the controller focusing on the electromagnetic stability only, we consider a rigid bar. The bar is connected to a mass through a non-linear electromagnetic force. The vehicle dynamics of the hyperloop are modelled as a 1.5-DOF system. The variables describing the system are the vehicle displacement and the electric current. The idea is to check the stability of the vehicle around a target airgap based on the proposed control strategy. The control strategy should ensure that the system in this configuration is stable, while the effect of dynamic instability is disregarded. Later in chapter 5, the effect of the moving load will be introduced by considering the continuous vehicle-beam coupled system. Figure 3.3 below presents a schematic diagram of the simplified system, with positive force and positive displacement oriented downward.

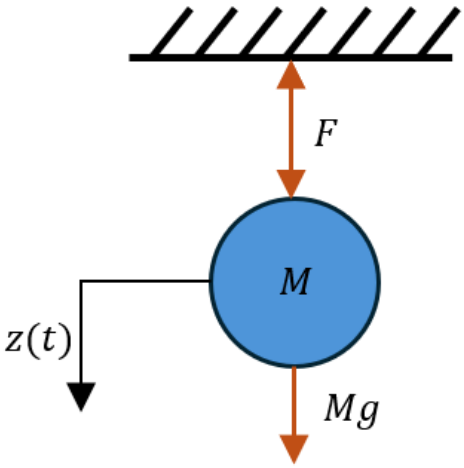

Figure 3.3 Simplified configuration of the hyperloop vehicle dynamics presented as a 1.5-DOF system.

The states that describe the system are defined as: $x_1 = \delta = z - w = z$, being the airgap between the rigid beam and vehicle, $x_2 = \dot{x}_1 =$ and $x_3 = I$. The equation of motion is reduced to the following state-space equations:

$$\begin{cases} \dot{x}_1 = x_2 \\ \dot{x}_2 = g - \dfrac{Cx_3^2}{mx_1^2} \\ \dot{x}_3 = \dfrac{x_2 x_3}{x_1} - \dfrac{Rx_1 x_3}{2C} + \dfrac{x_1}{2C}u \end{cases} \tag{3.2}$$

The governing equations are locally Lipschitz continuous in the region of interest.

Parameters

Numerical values of all the system parameters used in this thesis are given in table 3.1.

Parameter	Value
$\boldsymbol{R}$	$9.71\ Ohm$
$\boldsymbol{M, m}$	$7650\ kg$
$\boldsymbol{N}$	800
$\boldsymbol{A_m}$	$0.25\ m^2$
$\boldsymbol{\mu 0}$	$4\pi \times 10^{-7}\ Tm/A$
$\boldsymbol{C}$	$0.05\ Nm^2/A^2$
$\boldsymbol{g}$	$9.81\ m/s^2$
$\boldsymbol{\delta_0}$	$0.015\ m$
$\boldsymbol{EI}$	$25 \times 10^6 kNm^2$
$\boldsymbol{\rho}$	$1400\ kg/m$
$\boldsymbol{k_d}$	$28 \times 10^{\ 3}\ kN/m^2$
$\boldsymbol{c_d}$	$20\ kNs/m^2$

Table 3.1 Numerical values of the system parameters.

4. Control of the 1.5-DOF system

This section aims to develop an understanding of how different control methods influence the vehicle dynamics of the hyperloop system and provides a comparative analysis of their performance. This chapter focuses solely on the electromagnetic instability. Therefore, the simplified model (1.5-DOF system) is employed, in which the propagation of anomalous doppler waves is not possible.

4.1 Linear MPC

This section explores the potential of MPC control to achieve stabilization in an EMS, where the track beam is considered as rigid.

Linearisation

To write the nonlinear system in the standard state-space formulation, linearisation of Eq. (3.2) is needed. This research focuses on the system behaviour around the operating point of the hyperloop, corresponding to the setpoint δ_0. The equilibrium point (x_0, u_0) is determined, by setting $\dot{x} = 0$, as follows (Zhang et al., 2020):

$$\begin{cases} x_1 = \delta_0 = \dfrac{u_0}{R}\sqrt{\dfrac{k}{mg}} \\ x_2 = 0 \\ x_3 = I_0 = \dfrac{u_0}{R} \\ u = u_0 \end{cases} \tag{4.1}$$

The linear model is applicable when studying small variations $\tilde{x}, \tilde{u}$ and $\tilde{y}$ around the equilibrium. Define $\tilde{x} = \Delta x = x - x_0, \tilde{u} = \Delta u = u - u_0$ and $\tilde{y} = y - y_0 = \ y - \delta_0$. At the equilibrium point (x_0, u_0), equation Eq. (4.2) is linearized using Taylor expansion into:

$$\begin{aligned} \dot{\tilde{x}}(t) &= f(x_0, u_0) + A\tilde{x}(t) + B\tilde{u}(t) \\ \tilde{y}(t) &= g(x_0, u_0) + C\tilde{x}(t) - y_0 \end{aligned} \tag{4.2}$$

With $f(x_0, u_0) = 0$ and $y_0 = g(x_0, u_0)$, this reduces to:

$$\begin{aligned} \dot{\tilde{x}}(t) &= A\tilde{x}(t) + B\tilde{u}(t) \\ \tilde{y}(t) &= C\tilde{x}(t) \end{aligned} \tag{4.3}$$

When linearising with respect to (x_0, u_0): the A, B and C matrices are computed by:

$$A = \left.\frac{\partial f}{\partial x}\right|_{\substack{x=x_0 \\ u=u_0}}, \ B = \left.\frac{\partial f}{\partial u}\right|_{\substack{x=x_0 \\ u=u_0}}, \ C = \left.\frac{\partial g}{\partial x}\right|_{\substack{x=x_0 \\ u=u_0}} \tag{4.4}$$

This leads to the matrices being (Zhang et al., 2020):

$$\mathrm{A} = \begin{pmatrix} 0 & 1 & 0 \\ \dfrac{2g}{\delta_0} & 0 & -\dfrac{2}{\delta_0}\sqrt{\dfrac{Cg}{m}} \\ 0 & \sqrt{\dfrac{mg}{C}} & -\dfrac{R\delta_0}{2C} \end{pmatrix}, \quad \mathrm{B} = \begin{pmatrix} 0 \\ 0 \\ \dfrac{\delta_0}{2C} \end{pmatrix} \tag{4.5}$$

All states are assumed to be measurable, so matrix C is taken as the identity matrix. The matrix D is set to zero, since there is no direct effect from the input to the output (Hu et al., 2021). In addition, the model describing the plant is perfect. Therefore, no state observer is required. The problem is assumed to be time-invariant, so the system matrices are constant over time. With this, the linearisation around the equilibrium point is completed and the system can be written in the following form:

$$\begin{cases} \dot{\tilde{x}}(t) = A\tilde{x}(t) + B\tilde{u}(t) \\ \tilde{y}(t) = \begin{bmatrix} 1 & 0 & 0 \\ 0 & 1 & 0 \\ 0 & 0 & 1 \end{bmatrix} \tilde{x}(t) = \tilde{x}(t) \end{cases} \tag{4.6}$$

Discretisation

The problem is defined in Eq. (4.6) above as a continuous-time equation. However, the MPC algorithm used in research is based on a discrete-time formulated control problem. Therefore, a transformation should be done. This section briefly describes two main methods that are considered: Euler and Taylor.

Euler

the continuous problem is discretised using an explicit Euler Forward method. This method can be applied to both linear and nonlinear systems. Given a system in continuous time:

$$\dot{x} = f(x, u) \tag{4.7}$$

A discrete-time formulation can be obtained using a forward Euler approximation, resulting in the compact form:

$$x(k+1) = x(k) + f(x(k), u(k)) \cdot T_s. \tag{4.8}$$

For a linear state-space, the discretised matrices are given by: $A_d = I + AT_s$ and $B_d = BT_s$.

Taylor discretisation

The Taylor discretized version of a continuous-time LTI-system in its state space can be written as:

$$x\big((k+1)T_s\big) = \Phi(T_s)x(kT_s) + \Gamma(T_s)u(kT_s), \tag{4.9}$$

where $\Phi(T_s) = e^{AT_s} \in \mathbb{R}^{n\times n}$ and $\Gamma(T_s) = \int_0^{T_s} e^{A\tau}Bd\tau = (e^{AT_s} - I)A^{-1}B \in \mathbb{R}^{n\times m}$. These are constant state and input matrices respectively (Meena & Janardhanan, 2017). Another way to express this is by (DeCarlo, 1989):

$$e^{\begin{bmatrix} A & B \\ 0 & 0 \end{bmatrix} \cdot T_s} = \begin{bmatrix} A_d & B_d \\ 0 & I \end{bmatrix}. \tag{4.11}$$

This method assumes a zero-order hold on the input:

$$u(t) = u(kT_s), \text{ for } kT_s \le t < kT_s + T_s \tag{4.10}$$

Two discretisation methods are considered, each with distinct characteristics. Taylor-based discretisation is generally more computationally demanding, but it provides an exact discrete-time representation of the continuous-time system when the input is assumed to be constant over each sampling interval.

To compare the effect of discretisation on closed-loop stability, the stability regions of the same controller were evaluated for different sampling times using both the Euler method and the Taylor exact discretisation. The results showed that forward Euler exhibited significantly poorer performance as the sampling time increased, compared to backward implicit Euler and exact discretisation. The analysis further demonstrated that the exact discretisation method resulted in a larger stability region, allowing the use of larger sampling times while maintaining closed-loop stability.

The Taylor exact discretisation captures the continuous dynamics more accurately for larger timesteps, gives a closed-form solution for the LTI-system, and is therefore adopted in this thesis.

Design

For discrete systems, such as the one studied here, stability around a specific equilibrium point depends on the absolute value of the eigenvalues of the discrete A_d matrix, obtained via linearisation. Figure 4.1 illustrates that the open-loop system has three eigenvalues and shows where the instability of the system originates from. There is a pair of complex conjugates inside the unit circle, and a real valued one located just outside the circle. These results confirm the inherently unstable nature of the system, thereby requiring a closed-loop control strategy to achieve stable levitation of the vehicle.

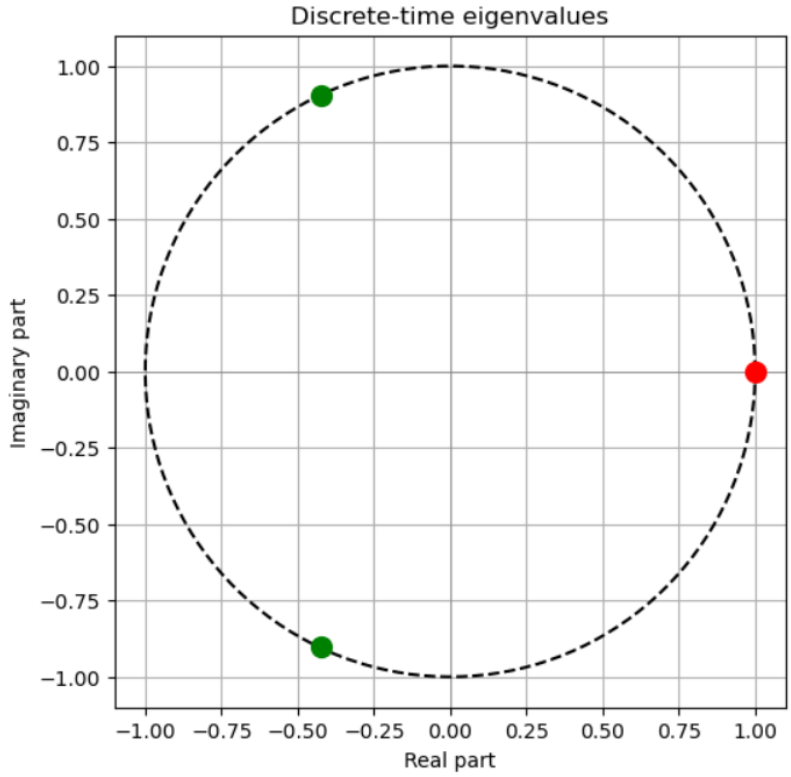

Figure 4.1 Open-loop system discrete eigenvalues, one eigenvalue just outside the unit circle.

Before designing a controller, the matrix pair (A, B) is examined, it turns out that the system is controllable. This means that, for any initial state, there exists a control input that can drive the system to any final state within a finite amount of time. This is confirmed by the fact that the controllability matrix W_r is full rank (Cavenago et al., 2023).

$$W_\mathrm{r} = (B \quad AB \quad \cdots \quad A^{n-1}B). \tag{4.12}$$

Stabilizability is a weaker condition than controllability, as it only requires that the unstable modes are controllable. This is verified by the controllability check, meaning that a suitable control law exists to place all eigenvalues of the closed-loop system in the stable region.

Another important concept to consider when designing a controller is the observability of the system. When all states are assumed to be known at every timestep, there is no need to verify observability. However, in practice, this assumption of the full state vector being directly available is often not realistic. Therefore observability is examined for the case where only the airgap displacement x_1 is measured, which corresponds to $C = [1 \quad 0 \quad 0]$. It can be shown that the observability matrix W_o has full rank in that case, which confirms that the internal states can be reconstructed based on measuring the airgap only (Astrom & Murray, 2008).

$$W_o = \begin{pmatrix} C \\ CA \\ CA^2 \\ \vdots \\ CA^{n-1} \end{pmatrix} \tag{4.13}$$

A model predictive control (MPC) has been applied to stabilize the system. The control variable is the input voltage of the electromagnet coil. The MPC control algorithm is described in more detail in section 2.3.

The optimization problem of the linear MPC will be formulated (Morari & Lee, 1999) as follows:

$$J_{(N_p,N_c)}(x_0) = \min_{u(\cdot)} \left[\tilde{x}^T(N_p) P \tilde{x}(N_p) + \sum_{i=0}^{N_p-1} \tilde{x}^T(i) Q \tilde{x}(i) + \sum_{i=0}^{N_c-1} \tilde{u}^T(i) R \tilde{u}(i) \right]. \tag{4.14}$$

The problem is now unconstrained with respect to its input.

The objective function is formulated to ensure that the system states follow a desired target, which in this case corresponds to the origin of the local coordinate system. After linearisation, the system is analysed in this reference frame, where $\tilde{x}$ represents the deviations from the equilibrium point. At every time step, the cost function from Eq. (4.14) is minimized over the prediction horizon, this gives a set of optimal control input values $\tilde{u}(k)$ for i from 0 to $N_c - 1$. Note that the control horizon can be shorter than the prediction horizon according to this formulation. In that case, when $N_p > N_c$, the last calculated input stays constant from timesteps N_c to N_p. The terminal cost term weighted by P is separated because it specifically penalized the final predicted state at the end of the prediction horizon and is often chosen based on stability guarantees, as mentioned in section 2.3.

The future states predictions over the prediction horizon will be determined according to the equation:

$$\tilde{x}(k) = \mathcal{M}\tilde{x}(k) + \mathcal{C}\tilde{u}(k) \tag{4.15}$$

The $\mathcal{M}$-matrix relates the current measured state $\tilde{x}(k)$ to the predicted future outputs. This matrix $\mathcal{C}$ propagates the effect of control inputs on the predicted states.

$$\tilde{x}(k) = \begin{bmatrix} x(k+1) \\ x(k+2) \\ x(k+N_c) \\ \vdots \\ x(k+N_p) \end{bmatrix}, \tilde{u}(k) = \begin{bmatrix} u(k) \\ u(k+1) \\ \vdots \\ u(k+N_c) \\ \vdots \\ u(k+N_p-1) \end{bmatrix}, \mathcal{M} = \begin{bmatrix} A \\ A^2 \\ A^3 \\ \vdots \\ A^{N_p} \end{bmatrix}, \mathcal{C} = \begin{bmatrix} B & 0 & \cdots & 0 \\ AB & B & \cdots & 0 \\ A^2B & AB & \cdots & 0 \\ \vdots & \vdots & \vdots & \vdots \\ A^{N_p-1}B & A^{N_p-2}B & \cdots & A^{N_p-N_p}B \end{bmatrix}. \tag{4.16}$$

By incorporating these matrices and vectors and reformulating, the relation given in Eq. (4.17) is obtained:

$$\begin{aligned} J(k) &= \tilde{u}^T(k) H \tilde{u}(k) + 2y^T(k) F^T \tilde{u}(k) + x^T(k) G x(k) \\ H &= \mathcal{C}^T Q \mathcal{C} + R \\ G &= \mathcal{M}^T Q \mathcal{M} \\ F &= \mathcal{C}^T Q \mathcal{M}. \end{aligned} \tag{4.17}$$

For this specific class of optimization problem (quadratic objective function, linear dynamics model and without constraints), an analytical solution can be found by taking the gradient of J with respect to u and setting that equal to zero:

$$\frac{\partial J}{\partial \tilde{u}} = 2H\tilde{u} + 2Fx = 0. \tag{4.18}$$

The optimal control sequence is then:

$$\tilde{u}^0(k) = -H^{-1}F\tilde{x}(k) = K\tilde{x}(k) \tag{4.19}$$

As this is a convex problem, the locally optimal solution is the global optimal. Following the receding horizon principle, we only implement the first value of the sequence.

4.1.1 Eigenvalue analysis

As can be seen from Eq. (4.19) above the unconstrained MPC results in a linear control law, with the controller gain remaining constant over time. The eigenvalues analysis can be used to study stability when the system is linear, however the mathematical model under control is nonlinear. The analysis could still be useful, since the controller is designed to levitate the vehicle around the equilibrium.

A closed loop system is obtained when substituting the control law: $x(k+1) = (A + BK)x(k)$, and the closed-loop matrix is:

$$A_{cl} = A + BK. \tag{4.20}$$

As is clear from the control law the factor K is dependent on tuning parameters. For a system that is discrete in time, stability can be achieved if and only if all eigenvalues of the closed-loop matrix lie strictly inside the unit circle (Van Den Boom, 2020).

Achieving stability can be challenging, the relationships between control performance and tuning parameters are mathematical complex (Camacho & Alba, 2013). The control parameters influencing matrix A_{cl} are tuned to satisfy the stability condition. The tuneable parameters are the sampling time T_s, the prediction horizon (N_p) and control horizon (N_c), as well as the penalties for reference tracking (Q) and input effort (R). The effect of these parameters on the closed-loop performance can be nonmonotonic (Garriga & Soroush, 2008). While, in the linearized case, explicit relationships can be formulated, deriving such relations becomes impossible when moving to nonlinear systems. There is no standard approach for tuning, literature provides some guidelines in terms of dynamic characteristics of the plant. Another method, increasingly used, formulates the tuning parameters as a decision variable within an optimization problem. However, in practice to avoid too much complexity, stability is achieved by carefully tuning the control parameters (Schmid et al., 2019). Accordingly, throughout this thesis, the parameters in all applications are selected using a heuristic trial-and-error approach.

To illustrate the effect of the tuning parameters on the closed-loop stability of the 1.5-DOF system under the discrete-time linear MPC, a stability parameter space is presented in the following paragraphs. The analysis focuses on the dominant eigenvalue that lies outside the unit circle in the uncontrolled system. For each controller configuration, every cross shown in the figure indicates the location of this eigenvalue. The remaining eigenvalues are not shown, unless stated otherwise, for clarity.

Sampling time (T_s)

A high sampling frequency is necessary to accurately capture the fast dynamical problem. The frequency influences the control results, so when changing this parameter, the control and prediction horizon should be tuned too. For the controller to be implementable, the sampling time should be larger than the time needed by the controller algorithm to determine optimal input. Its value affects both tracking performance and computational effort. The sampling time T_s is constrained by the technical specifications of the control equipment and is generally not considered as a tuneable parameter. In this thesis, the sampling time (T_s) is chosen as 0.005 seconds, the control action will then be executed at a frequency of 1/T_s. Every 0.005 s the optimization problem must be solved, and an optimal input will be computed and sent to the plant.

Prediction horizon (N_p)
A rule of thumb mentioned in literature is that the prediction horizon should at least be long enough to capture the effect of a change of the manipulated variable (Schwenzer et al., 2021). The crucial dynamics should also be considered within this interval, including the non-minimum phase time, which represents the duration of the initial inverse response. A larger prediction horizon generally improves stability. By taking a larger preview of the future dynamics, the controller can look ahead and predict a longer period and to anticipate, making it more robust. For computational reasons a prediction horizon should be not too large. In general, a shorter horizon also leads to lower control effort and a slower transient response.

Figure 4.2 shows the exact location of the two conjugate eigenvalues for each configuration, while a single cross is used to indicate the dominant eigenvalue near the unit circle boundary. Figure 4.3 then zooms in on this dominant eigenvalue. The control horizon is set equal to the prediction horizon in this configuration. A diagonal state weighting $Q = diag([10^6, 10^6, 10^6])$ and an input weighting $R = 1$ are used.

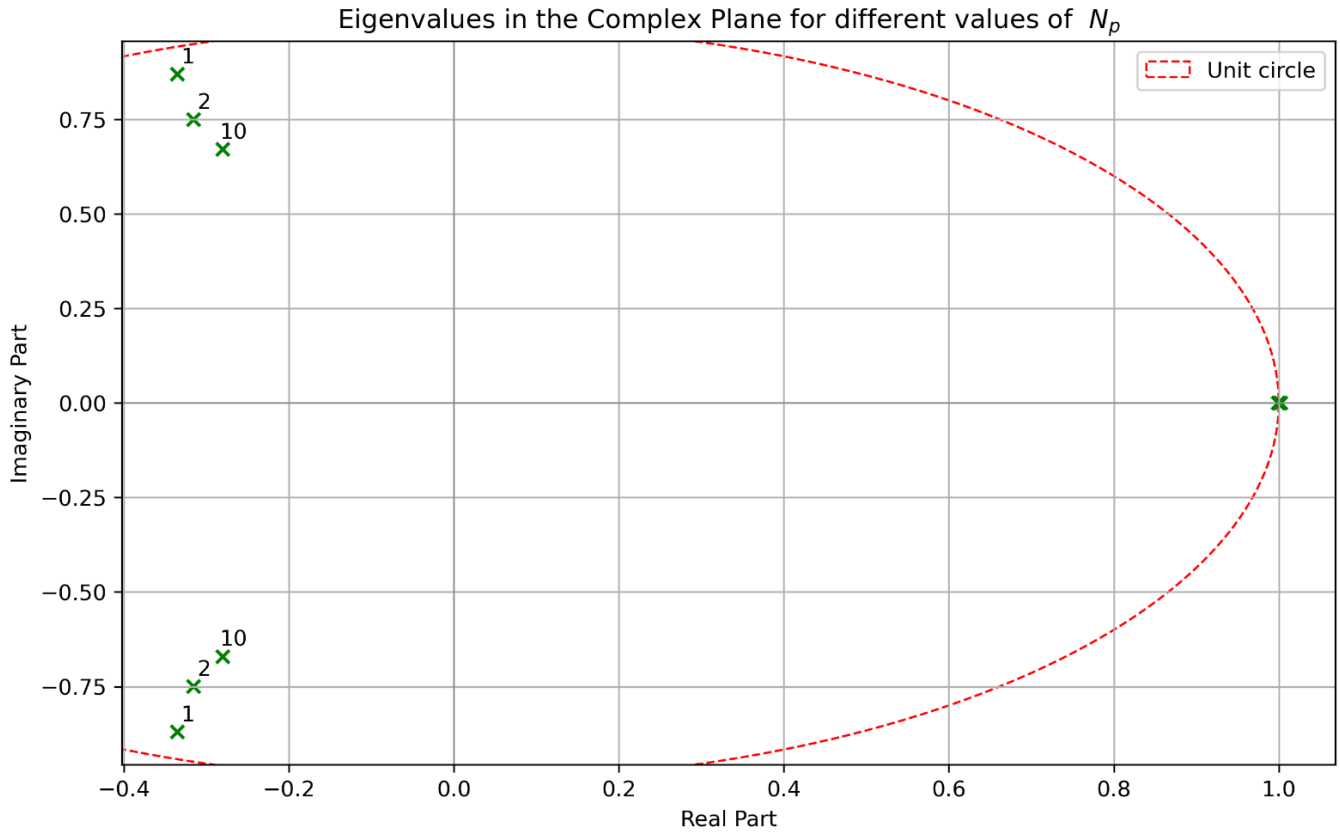

Figure 4.2 Eigenvalues in the Complex Plane for different values of N_p ($Q = diag([10^6, 10^6, 10^6]), R = 1, N_c = N_p$).

The effect on the complex-conjugate pair is visible in the figure. Figure 4.2 and 4.3 shows that, as the prediction horizon N_p, the dominant closed-loop eigenvalues initially move towards the interior of the unit circle, indicating improved closed-loop stability. Beyond a certain horizon length, further increases in N_p have little influence on the closed-loop behaviour.

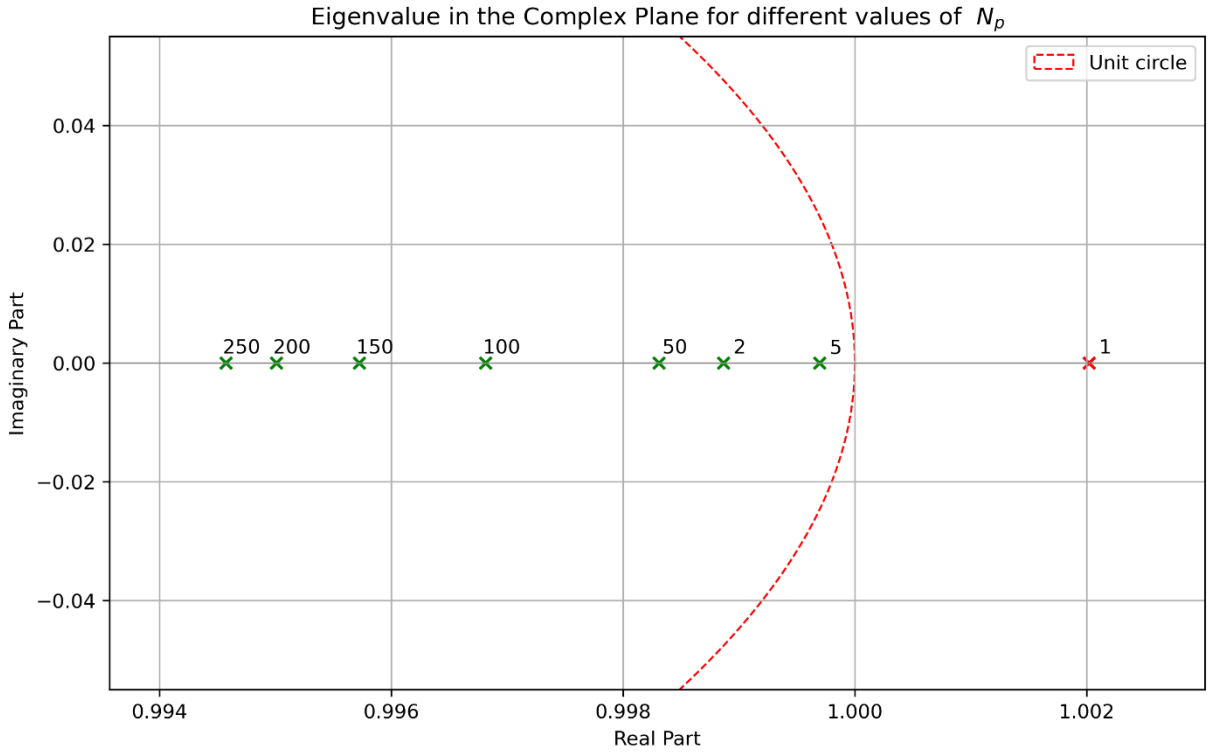

Figure 4.3 Zoomed-in view of the dominant eigenvalue in the Complex Plane for different values of N_p ($Q = diag([10^6, 10^6, 10^6])$, $R = 1$, $N_c = N_p$).

Control horizon (N_c)

In practice, the control and prediction horizon are set equal for convenience. However, the control horizon (N_c) is often chosen smaller than the prediction horizon, to reduce computational cost when calculating these inputs. This can significantly reduce the computational load when dealing with large optimization problems. Since, increasing the control horizon, means more variables to be optimized thus increasing the computational load. When decreasing the prediction and the control horizon, a more robust but less aggressive controller is obtained (Garriga & Soroush, 2008).

First only the dominant eigenvalue of the system is shown in figure 4.4:
A diagonal state weighting $Q = \text{diag}([10^3, 10^3, 10^3])$and an input weighting $R = 1$ are used. The prediction horizon is 300 steps.

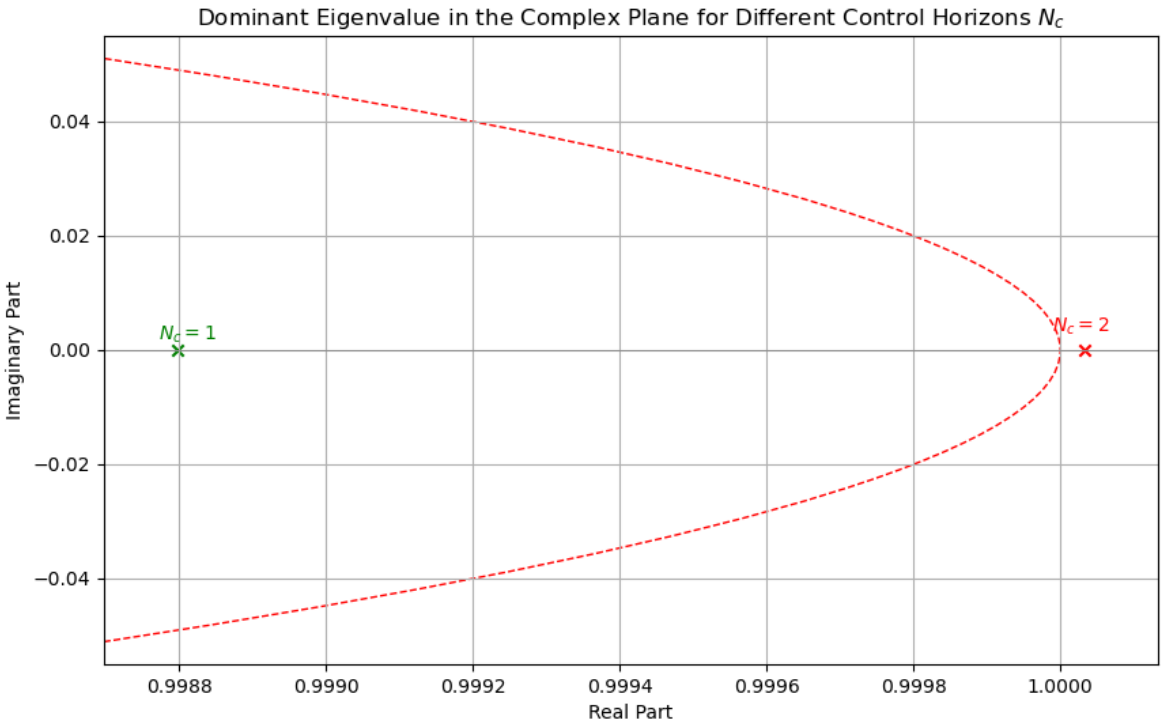

Figure 4.4 Dominant eigenvalue in the complex plane for different control horizons N_c ($Q = diag([10^3, 10^3, 10^3])$, $R = 1, N_p = 300$).

The eigenvalues for $N_c > 2$ are not shown in the figure 4.4, as they appear at the same location as $N_c = 2$. The effect of control horizon on the eigenvalue location inside unit circle, is not straightforward. Increasing the control horizon does not necessarily result in improved control performance or eigenvalues moving closer to the centre of the circle. Simulation results show that a longer control horizon led to smaller input voltages applied, resulting in insufficient force to control the airgap.

However, when increasing Q to $\mathrm{diag}([10^6, 10^6, 10^6])$ this effect is no longer observed. With such a low relative penalty on the inputs, increasing the horizon allows the controller to apply the higher control input values that are needed for stabilization. This occurs because the contribution of the input penalty to the objective function remains relatively small, even though the number of penalized control terms increases with a longer control horizon. This effect becomes apparent when plotting the dominant eigenvalues of the system. Figure 4.5 shows the location of the complex conjugate eigenvalue pair for different N_c, while the dominant right-half-plane eigenvalue does not move much and is therefore shown as a single cross. The figure shows that the eigenvalues initially move towards the origin, resulting in more stable system dynamics. But from a certain horizon value it moves to another location in the complex plane, after which their position no longer changes. This behaviour is consistent with the findings of Garriga et al. (2010).

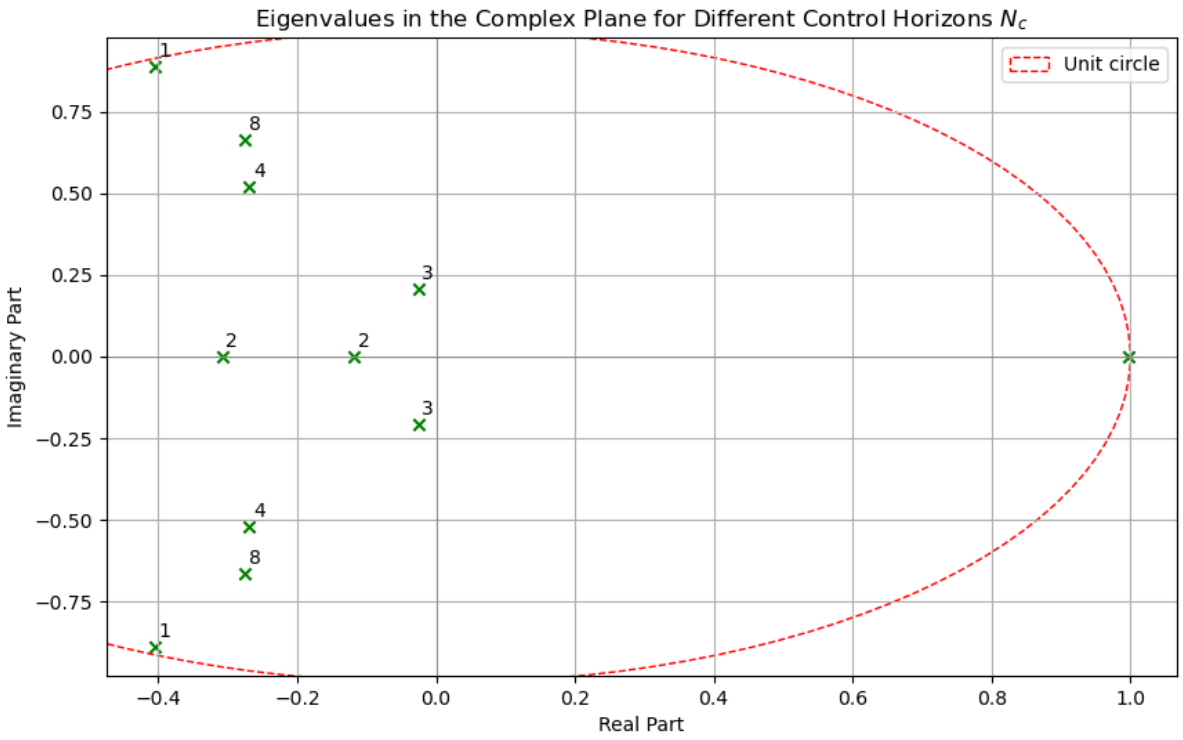

Figure 4.5 Eigenvalues in the complex plane for different control horizons N_c ($Q = diag([10^6, 10^6, 10^6])$, $R = 1$, $N_p = 300$).

Further increasing the control horizon gives eigenvalue at almost same location as $N_c = 8$, and is not reported in figure 4.5 for clarity. Increasing Q or reducing R further leads to the same effect on the eigenvalues.

This non-monotonic relation is reflected when evaluating the performance of this configuration using the infinite horizon cost as formulated in Eq. (4.21) as performance indicator. Although the infinite-horizon cost of this system can be computed exactly, it is here approximated by evaluating the cost over a sufficiently long finite time to ensure convergence to a steady-state.

$$J_{\mathrm{IH}}(x, u_\infty) = \sum_{k=0}^{\infty} x(k)Qx(k) + u(k)Ru(k) \tag{4.21}$$

The counterintuitive behaviour found is also observed in a study by Di Palma and Magni (2006), where it occurs in an unstable and unconstrained linear system. This shows that increasing control horizon does not always lead to improved closed-loop performance.

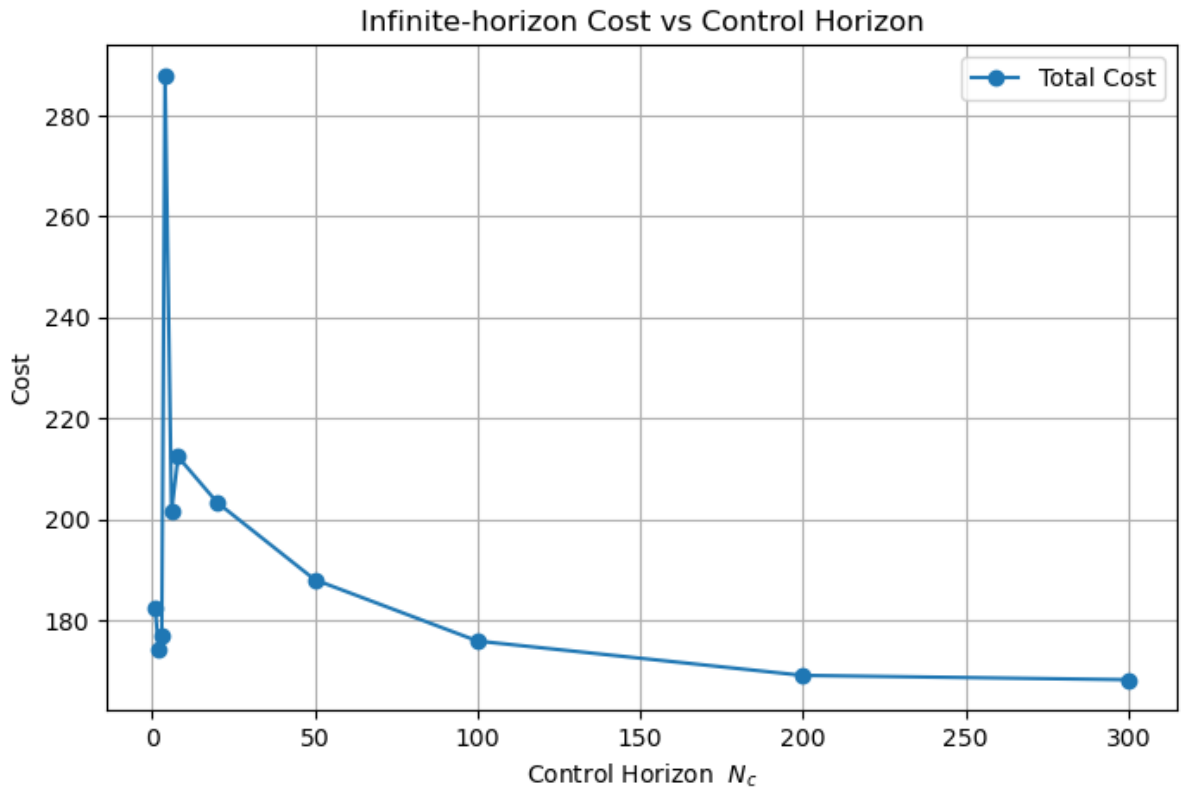

Figure 4.6 Infinite-horizon MPC cost against control horizon lengths ($Q = diag([10^6, 10^6, 10^6])$, $R = 1$, $N_p = 300$).

Penalty terms

The weighting factors Q and R define the relative importance of different control objectives and have no unit. The positive definite weighting matrices factors Q and R are determined based on process requirements. There are no guidelines related to the plant like for horizons, as the factors are influenced by scaling of the different states. By tuning these parameters, the emphasis can put on tracking performance or on input effort. By increasing the Q, the reference tracking error is penalized higher. The figure below depicts an expected influence of the weight Q. When increasing the diagonal values of the state weighting matrix Q, the eigenvalues move towards the origin and thereby the closed-loop system becomes 'more stable'. Each cross is labelled with the corresponding diagonal entry of the matrix Q.

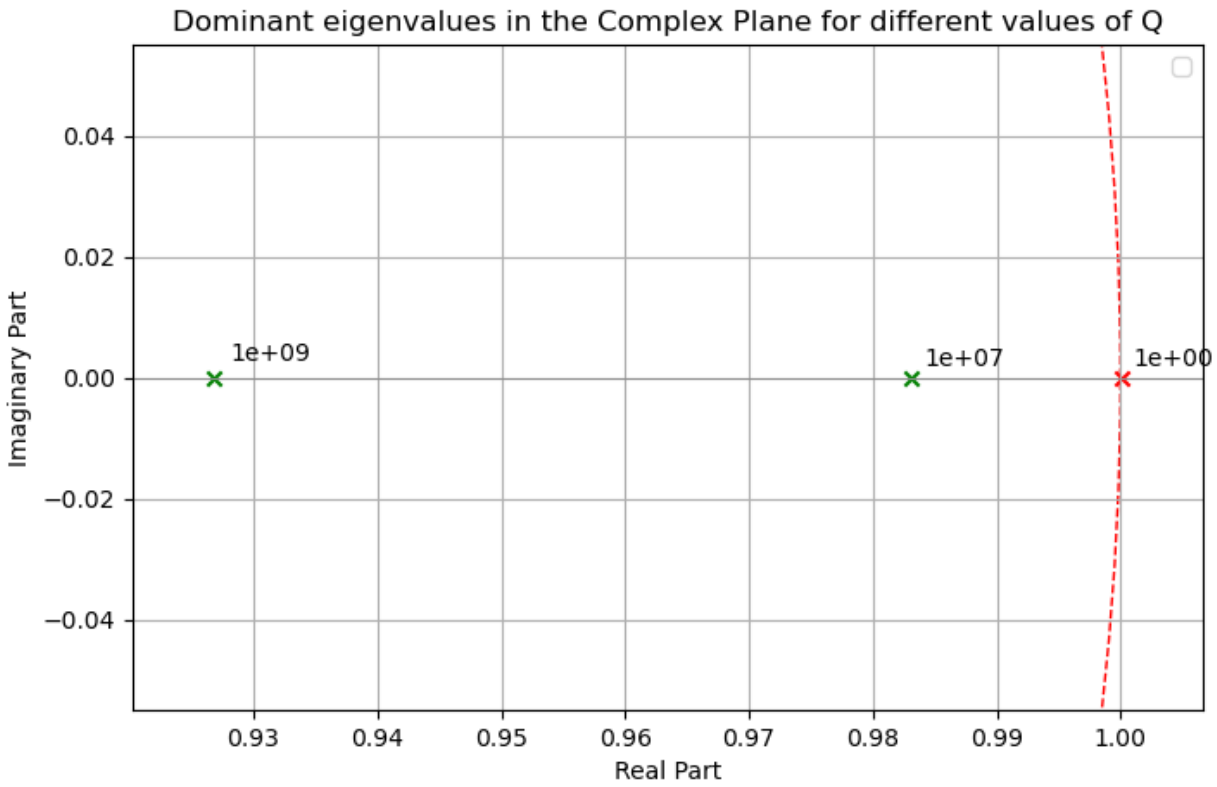

Figure 4.7: Effect of increase of penalty Q on the dominant eigenvalue for N_c=N_p=200 and R = 1

Validation of the eigenvalue analysis

Here, the combined effect of the horizon length and state weighting matrix are presented. Figure 4.8 shows stability based on the closed-loop eigenvalues for the linearised 1.5-DOF system. The Q-value varies and is applied to the diagonal entries of the state weighting matrix, the input penalty factor R is set to 1, and the prediction horizon is varied, while the control horizon is set equal to 1. For low diagonal values of Q, the system remains unstable for all horizon lengths, indicating insufficient penalisation of state penalty. As Q increases, stability becomes dependent on the prediction horizon. For large Q around 10^6, the system is stable across nearly the entire range of horizons.

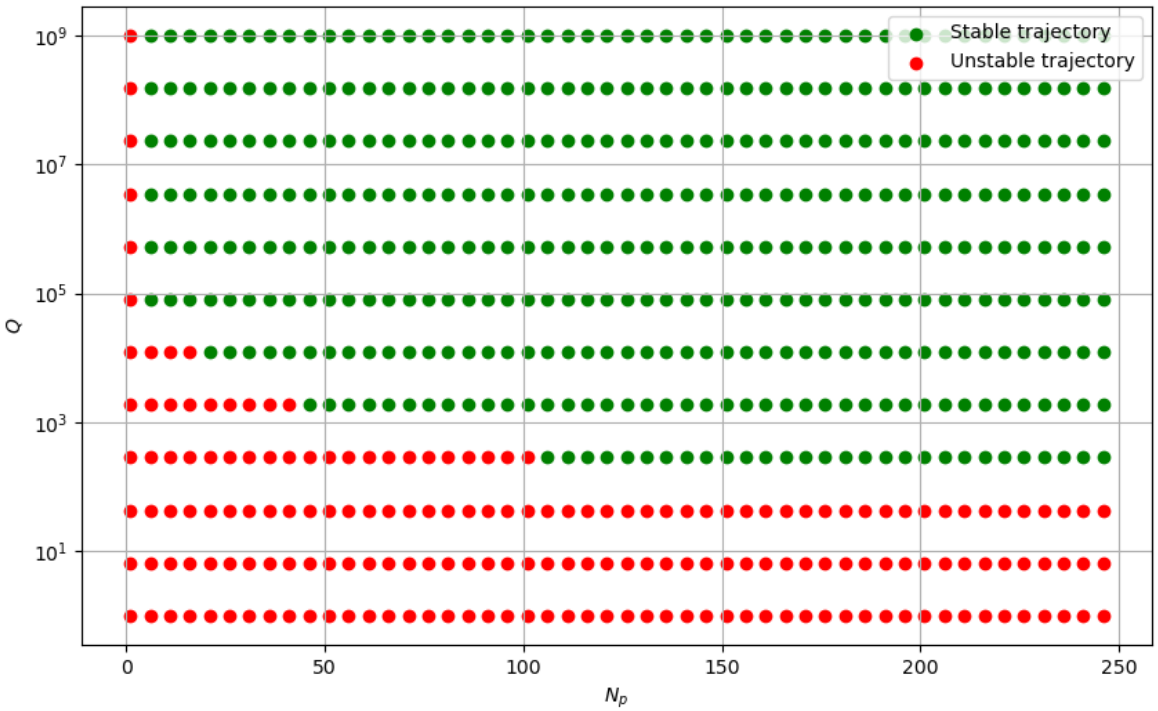

Figure 4.8: Closed-loop stability map for varying control parameters Q and prediction horizon N_p, control horizon N_c taken equal to 1.

To assess the validity of the stability statements made based on the eigenvalues of the linearized system, a comparative analysis is performed using nonlinear closed-loop simulations. For different combinations of parameter values, it was evaluated whether the nonlinear simulations exhibited the (un)stable trajectory the figures above suggest. In that analysis, large discrepancies were observed between the linear and on nonlinear MPC simulations. The stability should therefore be verified through nonlinear closed-loop simulations, even when giving a very small perturbation from the equilibrium.

In contrast, such behaviour is not observed when using a PD-controller. In that case, the trajectories of the linear and nonlinear responses remain show similar behaviour when the system operates close to the equilibrium point. A possible explanation may be the fact that MPC relies on model-based predictions to derive the control law, making it more sensitive to linearisation errors.

4.1.2 Results

The MPC problem is solved based on the linearized model, determining the control input by using the linearized system dynamics as a simplified representation of the original nonlinear system. The control input from this linearized MPC was then applied to the actual nonlinear system. This approach allowed the application of a linear control law for the nonlinear system, but it resulted in very poor performance. The controller was unable to stabilize the linearized system for initial conditions near the equilibrium, even for small perturbations.

Even when applying sequential linear MPC, whereby at every new state the system is linearized around the current operating state, the controller fails to achieve stabilization. The limited controllability is likely due to the inherent instability of the system and its strongly nonlinear dynamic. A more accurate model is needed to capture the nonlinear behaviour.

4.2 LQR

When the prediction horizon in the objective function approaches infinity and no constraints are imposed, the resulting controller corresponds to a linear quadratic regulator (LQR). LQR belongs to the family of optimal control problems. Similar to the linear MPC case discussed in the previous section, the LQR control input is derived from the linearized system dynamics, and the resulting control input is applied to the nonlinear system. The term quadratic refers to the structure of the cost function, which penalizes both the system states and the control inputs through quadratic weighting. The objective in this study is to track the desired reference by minimizing that cost function, resulting in an optimal control law that guarantees stability for the nominal linear system.

When dealing with a linear time-invariant (LTI) system and constant weight matrices, the control law for an infinite-horizon system becomes constant. This control law is based on the linearized system derived in the previous section is used for the controller design and can then be applied to the nonlinear system. The finite horizon discrete LQR feedback control law is given by:

$$u(k) = K_\infty x(k) \text{ with } K_\infty = -(B^T P_\infty B + R)^{-1} B^T P_\infty A \tag{4.22}$$

To implement LQR, all states of the system must be measurable, and the model of the plant should accurately describe the real system.

Here, P is the solution of the discrete algebraic Riccati equation:

$$P_\infty = A^T P_\infty A + A^T P_\infty B K_\infty + Q \tag{4.23}$$

The parameters used for the LQR controller are chosen as:

$$Q = \begin{bmatrix} 1 \cdot 10^{12} & 0 & 0 \\ 0 & 1 \cdot 10^{7} & 0 \\ 0 & 0 & 1 \cdot 10^{4} \end{bmatrix}, R = [0.0001], T_s = 0.0001\ s \tag{4.24}$$

Using these matrices, the discrete algebraic Riccati equation was solved using a Python package, resulting in the following solution for the matrix P:

$$P = \begin{bmatrix} 4.51 \cdot 10^{12} & 2.90 \cdot 10^{9} & -1.28 \cdot 10^{8} \\ 2.90 \cdot 10^{9} & 1.57 \cdot 10^{7} & -3.62 \cdot 10^{5} \\ -1.28 \cdot 10^{8} & -3.62 \cdot 10^{5} & 3.90 \cdot 10^{4} \end{bmatrix} \tag{4.25}$$

While the chosen R value may appear negligible, setting $R = 0$ resulted in a noticeable increase in control effort, which cannot be neglected. Conversely, increasing R to 0.1 or decreasing Q led to instability. Considerable effort was required for tuning Q and T_s, as stable trajectories were obtained for only a limited set of parameter values.

Results

A simulation was conducted to evaluate the behaviour of this type of linear controller. A small perturbation was applied to the airgap, the input obtained is applied to the actual nonlinear system dynamics and its response is shown in figure 4.9 below. A minor initial overshoot and oscillations are observed. However, the system converges relatively quickly towards the desired reference by using a relatively large control effort.

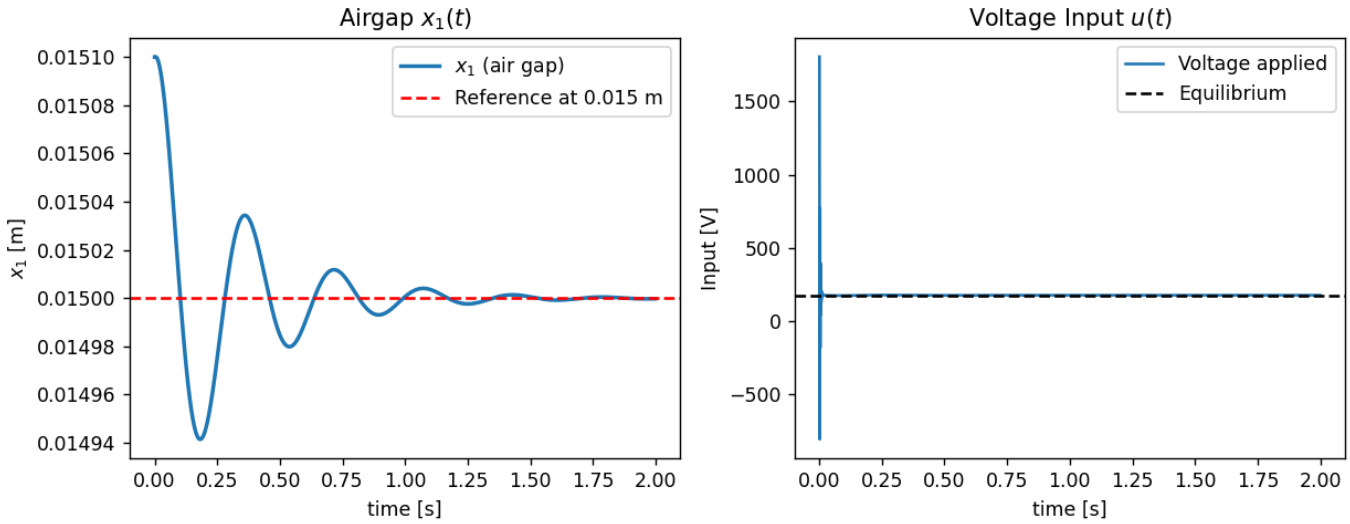

Figure 4.9 LQR controller trajectories of the vehicle position and control input following from Eq. (4.22)

The effect of sampling on the performance is shown in figure 4.10. The improved faster convergence, caused by increasing sampling frequency, might sound logic as you will respond earlier to fast changing dynamics. However, there is no guarantee that this will always be the case as shown in Bachtiar et al. (2015).

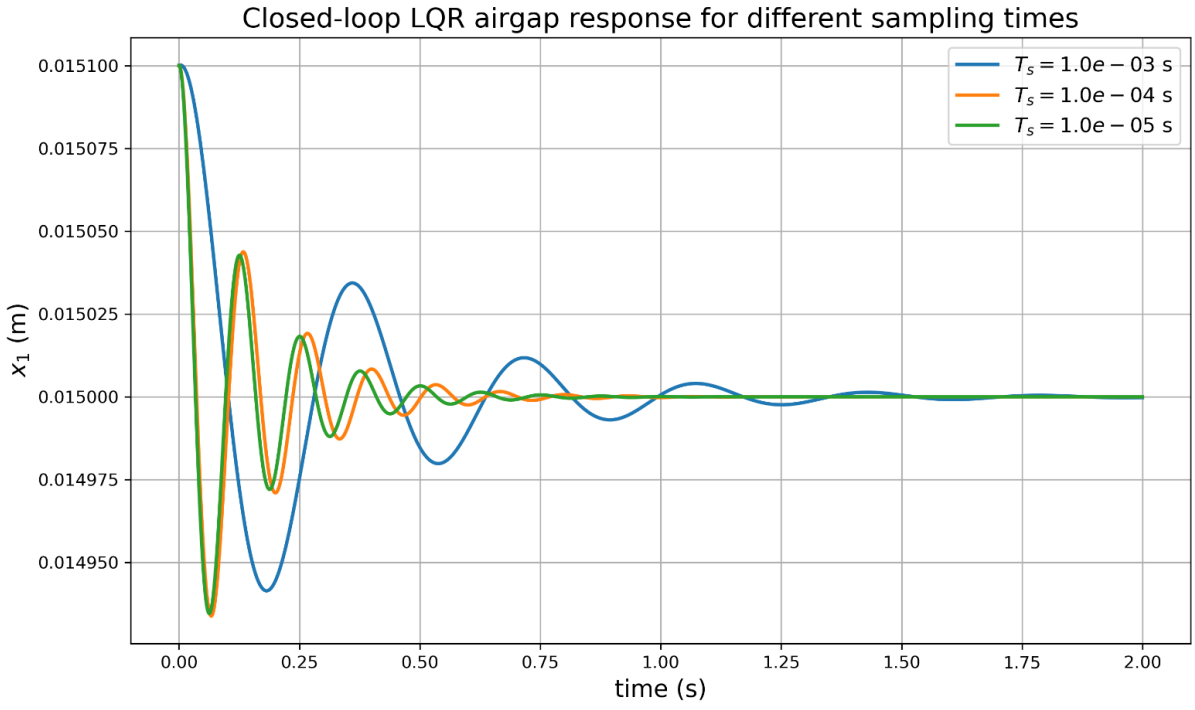

Figure 4.10 Effect of sampling time on the closed-loop airgap response of LQR controller, using the parameters presented in Eq. (4.24.)

Stability plot:
To evaluate and validate the performance of a controller, its region of attraction (ROA) is computed. The ROA of a system is a set of states for which a trajectory starting within that set will converge to the equilibrium value. In literature, several methods have been proposed to estimate that region. In this work, the performance of LQR control is investigated through simulations. The stability region is determined by computing trajectories over a grid of initial conditions. Perturbations were imposed to the initial vehicle position (x_1) and velocity (x_2) while x_3 is maintained at its equilibrium. The considered state region is representative of disturbance that may occur when operating a hyperloop. Perturbations occur whenever the net vertical force is unbalanced, which can happen because of passenger weight change. For each initial condition, stability is considered achieved if the final value at the end of the simulation time remains within a small threshold of the setpoint. Even though this method is computationally demanding, the techniques here is employed because of its simplicity for lower order systems.

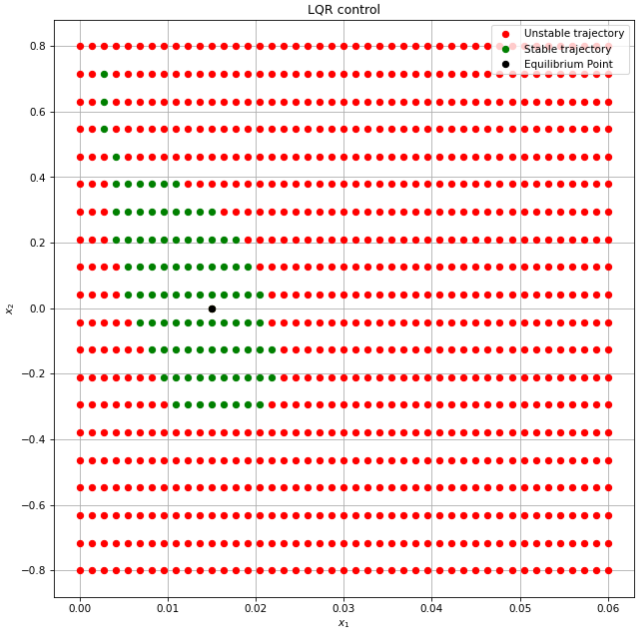

Figure 4.11 Region of attraction for a LQR controller.

The results indicate that the LQR controller stabilizes the nonlinear system, but only within a limited region around the equilibrium, as shown in figure 4.11. When the initial condition is outside the stable region (in green), the controller can no longer compensate for the destabilizing effects.

4.3 Nonlinear MPC

The MPC controller used in the previous section was based on a linearized prediction model around the target airgap. However, using a linear model is an inadequate representation of the vehicle dynamics when operating farther away from equilibrium. In order to meet the tight performance requirements of the levitation control of the hyperloop, a more accurate description of the system dynamics might be needed. This appeals the need for a nonlinear model predictive control (NMPC), which incorporates the highly nonlinear dynamics of the levitation system (Findeisen & Allgöwer, 2002) into the prediction model. NMPC is expected to result in improved performance compared to linear controllers. However, applying a nonlinear controller makes the analysis less tractable, since the nonlinear MPC applied to both the simplified model and the vehicle-guideway model does not have an explicit control law. Hence, an analytical study of how the control law affects the instability boundaries cannot be performed as was done for the PD and linear MPC analysis.

Formulation of NMPC:

The prediction model is written in a discretised form using the Euler forward discretisation method, enabling the use of available solvers (Zietkiewicz & Owczarkowski, 2017). A numerical study of different integration schemes shows that both the implicit Runge-Kutta integration and the Euler forward scheme are both suitable as can be seen from figure 4.12. A difference is observed between the methods. Over a wide range of time steps, both the Euler forward method and the RK4 method produce nearly identical trajectories. The RK4 method demonstrates slightly better tracking performance by reducing overshoot and undershoot.

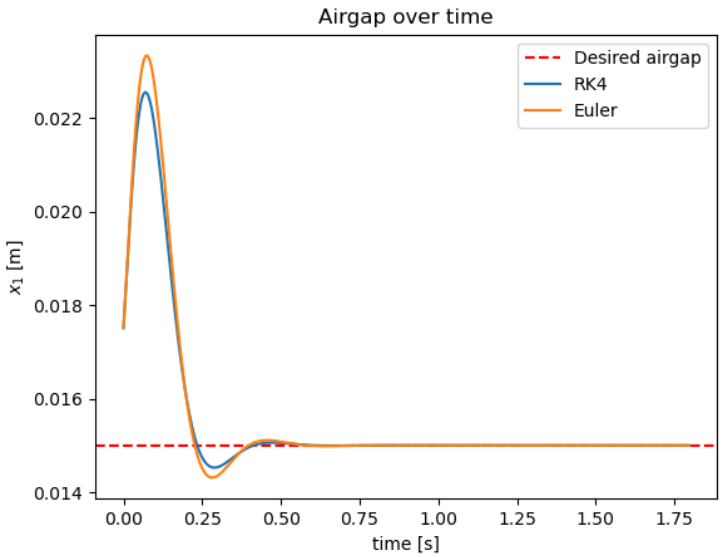

Figure 4.11 Simulation of NMPC for two numerical time integration methods

The prediction model using forward Euler is expressed as follows:

$$\begin{cases} x_{1,k+1} = x_{1,k} + T_s \cdot x_{2,k}, \\ x_{2,k+1} = x_{2,k} + T_s \cdot \left(g - \dfrac{C x_{3,k}^2}{m {x_{1,k}}^2} \right), \\ x_{3,k+1} = x_{3,k} + T_s \cdot \left(\dfrac{x_{2,k} x_{3,k}}{x_{1,k}} - \dfrac{R x_{3,k}}{2C} + \dfrac{x_{1,k}}{2C} u_k \right). \end{cases} \tag{4.26}$$

The prediction model above gives the predicted states for every time instant over a horizon of length N. here the prediction horizon and control horizon are set equal ($N_p = N_c$). The optimization to be solved is then formulated as:

$$J = \sum_{k=0}^{N} \left(x_{k+1} - x_{ref}\right)^T Q\left(x_{k+1} - x_{ref}\right) + \sum_{k=0}^{N-1} \left(u_k - u_{ref}\right)^T R\left(u_k - u_{ref}\right) \quad (4.27)$$
$$u_{min} \leq u_{k+i} \leq u_{max} \;\; \forall\, k = 0, 1 \ldots . N-1.$$

Here Q and R are factors penalizing the tracking error and control effort respectively. The objective is for the predicted states to follow the desired trajectory, while satisfying the lower and upper limit of the voltage input. The term x_{k+1} represents the vector of predicted values at time k. The optimizer calculates the optimal control over a horizon of length N. As is evident from the equations above, the system dynamics are now nonlinear, making the NMPC optimization a non-convex problem (Cannon, 2004).
When solving a nonconvex problem, one encounters difficulties. Since multiple local minima exist, the solver may converge to suboptimal solutions. Secondly, the computation of the solution is much slower, while the MPC relies on solving the optimization problem online at every timestep. The computation time for a single optimization for the designed controller should satisfy the real time constraint to be suitable for fast systems (Van den Boom & De Schutter, 2018).

This new type of problem demands a more advanced type of optimization method than was needed for convex QP problems in linear MPC. The two most used methods for addressing these types of optimization problems are interior-point (IP) and sequential quadratic programming (SQP). SQP is considered as the most efficient method for solving constrained nonlinear optimization problems in literature and remains widely used today, appearing in various variants across recent research (Quirynen & Di Cairano, 2021). Furthermore, the application of a SQP algorithm has appeared to be a popular method for solving NMPC problems (Zietkiewicz & Owczarkowski, 2017; Mayne, 2014). Therefore, the SQP method is chosen as technique in this study to address the inequality constrained optimization problem in Eq. (4.27).

SQP method
SQP is a Newton-based optimization method that uses a second-order Taylor approximation and is applicable for constrained optimization problems.
This method transforms the original NLP problem into a sequence of simpler linearly constrained QP subproblems (Cannon, 2004).
This method will be described and explained in this paragraph (Van den Boom & De Schutter, 2018).
Solve an algebraic equation to get the optimal control sequence.

The optimization problem is defined in standard form: minimizing the objective function *f*, subject to the nonlinear inequality constraint *g*.
$$\min_x f(x) \text{ subject to } \; g(x) \leq 0 \quad (4.28)$$

In our specific problem, the decision variable is the input: $x = [u]^T = [u_0, \ldots, u_{N-1}]^T$.

The Lagrange function is introduced, enabling handling of constraints in the cost function:
$$\mathcal{L}(x, \lambda) = f(x) + \lambda g(x) \quad (4.29)$$
, where λ is a Lagrange multiplier associated to the inequality constraint.

The Lagrangian in Eq. (4.29) is approximated by a second-order Taylor expansion, following the Newton-based method applied:
$$L(x, \lambda) \approx L(x_k, \lambda) + \nabla_x^T L(x_k, \lambda)(x - x_k) + \frac{1}{2}(x - x_k)^T H_L(x_k, \lambda)(x - x_k) \quad (4.30)$$

The inequality constraint is then linearized:
$$g(x) \approx g(x_i) + \nabla^T g(x_i)(x - x_i). \quad (4.31)$$

Computation of the Hessian H_L, describing the curvature of the Lagrangian with respect to the decision variable, is computational expensive. Therefore, the optimization algorithm employs a quasi-Newton, approximating the Hessian. Where $\hat{H}_k$ is the approximation of the Hessian, updated at every iteration.

The original problem is now approximated by a quadratic programming (QP) subproblem:

$$\begin{aligned} &\min_d \frac{1}{2} d^T \hat{H}_i d + \nabla^T f(x_i) d, \\ &\text{subject to } g(x_i) + \nabla^T g(x_i) d \leqslant 0. \end{aligned} \tag{4.32}$$

The subproblem solves the search direction d_k ($d_k = x - x_k$). Consequently, a line search method is applied to determine an appropriate step size along the direction d_k, ensuring convergence to a local optimum regardless of the chosen starting point.

$$s_i = \arg\min_s \psi(x_i + s d_i) \tag{4.33}$$

Where ψ is a merit function, combining the objective function and the constraints.
Subsequently, the kth estimate can be generated:

$$x_{i+1} = x_i + s_i d_i \tag{4.34}$$

This procedure will be repeated until convergence towards the optimal value x^0, which satisfies the optimality conditions shown below. If convergence is not achieved, the process is repeated, starting with the calculation of the Lagrangian at the latest estimation of x_{i+1} (Van den Boom & De Schutter, 2018).

The necessary optimality conditions that any solution of the optimization problem of Eq. (4.28) should satisfy are given by the Karush-Kuhn-Tucker (KKT) condition:

$$\begin{aligned} \nabla f(x) + \nabla g(x) \lambda = 0, \\ \lambda^\top g(x) = 0, \\ \lambda \geq 0, \\ g(x) \leq 0. \end{aligned} \tag{4.35}$$

In short, the goal is to find the optimal solution of the original nonlinear problem satisfying the KKT conditions, by iteratively solving a simpler quadratic problem. That gives a search direction and together with the step size obtained from the line search, the estimate x_{i+1} will be iteratively updated until convergence to the optimal solution x^0.

The Sequential Least SQuares Programming (SLSQP) method from the SciPy.optimize module (Joshy & Hwang, 2024) in Python is used to solve this type of optimisation problem. SLSQP is generally well suited for problems up to hundred decision variables and having a relatively coarse discretisation. A number of alternative SQP-solvers have been developed since then. These solvers include both algorithmic advances and new functionalities (Joshy & Hwang, 2024). Nevertheless, SLSQP from SciPy is chosen here because it is easy to apply.

This solver requires the definition of a cost function as an input argument, along with an initial guess for the decision variables. Additionally, relevant problem parameters can be passed via an optional argument tuple. If needed, constraints on the optimisation variables can be specified. The function returns several useful attributes, such as the final value of the cost function, details about the optimisation process, and most importantly, the optimised array of control inputs.

SLSQP is a particular variant of the SQP, that employs a least-squares formulation instead of a QP subproblem. This algorithm formulates the problem as a least square one, by LDL^T factorizing the Hessian matrix.
The optimization problem is solved in the following form (Kraft, 1988):

$$\min_{d \in R^n} \left\| \left(D^k\right)^{\frac{1}{2}} \left(L^k\right)^T d + \left(D^k\right)^{-\frac{1}{2}} \left(L^k\right)^{-1} \nabla f\left(x^k\right) \right\|_2, \tag{4.36}$$

subject to constraints:

$$\nabla g(x^k)d + g_j(x^k) = 0. \tag{4.37}$$

The iterative SQP approach requires an initial guess, the concept of warm starting is applied in order to accelerate convergence. Since consecutive problems are similar, the solution to these problems will be similar as well. By assuming the solution of the previous optimization problem as the initial guess for the current time instance, the algorithm will start search more closely to the optimal solution (Cannon, 2004). In expressions: if the optimal control calculated at time t is (Gros et al., 2016): $u_t^0 = [u_{t,0}^0, u_{t,1}^0, \dots, u_{t,N-1}^0]$. Then the initial guess at time step $t+1$ is given by:

$$u_{t+1}^{\text{guess}} = [u_{t,1}^0, u_{t,2}^0, \dots, u_{t,N-1}^0, u_{t,N-1}^0]. \tag{4.38}$$

This warm-starting initial guess resulted in a reduction of around 50% in computation time and, in some scenarios, improved stability compared to a poor initial guess.

The applied solver is a local optimizer. The choice of initial value can lead the iterations towards different local optima. Providing equilibrium values as the initial guess at the first step and applying warm-starting from equation Eq. (4.38) appears to give sufficiently good results and is therefore used.

The algorithm described below provides a structured description of the method applied for the NMPC of the 1.5-DOF system.

Algorithm 4.1: *NMPC using SQP for reference tracking.*
Input: Initial condition $\boldsymbol{x}_k$
Output: Control input u_k

Initialize: *controller parameters*
for each time step t:

1. Obtain new state (new “measurements”) and store it
2. Solve optimization problem, using SLSQP, gives $\boldsymbol{u}_t^0$
3. Apply just first input $u_{t,0}^0$ to the nonlinear system
4. Shift initial guess

Note that in this section the discrete-time index k refers to the MPC time step, and index i denotes the SQP iteration number within the solver.

Closed-loop simulation results
The SLSQP-method is verified by performing an unconstrained linear MPC simulation using the known analytical solution for the control input given in Eq. (4.19). The simulation is then repeated under the same parameters, but with the control inputs resulting from the numerical SLSQP method. The resulting states and input trajectories from both methods match exactly, validating the implementation of the SLSQP solver.

This section illustrates the effect of different MPC parameters on the nonlinear response. The ranges of tuneable parameter values that ensure the closed-loop system is asymptotically stable is small.

The effect of the control horizon on the closed-loop performance is depicted in figure 4.13, an unexpected effect of the horizon length N on stability is observed from that figure. This counterintuitive behaviour of the controller is also reported by Bachtiar et al. (2015). Although that paper considers a constrained and linear system.

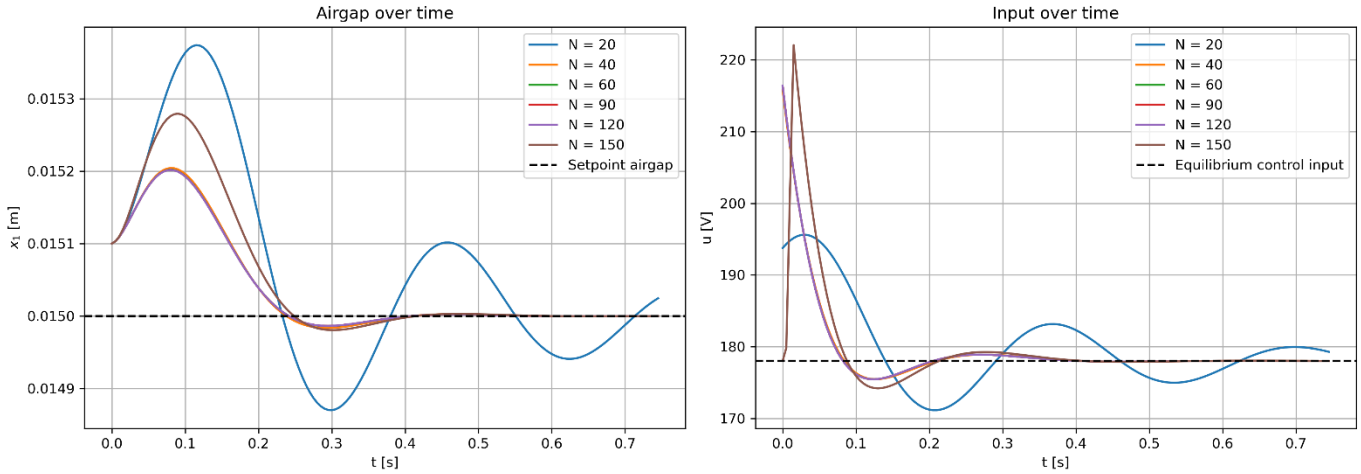

Figure 4.13 Effect of the horizon length on the closed-loop trajectory for NMPC with a fixed Q, R and T_s (N_p=N_c).

When the horizon length N is smaller than the 'optimal' horizon length, the closed-loop simulation results in a large reference tracking error or even causes divergence as one may expect. However, when increasing the horizon length further, the control performance deteriorates, as illustrated in the figure above. This happens from H =150 onward, as the input takes unrealistic values, which causes a larger tracking error.

One could argue that lower horizon has less performance because of less decision freedom. But the larger horizon doesn't find an optimum because of complex shape of the cost function.
To better understand the behaviour, the message returned by the optimizer was inspected to find the cause of this counterintuitive behaviour. Since the solver did not report that a successful termination was reached, this indicates that it did not converge to a global or local minimum. The SciPy solver provides limited information on the optimization process. At least what can be derived is the large Jacobian values, meaning that the change in input has a large influence on cost the optimization makes some jumps in optimization surface. These observations suggest that the solver struggles to converge due to numerical issues, such as ill-conditioning of the problem, resulting in abrupt jumps across the cost surface. When the initial guess is improved for this configuration by using the closed-loop optimal input obtained from a shorter horizon, the performance improves and the solution follows the same trajectory as the well-performing cases.

The weighting factor Q shows similar behaviour, as shown in the figure 4.14. Increasing Q initially improves performance, but beyond a certain value it introduces similar numerical issues as discussed in the previous paragraph. The figure presents the airgap trajectories given different diagonal matrices with same diagonal values, and a configuration in which only electrical current x_3 is penalized. The results indicate that applying a penalty to that variable has the most influence on the system's behaviour.

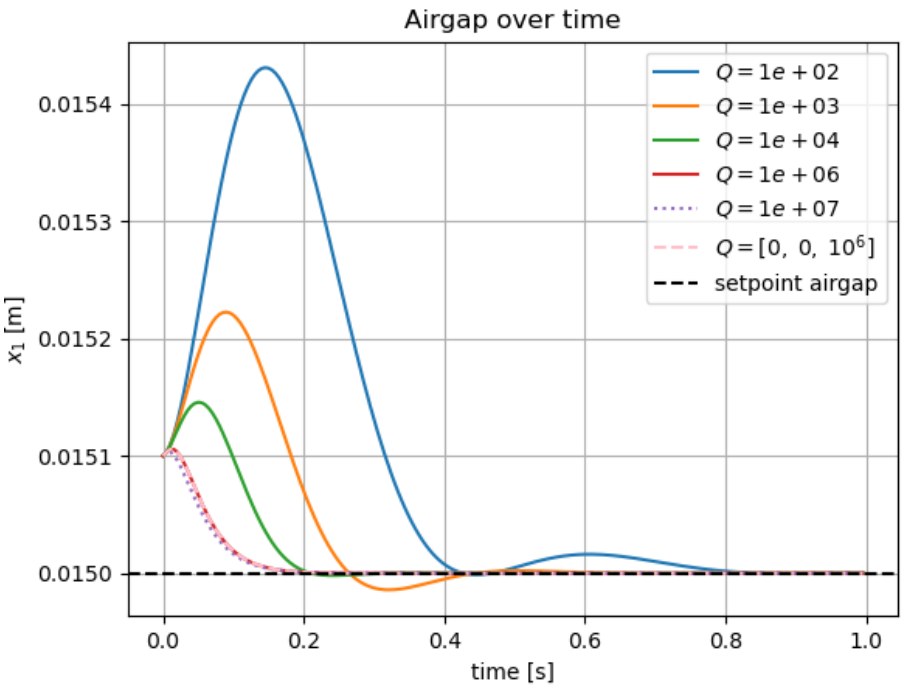

Figure 4.14 Airgap over time for different state weighting matrices Q.

After tuning the controller and considering robustness under larger deviations, the parameters were set to be:

$$Q = \begin{bmatrix} 1 \cdot 10^9 & 0 & 0 \\ 0 & 1 \cdot 10^3 & 0 \\ 0 & 0 & 1 \cdot 10^3 \end{bmatrix}, R = [1], N = 40, T_s = \ 0.005\ s \tag{4.40}$$

Figure 4.15 depicts the achieved stabilization under the initial condition: $[x_1, x_2, x_3] = \ [\delta_0 + 10^{-4}, 0, I_0]$ for the designed controller. The applied controller stabilizes the system. The overshoot is small and can be considered as acceptable, while the system fast settles towards the setpoint.

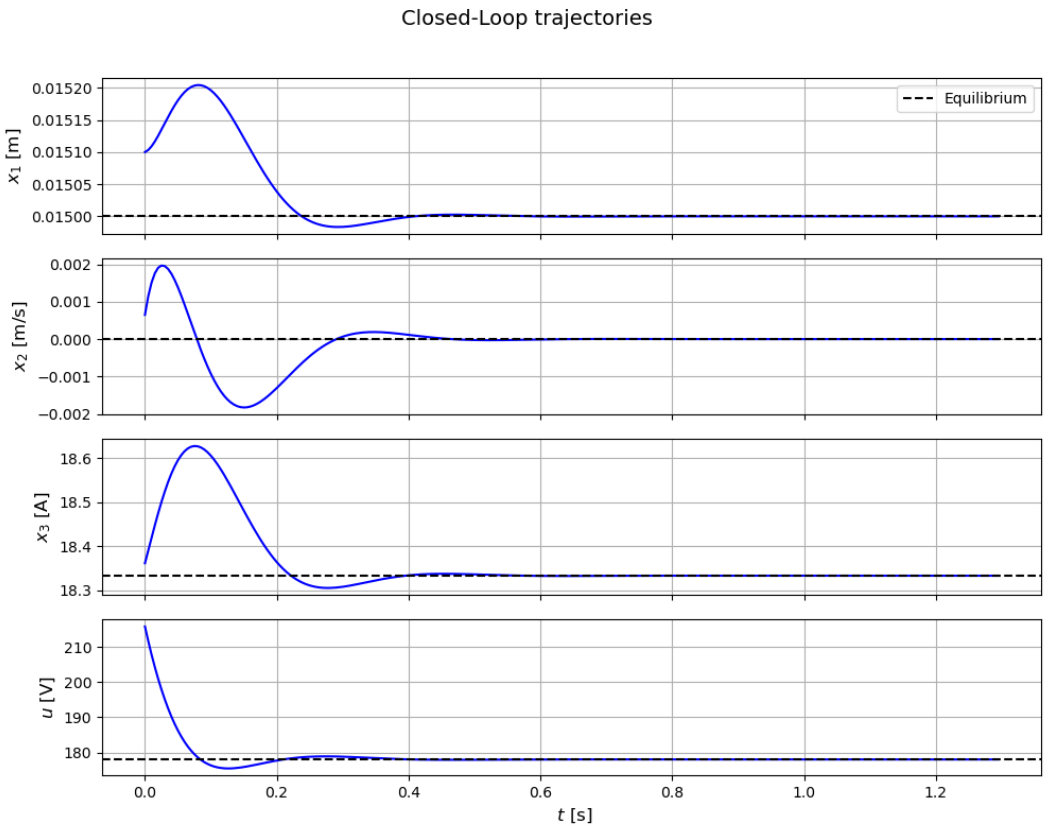

Figure 4.15 Closed-loop NMPC trajectories for the different states and input.

Sensitivity analysis:
This section investigates the performance of NMPC across different initial conditions, as was done for LQR in section 4.2. Since standard stability analyses are not applicable to optimization problems subject to constraints, alternative techniques were applied (Schwenzer et al., 2021).

Consider first an unconstrained NMPC controller. The region of attraction is not a single area but appears scattered. There is a large region of attraction around equilibrium point (indicated by a green dot). But there are also some initial conditions leading to unstable trajectories when the vehicle (x_1) is close to the guideway and moves with downwards or upwards velocity.

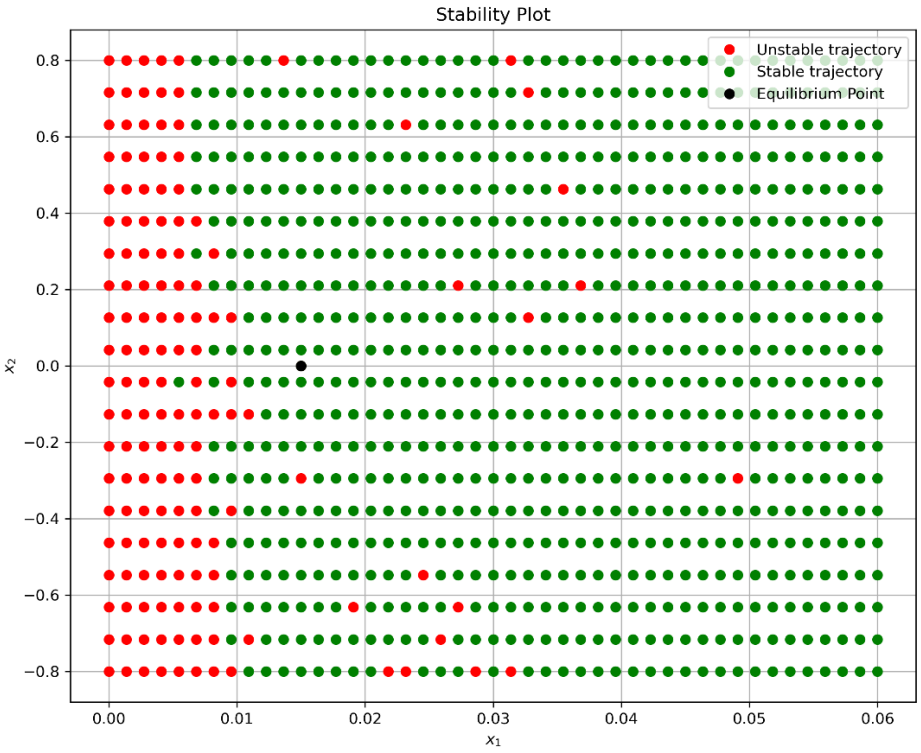

Figure 4.16 Stability plot for an unconstrained NMPC

In figure 4.17, a stability plot is presented for a constrained NMPC controller with a realistic input range of -2000 V to 2000 V. The observed asymmetry with respect to the velocity state x_2 can be explained by the direction of motion of the vehicle relative to the track. As shown, the controller loses stability in the upper right region of the plot, corresponding to large positive velocities, meaning the vehicle moves away from the track. This results in an attractive force that is too small to be compensated by any feasible voltage, thereby leading to divergence of the vehicle. In contrast, for the same initial vehicle position, a negative velocity of equal magnitude directed towards the track allows the controller to stabilise the system.

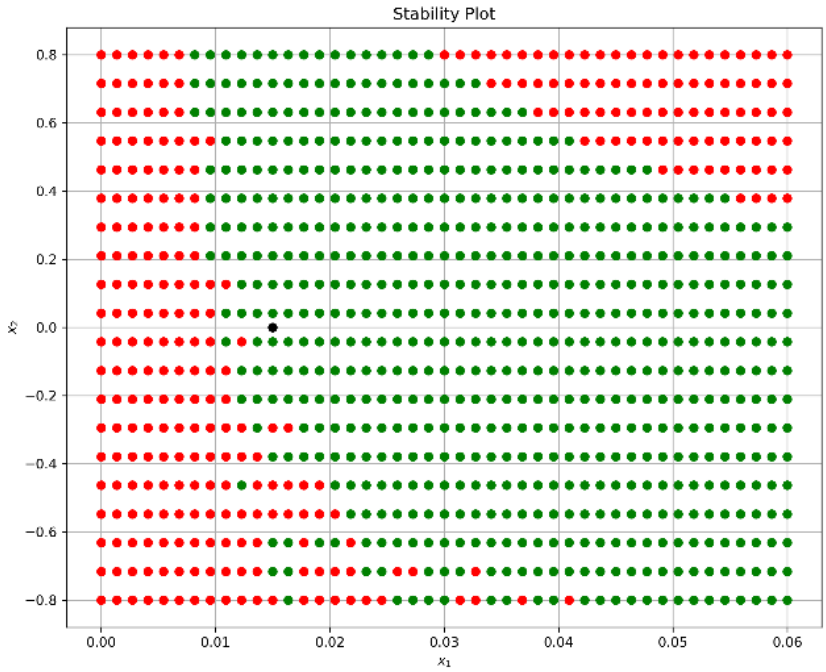

Figure 4.17 Stability plot for different scenarios, input limit: -2000 V <u <2000 V

In figure 4.18, a smaller input range from -400 V to 400 V is considered. The controller is unable to handle even small perturbations to the system, demonstrating that the limited input significantly restricts its ability to maintain stability.

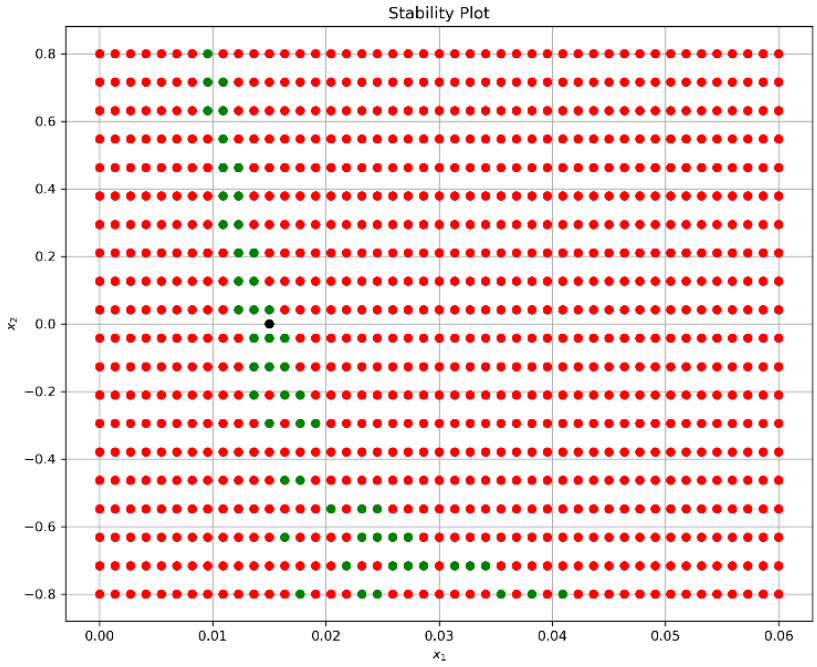

Figure 4.18 Stability plot for different deviations, input limit: -400 V <u <400 V

An unstable region can be observed from these stability figures that for small values of x_1, corresponding to initial vehicle positions close to the guideway (smaller than the equilibrium position). In this region, achieving stable levitation becomes infeasible. This is caused by the strongly nonlinear magnetic force on the vehicle being inversely proportional to the square of the airgap. As a result, the magnetic force increases rapidly as the vehicle approaches the guideway ($x_1 \to 0$). The control input cannot be adjusted sufficiently to reduce the current and thereby counteract the rapid increase in attraction force caused by the decreasing denominator. This complicates the stabilization of the system when the vehicle is closer to the track than the nominal levitation height, causing the vehicle to be pulled toward the guideway.

Despite the observed behaviour, the controller maintains stability over a large region of the state space. This demonstrates NMPC's ability of dealing with electromagnetic instability and simultaneously adhering to the imposed constraints.

4.4 PD

One of the most used controllers in engineering, and the basis on which this study builds, is the PID controller. PID control is often used because of its simplicity. Often this controller consists of three components: the proportional, integral and derivative term. Together, these terms influence the system's response characteristics.

In J. Mas Soldevilla (2022) stabilization was achieved using PD terms only. The integral component, which removes the steady-state error, was omitted to avoid complexity. The proportional gain K_p was found to affect both the location of the fixed points and how fast the system converges towards the equilibrium. The derivative term K_d defines the type of that fixed point and influences the change of the error, thereby damping out oscillations and reducing overshoot. This term is seen as a form of feedforward control. A drawback of this feedback mechanism is that constraints cannot be included explicitly. However, the controller parameters could be tuned to operate within the allowable input limits.

The control law for this application is formulated as:

$$u = K_p(x_1 - \delta_0) + K_d \frac{\partial(x_1 - \delta_0)}{\partial t} + u_0 = K_p(x_1 - \delta_0) + K_d x_2 + u_0 \tag{4.41}$$

The gains are manually tuned, trying to find the most optimal configuration in terms of stability and tracking performance. The gains are selected as: $K_p = 28\ kV/m$ and $K_d = 27\ kVs/m$.
A trade-off was observed between fast convergence (K_p) and error amplitude (K_d) (J. Mas Soldevilla, 2022). When aiming for a faster convergence, the K_p value has to be increased, however this causes an increase in overshoot. This can then be decreased by implementing a higher derivative term K_d, but at the same time this term slows down the response.

Figure 4.19 shows the state and input trajectory. The response exhibits no overshoot, but small oscillations are present as the vehicle moves towards the setpoint. The settling time is around 3s.

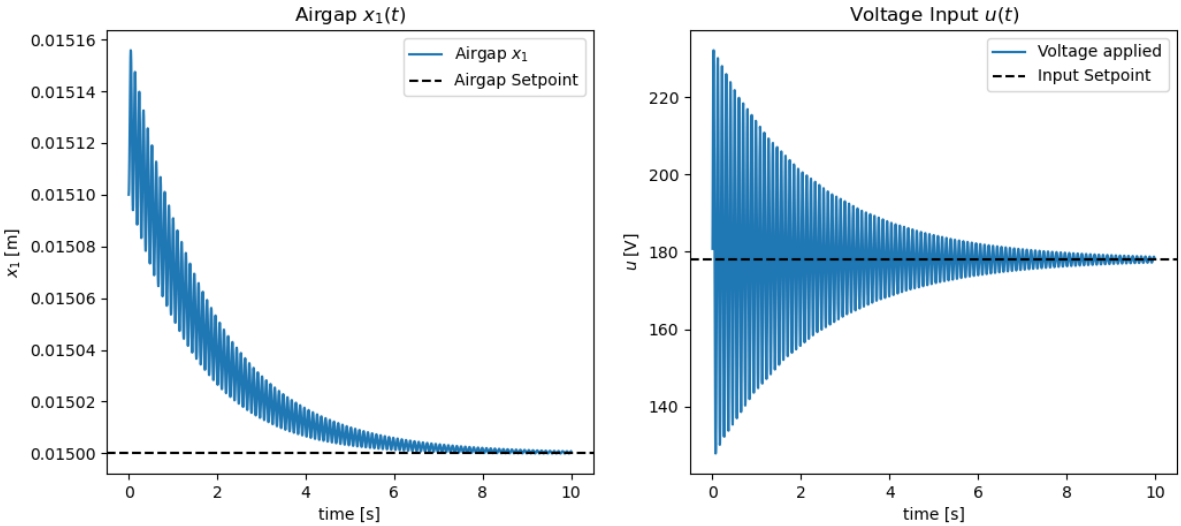

Figure 4.19 PD controller trajectories given a small initial perturbation on the airgap.

In both the MPC and PD closed-loop trajectories, an inverse transient response is observed, where the airgap initial increases before converging towards the desired reference. Such behaviour is often associated with a right-half-plane zero. However, after analysing the open and closed loop poles and zeros, there are no zeros found in that region. The observed behaviour is instead caused by explained by the inherent unstable poles few time steps, the control input u might not have fully taken effect, causing a temporary increase in the airgap as the control system is catching up to the unstable dynamics of the system. The initial magnetic force is insufficient to is to counteract the vehicle gravity, causing a temporary increase of the airgap before convergence.

By running simulations using the controller configuration given above and applying the control law defined in Eq. (4.41) to the nonlinear 1.5-DOF system, a stability plot is obtained, similar to that for the NMPC and LQR controller. The resulting region of attraction shows that the PD controller stabilizes the system in a convex region as is clear from figure 4.20.

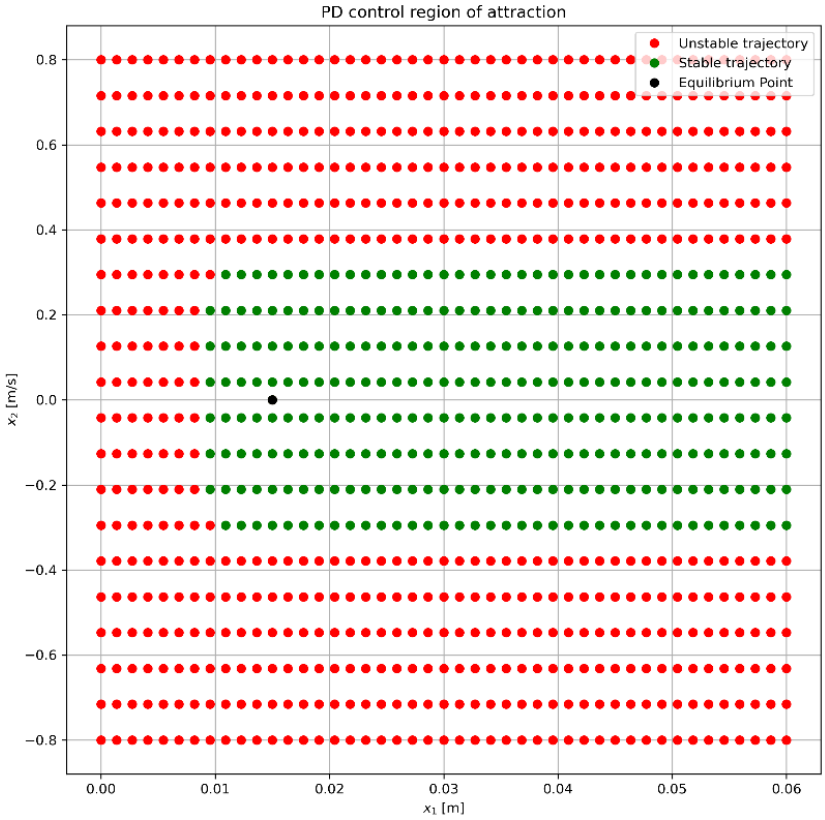

Figure 4.20 Region of attraction of a PD controller ($K_p = 28\ kV/m$ and $K_d = 27\ kVs/m$).

4.5 Comparative analysis

Comparing the effect of the MPC and PD control methods is somehow challenging since many tuning options are possible. To ensure a fair comparison, the sampling interval is kept equal, and an optimal tuning configuration for the goal of reference tracking is found for both the controllers. Only the airgap and voltage are considered in this analysis, while the other states are left out. This is justified because the other states are strongly coupled and show similar qualitative behaviour in closed-loop dynamics.

The different control strategies are first evaluated using quantitative performance criteria. Observations from previous results are then presented and compared to assess their relative performance.

Travel comfort
Official standards exist for the travel comfort, however in this study it is quantified by calculating the root-mean-square (RMS) value of the unfiltered accelerations in discrete time (Oppeneiger et al., 2024) .

$$\mathrm{RMS} = \sqrt{\frac{1}{N}\sum_{k=0}^{N_f}\left(\frac{x_{2,k+1} - x_{2,k+1}}{T_s}\right)^2} \tag{4.42}$$

The N_f denotes the number of steps considered in the calculation and is chosen equal to the number of steps needed to reach the settling time.

Control effort
The control trajectories all have a similar order of magnitude but differ in how they converge to the equilibrium. To capture this behaviour and highlight the obtained inputs, the following quadratic variation measure is used to quantify the control effort: (Oppeneiger et al., 2024)

$$\mathrm{Var}_2(u) = \sum_{k=0}^{N_f} (u_{k+1} - u_k)^2 \tag{4.43}$$

Results

	RMS [m/s²]	*quadratic variation [V²]*	*Computation time [s]*
NMPC	*0.0212*	*105*	*20*
PD	*0.0312*	*35500*	*1*

Table 4.1 Control performance metrics.

The acceleration RMS is higher for the PD controller, but these values remain within comfortable limits. Additionally, the control effort is much higher for PD, a too large quadratic variation in control input could potentially cause actuator problems.

This unconstrained optimization problem can be solved within a sufficiently small computation time. However, solving a nonconvex NMPC problem requires an iterative solver, which generally takes longer to solve. The nonlinear solver method used for NMPC resulted into a significantly bigger computation time, as can de be seen in table 4.1.

Figure 4.21 shows a comparison of the airgap response obtained using the PD and NMPC controllers. Both responses are evaluated under the same perturbation and with optimally tuned controller parameters, allowing a consistent comparison of their dynamic behaviour.

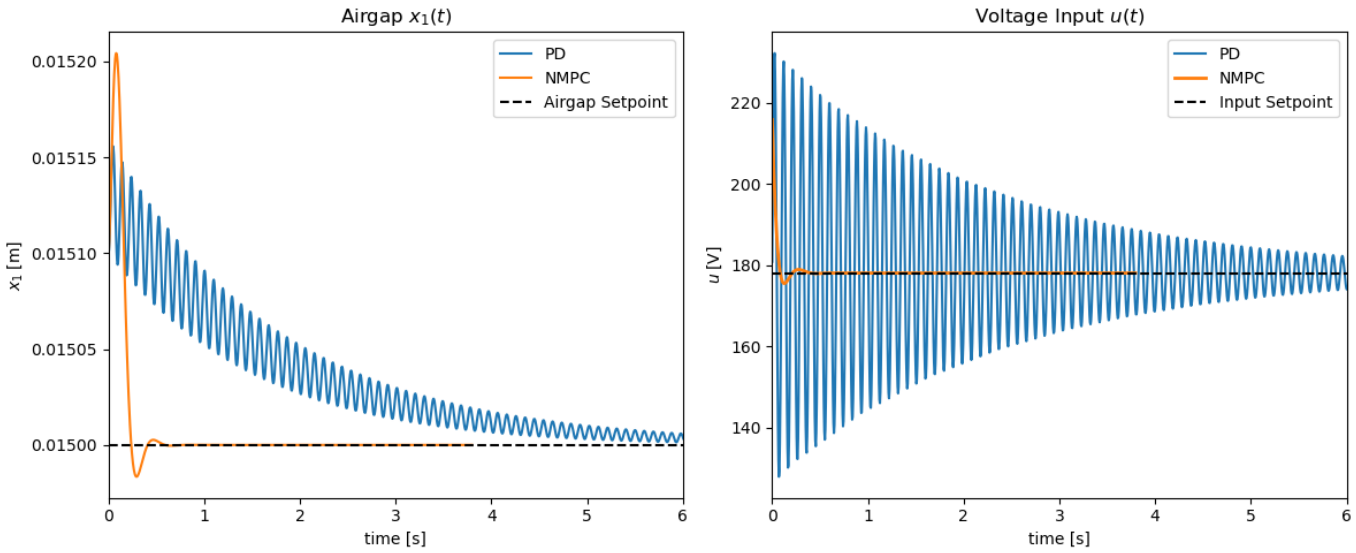

Figure 4.21 Comparison of PD and NMPC trajectories using same control parameters as for the performance metrics above

Summary
The PD-controller showed strong oscillatory behaviour at the start of the simulation. In contrast, the LQR controller demonstrates satisfactory performance, with only a minor initial overshoot and small oscillations around the setpoint. It is, however, not able to handle constraints.
Linear MPC did not achieve stabilization at all. In contrast, when the nonlinear model is used, MPC has demonstrated to be able to accurately track the desired set point, with reduced overshoot and oscillations. One second after the perturbation is applied, the vehicle is already very close to the reference. It can be concluded that the MPC controller allows for much faster convergence, without causing overshoot. A large

region of attraction for MPC, compared to PD, is observed from the stability plots in the previous paragraphs. This is because of MPC being a more advanced control strategy, looks ahead and incorporates a prediction of future behaviour. This leads to an improved controller performance. This can be explained by the fact that controller uses only the current measurements. In this PD-controlled case, faster convergence led to overshoot and a large amplitude of oscillation around the equilibrium point.

Overall, MPC shows improved performance on the 1.5-DOF system compared to the other control strategies.

5. Control of the continuous guideway model

To account for the frequency and velocity dependent reaction force of the Hyperloop system during motion of the vehicle along the guideway, the assumption of a rigid track is not valid anymore and elasticity of the guideway should be considered. This changes the system from a 1.5-DOF to an infinite-DOF system, thereby allowing wave-induced instability to occur. Following the model description provided in chapter 3, this chapter describes the method of solution and evaluates the effect of MPC on the infinite-DOF system. The results are then compared with the PD-controller applied in previous studies.

5.1 Method

The EOM of the load-structure coupled system is described by the nonlinear PDE in Eq. (3.1), thus requiring a numerical approach. The EOM of the beam will therefore be written in the following form:

$$w_0(t) = -\int_0^t G_0(t-\tau)F(\tau)d\tau + w_0^{ic}(t) \tag{5.1}$$

The first term of Eq. (5.1) captures the response at the location of the load ($F(\tau)$) given trivial initial condition, so $w_0^{\mathrm{ic}}(t)$ is needed to complement the displacement of the beam due to initial conditions. The Green's function of the beam, G_0, is the response to a moving unit impulse load. Once this is known, the response to any force can be calculated by applying the convolution integral, corresponding to the first term in Eq. (5.1).

To obtain the general solution, G_0 should be determined. Therefore, a few steps are taken to arrive at an algebraic equation. First, the Laplace transform with respect to time will be applied, followed by the Fourier transform with respect to the longitudinal coordinate, using the definitions:

$$W(k,s) = \int_{-\infty}^{\infty} V(\xi,s)e^{-\mathrm{i}k\xi}\mathrm{d}\xi, \qquad \mathrm{V}(\xi,s) = \int_0^{\infty} w(\xi,\tau)e^{-s\tau}\mathrm{d}\tau \tag{5.2}$$

, where $s = \sigma + j\omega$. Trivial initial condition and vanishing boundary conditions are assumed. Applying these definitions to the PDE in Eq. (3.1) results in:

$$\begin{aligned} D(k,s)W(k,s) &= \frac{F_{EM}(s)}{EI}, \\ D(k,s) &= k^4 - \frac{\rho v^2}{EI}k^2 - \frac{(2i\rho vs + icv)}{EI}k + \frac{\rho s^2 + k_d + c_d s}{EI}. \end{aligned} \tag{5.3}$$

Applying an inverse Fourier transform to obtain the solution in the Laplace domain leads to:

$$V(\xi,s) = \frac{F_{EM}(s)}{2\pi EI}\int_{-\infty}^{\infty}\frac{e^{\mathrm{i}k\xi}}{D(k,s)}\mathrm{d}k = F_{EM}(s)\hat{G}_0\,(\xi,s). \tag{5.4}$$

To obtain the response to a time varying force, the Green's function $\hat{G}_0\,(\xi,s)$ is used. This transfer function is the response to a unit impulse and can be isolated by taking the transform of a unit impulse ($F(s) = 1$). This results in: $V(\xi,s) = \hat{G}_0\,(\xi,s)$. Evaluating that expression at $\xi = 0$ to capture the location of the moving load interaction leading to the instability, yields the relation:

$$\hat{G}_0\,(0,s) = \frac{1}{2\pi EI}\int_{-\infty}^{\infty}\frac{1}{D(k,s)}\mathrm{d}k. \tag{5.5}$$

To calculate the complex Green's integral, the following Cauchy's Residue Theorem (Brown & Churchill, 1996) will be applied:

Let C be a simple, closed, positively oriented contour. If a function $f(z)$ is analytic on and inside C, except for a finite number of singularities z_k, then:

$$\int_C f(z)dz = 2\pi i\sum_{k=1}^{n}\lim_{z\to z_k}(z-z_k)f(z). \tag{5.6}$$

The roots of $D(k,s)$ from Eq. (5.3) are taken as the singularities, and the path along the upper half of the complex plane is considered, since the two positive imaginary wavenumbers contribute to the displacement in front of the moving load. By applying the theorem in Eq. (5.6), the complex integral from Eq. (5.5) can be evaluated and written in the following form:

$$\hat{G}_0\,(0,s) = \frac{i}{EI}\sum_{k=1}^{n} \lim_{k\to k_n} \frac{(k-k_n)}{(k-k_1)(k-k_2)(k-k_3)(k-k_4)}. \tag{5.7}$$

The Green's function in Eq. (5.7) is now expressed in the Laplace domain. The inverse Laplace is then applied, and the integral will be approximated by the trapezoidal rule to obtain G_0 in the time domain.

To solve the transformed EOM, the convolution integral from Eq. (5.1) is approximated by a trapezoidal resulting in the following expression. Therein the sum is split into contributions from the initial conditions, the known past ($w_{0,n}^{\mathrm{hist}}$) and an instantaneous unknown term at t_n. The following formulation is based on Faragau et al. (2023):

$$\begin{gathered} w_{0,n} = w_{0,n}^{\mathrm{ic}} + w_{0,n}^{\mathrm{hist}} + F_n\big(w_{0,n}\big)\mathcal{R}_0, \\ w_{0,n}^{\mathrm{hist}} = \sum_{\tilde{n}=0}^{n-2} \left[F_{\tilde{n}}\big(w_{0,\tilde{n}}\big)\mathcal{L}_{n-\tilde{n}-1} + F_{\bar{n}+1}\big(w_{0,\tilde{n}+1}\big)\mathcal{R}_{n-\bar{n}-1}\right] + F_{n-1}\big(w_{0,n-1}\big)\mathcal{L}_0, \\ \mathcal{R}_{n-\tilde{n}-1} = \int_{t_{\tilde{n}}}^{t_{\tilde{n}+1}} G_0(t_n-\tau)\frac{\tau - t_{\tilde{n}}}{\Delta t}\,\mathrm{d}\tau, \\ \mathcal{L}_{n-\tilde{n}-1} = \int_{t_{\tilde{n}}}^{t_{\tilde{n}+1}} G_0(t_n-\tau)\left(1-\frac{\tau - t_{\tilde{n}}}{\Delta t}\right)\mathrm{d}\tau. \end{gathered} \tag{5.8}$$

The displacement can be seen calculated using $\mathcal{L}$ and $\mathcal{R}$, being the contribution from the pulse at the left and right of the interval between running time index $\bar{n}$ and $\bar{n}+1$, observed at the observation time n.

When substituting the formula for F_n from Eq. (3.1) into the first equation of Eq. (5.8), the next third-order polynomial can be solved:

$$\begin{gathered} w_{0,n}^3 + a_{2,n}w_{0,n}^2 + a_{1,n}w_{0,n} + a_{0,n} = 0 \\ a_{2,n} = -w_{0,n}^{\mathrm{ic}} - w_{0,n}^{\mathrm{hist}}, a_{1,n} = -u_n^2, a_{0,n} = \big(w_{0,n}^{\mathrm{ic}} - w_{0,n}^{\mathrm{hist}}\big)u_n^2 + CI_n^2\mathcal{R}_0. \end{gathered} \tag{5.9}$$

The resulting discretised system of equations is given in Eq. (5.10) below, and will be solved by using the Runge-Kutta 4 method:

$$\begin{gathered} w_{0,n} = f\big(w_{0,n}^{\mathrm{ic}}, w_{0,n}^{\mathrm{hist}}, z_n, I_n\big), \\ M\ddot{u}_n = C\frac{I_n^2}{\big(w_{0,n}-z_n\big)^2} - Mg, \\ \dot{I}_n = \frac{w_{0,n}-z_n}{2C}\left(U_n - I_nR + 2C\frac{I_n}{\big(w_{0,n}-z_n\big)^2}\big(\dot{w}_{0,n}-\dot{z}_n\big)\right), \\ U_n = \kappa_{MPC} \end{gathered} \tag{5.10}$$

This polynomial in the first line of Eq. (5.10) can be calculated using a mathematical symbolic package and gives one physical admissible root.

By using the equations above as a prediction model, future states over the prediction horizon can be determined. The objective function defined in Eq. (5.11) is formulated based on the "measurements" up to time $\bar{n} = n$, and the predictions are calculated over a horizon of length H. The objective function again consists of two terms. However, in this case, not all states describing the system are taken into account. Only the deviations from the target airgap and airgap velocity are penalized. The second term punishes deviations of the input from the equilibrium voltage (U_0), which maintains the vehicle at the desired airgap when the electromagnetic force equals $F_{EM}(t) = mg$. Compared to the 1.5-DOF system, the vehicle-guideway coupled model exhibits history-dependent behaviour. This is evident from the first line of Eq. (5.10), where the future states are determined by the past trajectory rather than solely by the initial conditions, as in the MPC formulation of previous chapter was the case. The optimal control input is computed with the SLSQP optimizer, following the same approach control as in the NMPC control of the 1.5-DOF system in section 4.3.

$$J = \sum_{\bar{n}=n+1}^{\bar{n}=n+H} \left(x_{\bar{n}} - x_{ref}\right)^T Q \left(x_{\bar{n}} - x_{ref}\right) + \sum_{\bar{n}=n}^{\bar{n}=n+N-1} \left(u_{\bar{n}} - u_{ref}\right)^T R \left(u_{\bar{n}} - u_{ref}\right) \tag{5.11}$$

Where $\boldsymbol{x}_{\bar{n}} = \begin{bmatrix} w_{0,\bar{n}} - z_{\bar{n}} \\ \dot{w}_{0,\bar{n}} - \dot{z}_{\bar{n}} \end{bmatrix}, x_{ref} = \begin{bmatrix} \delta_0 \\ 0 \end{bmatrix}, u_{\bar{n}} = U_n$ and $u_{ref} = U_0$

5.2 Results

The effect of the MPC on the beam model is demonstrated through comparative simulations in this chapter, comparing for different parameters and operating conditions. A numerical method is used to study the system behaviour. However, the underlying type of stability it exhibits will not become clear from this study, since such an analysis is less tractable to perform for the MPC system.
Different scenarios are considered, varying in applied constraint, applied perturbations and in the longitudinal velocity of the vehicle. These results provide insight into the practical performance of the controller, showing it robustness, how it deals with constraint, and ability to deal with electromagnetic and wave-induced instability.

After the tuning process, the controller parameters are chosen to be:

- $T_s = 0.00025$ s, is the applied and maximum sampling time following from Nyquist-Shannon sampling theorem
- $H = 80$
- $Q = \begin{bmatrix} 1e^6 & 0 \\ 0 & 1e^3 \end{bmatrix}$
- $R = 1e^{-6}$

One may think that the penalty factor $R = 1e^{-6}$ could be neglected, but it appeared to have still a significant effect compared to the case with $R = 0$.
The simulations are carried out for different values of the vehicle's horizontal velocity, relative to the critical velocity. Define the critical velocity to be:

$$v_{cr} = \sqrt[4]{\frac{4k_d EI}{\rho^2}} \tag{5.12}$$

See the graphs below for the simulation results under different scenarios. For each simulation, the closed-loop trajectories of the nonlinear system are shown. The vehicle displacement, beam displacement, and attractive force are presented one below the other. The applied input voltage is also shown.
The steady-state values are indicated by a black horizontal line. Under good control, the trajectories should approach these values, which results in the airgap being equal to the setpoint δ_0.

$\boldsymbol{v = 0.1\, v_{cr}}$

An initial perturbation of -0.1 m/s in vehicle velocity and a small perturbation around equilibrium for the initial vehicle displacement is standard used in the following scenarios, unless stated otherwise.

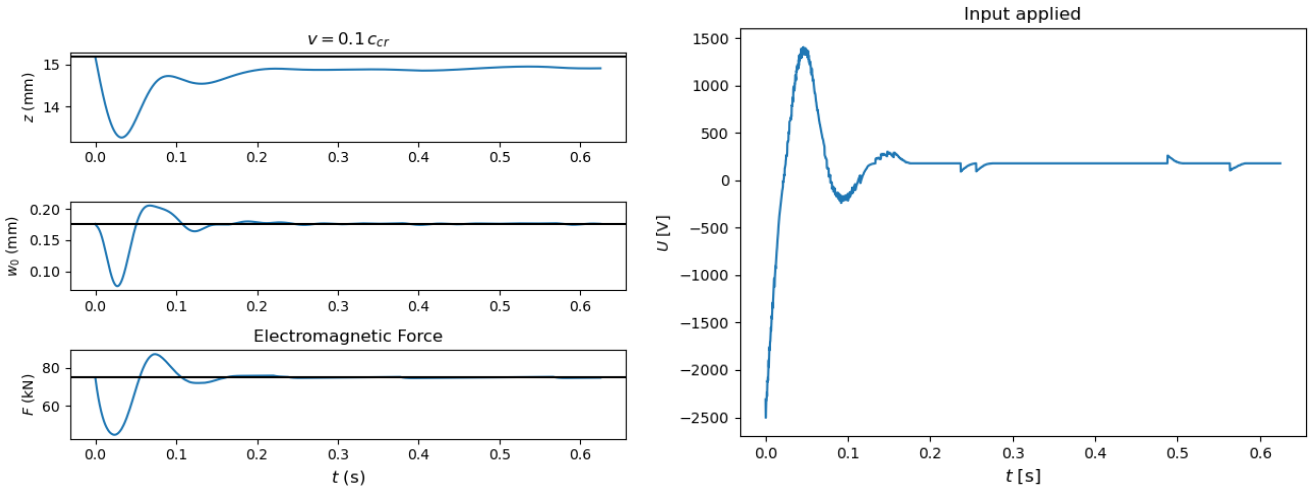

Figure 5.1 Closed-loop time responses for an unconstrained NMPC ($v=0.1v_{cr}$), z denotes the vehicle displacement and w_0 represents the beam displacement at the vehicle location

From figure 5.1 it may appear that the mass position is being penalized to reach the reference airgap. However, the controller is penalizing the difference between beam and mass displacement. This will become clear later in this study, when using a larger horizon length.

The performance is now evaluated under a larger perturbation, using an initial vehicle displacement of 0.03 m, as shown in figure 5.2. As a result, a larger input voltage is required to counteract this perturbation.

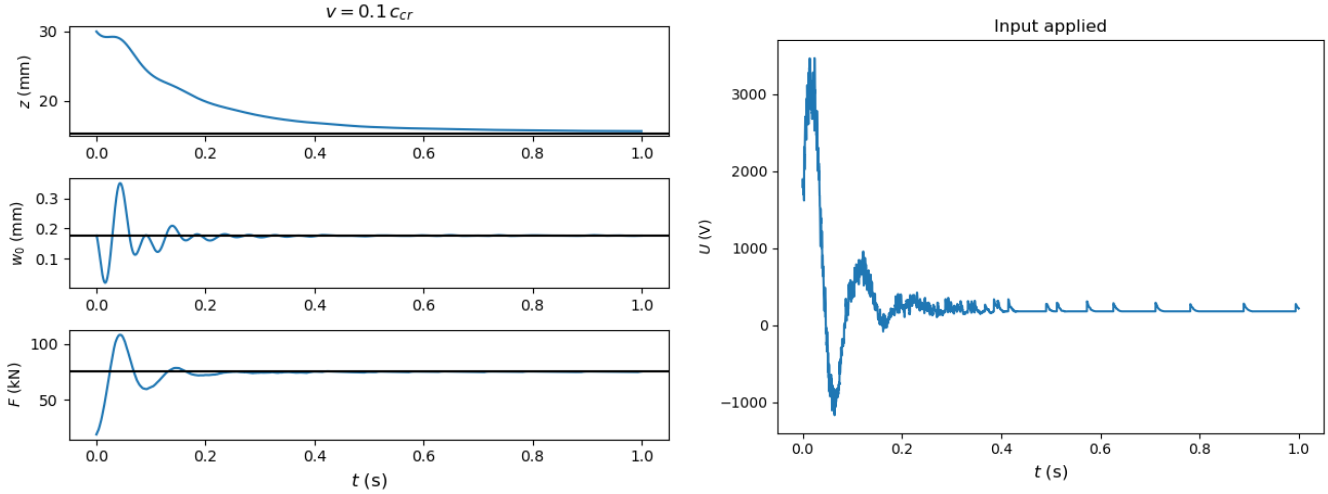

Figure 5.2 Closed-loop time responses for an unconstrained NMPC given a larger vehicle perturbation at a velocity of $v = 0.1v_{cr}$

$\boldsymbol{v = 0.7\, v_{cr}}$

Figure 5.3 illustrates the effect of an increased vehicle velocity.

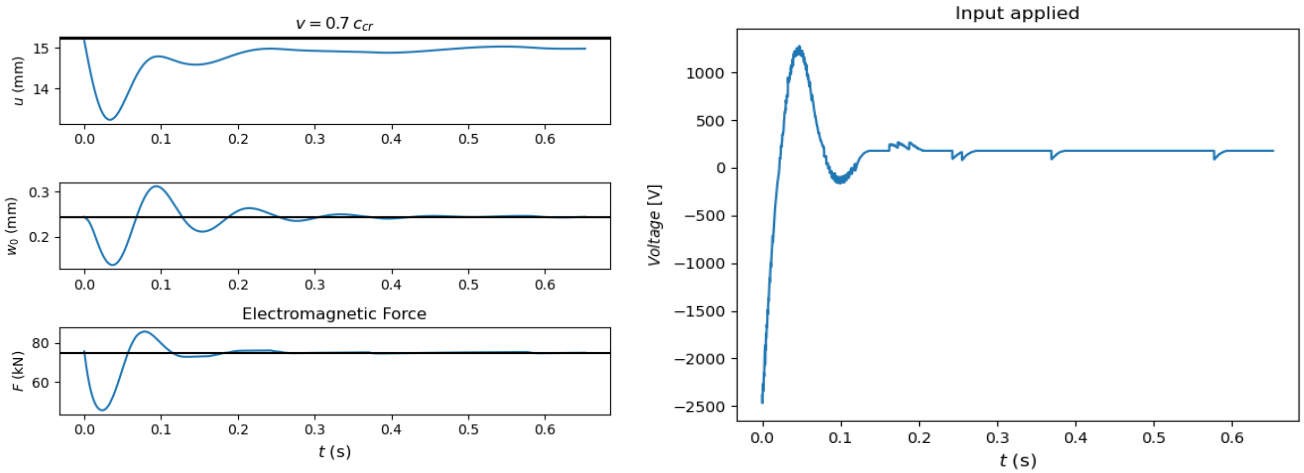

Figure 5.3 Closed-loop time responses for an unconstrained NMPC ($v=0.7v_{cr}$)

$\boldsymbol{v = 1.0\, v_{cr}}$

Figure 5.4 illustrates the system response when the vehicle velocity is equal to the critical velocity.

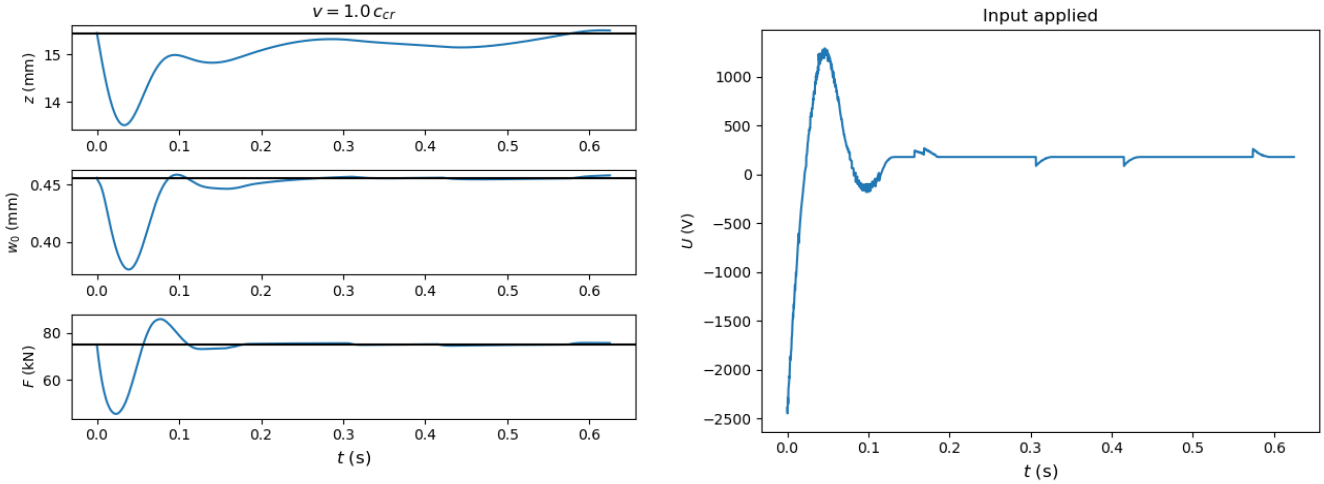

Figure 5.4 Closed-loop time responses for an unconstrained NMPC ($v=v_{cr}$)

$\boldsymbol{v = 1.3\, v_{cr}}$

Figure 5.5 presents the trajectories for a supercritical velocity.

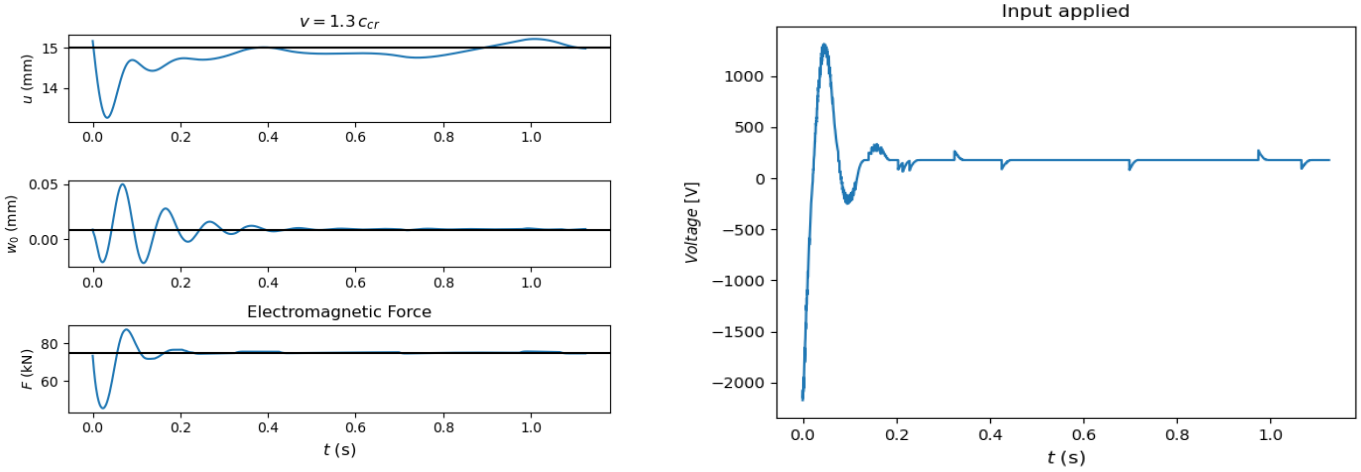

Figure 5.5 Closed-loop time responses for an unconstrained NMPC ($v=1.3v_{cr}$)

$\boldsymbol{v = 1.6\, v_{cr}}$

Figures 5.6 and 5.7 show the influence of imposing input constraints on the time response.

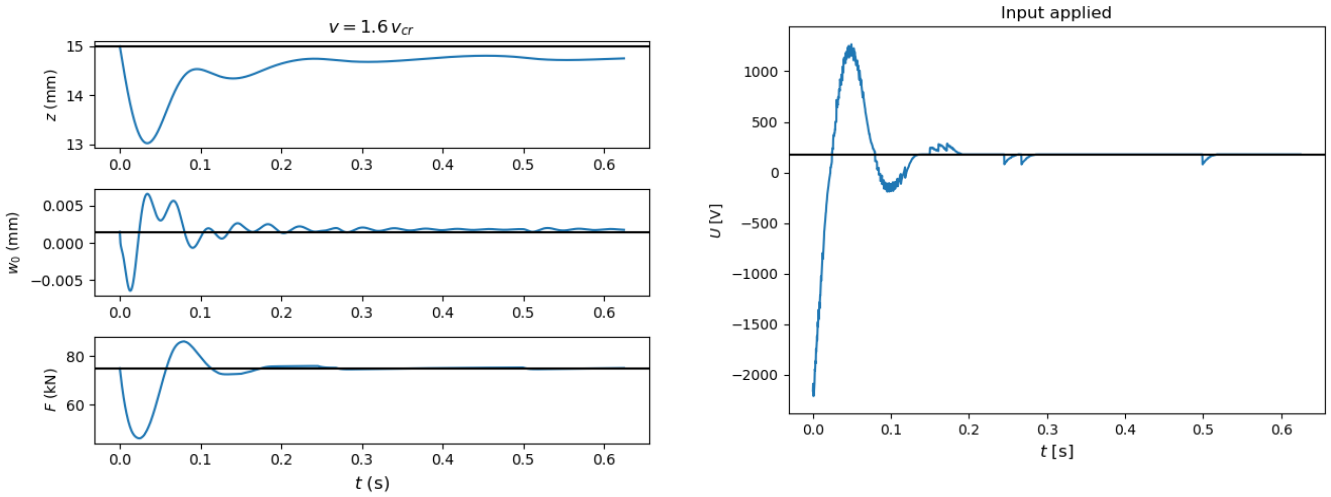

Figure 5.6 Closed-loop time responses for an unconstrained NMPC ($v=1.6v_{cr}$)

Figure 5.7 shows the time response of the system under a constrained input of -2000 to 2000 V.

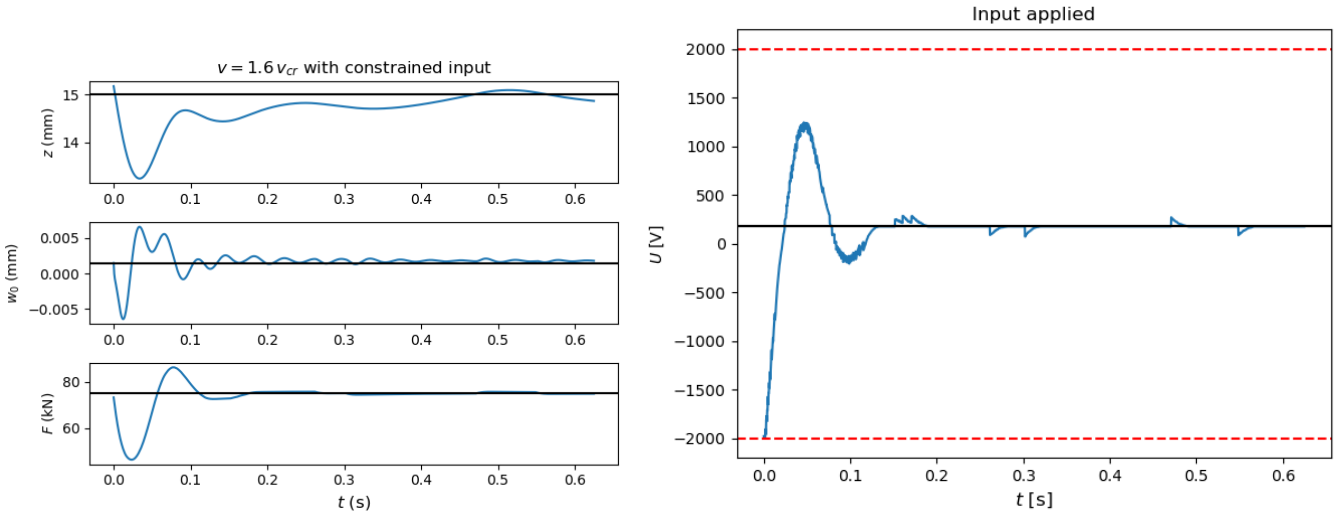

Figure 5.7 Closed-loop time responses for a constrained NMPC ($v=1.6v_{cr}$), constraints are shown by red dashed lines.

$\boldsymbol{v = 2.0\, v_{cr}}$

The time-history responses for a supercritical longitudinal velocity is shown in figure 5.8.

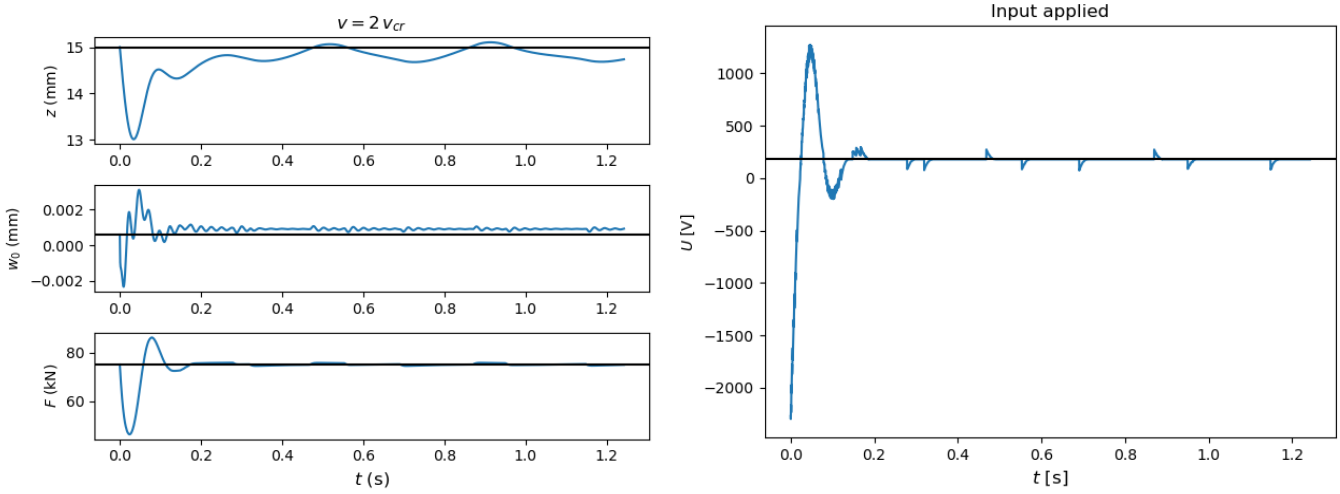

Figure 5.8 Closed-loop time responses for an unconstrained NMPC ($v=2v_{cr}$), over a longer time interval.

Evaluation

Figures 5.9 and 5.10 show the airgap responses obtained using PD control and MPC for sub- and supercritical velocities, respectively. The PD controller parameters were selected such that the largest stability region was achieved across different vehicle velocities. This may be regarded as a practical design choice, since in practice it is desirable to select parameter values that provide robust performance over a wide operating range. So, although increasing K_d could ensure that the airgap reaches faster the steady state, this may also lead to unstable trajectories for vehicle velocities around 1.7 to 2 times v_{cr}. the values applied in the comparison, however, remain stable in that region.

When analysing the trajectories in the figures, a clear difference can be observed. The PD controller shows oscillations, while the MPC response reaches the target more smoothly.

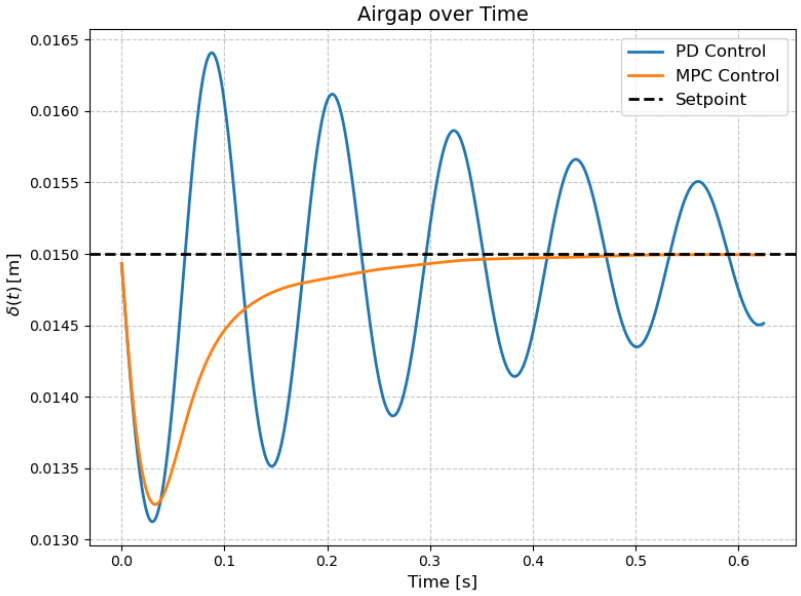

Figure 5.9 Airgap over time for a subcritical velocity ($v=0.7v_{cr}$) using PD (K_p =40 kV/m and K_d =20 kVs/m) and MPC control (H=150)

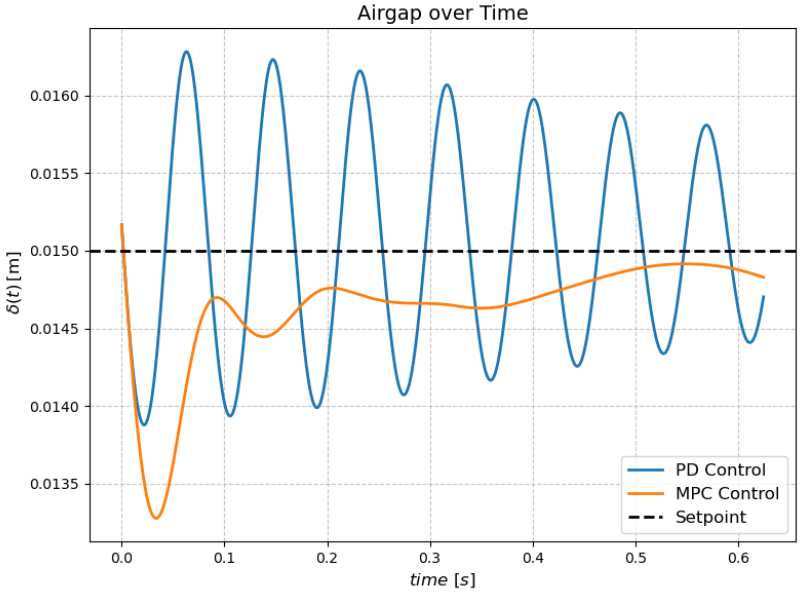

Figure 5.10 Airgap over time for a supercritical velocity ($v=1.3v_{cr}$) using PD(K_p =40 kV/m and K_d =40 kVs/m) and MPC control (H =80).

This predictive advantage of MPC is further illustrated by comparing the response obtained using $H = 80$ in figure 5.3 with the response for $H = 150$ in figure 5.11, under identical parameter settings. The larger horizon case in the figure below shows slightly smaller oscillations and a faster transient response.

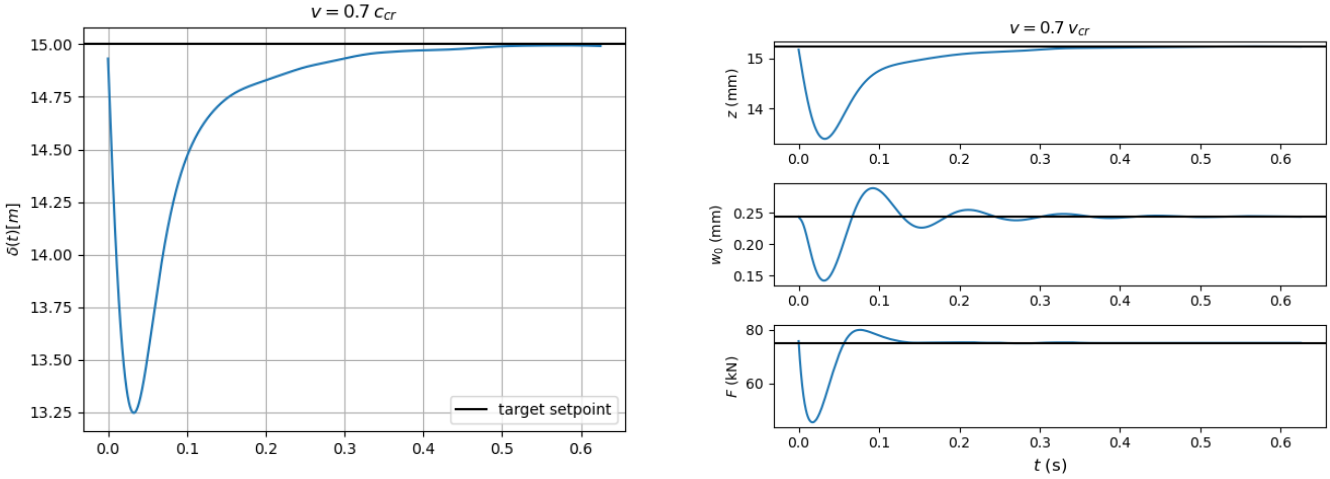

Figure 5.11 Response for an unconstrained MPC controller using an increased horizon length of H = 150. In the left plot the airgap is shown.

The simulations performed demonstrate a control performance capable of achieving close trajectory tracking in the vehicle-guideway model, around the tested scenarios. The control strategy appears to be effective in counteracting the effect of both instability mechanisms, provided that the controller parameters are tuned appropriately. Even, in the scenarios with larger perturbation, the controller demonstrates good performance. Moreover, when realistic voltage limits are applied, the MPC controller is still able to maintain close tracking of the target. Compared to the PD controller, the MPC controller converges faster to the setpoint with smaller oscillations, under the same conditions. Within the limited set of simulated scenarios considered in this study, no limit cycles were observed. However, this observation is based on a limited number of simulations, and greater confidence in this conclusion would require a more extensive parametric study.

At high supercritical longitudinal vehicle velocities, such as $v = 2.0\, v_{cr}$, an interesting difference between PD and MPC becomes visible**.** The PD controller only remains stable for parameter settings that lead to poorer tracking performance at lower velocities. Parameters setting that performed comparable to MPC at lower velocities do not maintain stability at this velocity. MPC, on the other hand, allows parameter choices that preserves both stability and satisfactory tacking performance. This suggests that MPC is better able to achieve fast convergence while also suppressing wave-induced instability.

A major limitation of applying MPC to this system is the computation time, as simulating just a few seconds of system behaviour takes a few hours of computation time. This is due to the nature of the problem, which is unstable, nonconvex and highly nonlinear, leading to a large amount of function evaluations when searching for the optimal input.

6. Conclusion

This thesis studies the effect of MPC on an inherently unstable EMS system subject to dynamic instabilities arising at high longitudinal velocities. Both analytical methods and numerical simulations were carried out to evaluate and compare the performance of MPC with that of a conventional PD controller. This work contributes by extending MPC analysis to include wave-induced instability and its interaction with electromagnetic instability.

It is demonstrated that identifying an appropriate tuning configuration is not straightforward for the unconstrained linearized 1.5-DOF system. The control horizon should not be penalized too much, as this restricts the controller's ability to apply the required control input. When a lower penalty is applied to the input effort, the closed-loop performance degrades at a small horizon value. However, the performance improves again from a certain horizon length.
The effects of the state weighting matrix Q and prediction horizon N_p show a more predictable effect on the closed-loop behaviour, increasing them leads to improved closed-loop performance up to a point at which a further increase results in stagnation.
Although the dynamics are nonlinear and no stabilization is achieved after linearisation, the presented analysis provides additional insight into the tuning behaviour of an unstable 1.5-DOF system. The results complement existing tuning studies and may help guide the search toward optimal configuration when using a nonlinear prediction model in NMPC.
When considering the nonlinear prediction model of the simplified system, the effects of the horizons and penalty factors follow an intuitive trend. However, a numerical effect is observed leading to a non-optimal control sequence that deteriorates closed-loop performance.

A comparison is presented between PD and NMPC controller. A nonlinear MPC was therefore designed, which achieves successful stabilisation. The region of attraction of the constrained NMPC becomes smaller because of the imposed input limits, but it still demonstrates stable levitation over a wider range of initial conditions than the unconstrained PD controller.
Based on simulations performed under identical scenario to ensure consistency, MPC performs significantly better in following the desired reference. The NMPC also shows dominant performance when measuring it by travel comfort and controller effort. This can be explained by the principle of predicting the future behaviour over a horizon of MPC, whereas PD control acts on the current error and lacks the predictive ability.

The controller performance is then studied through closed-loop simulations of the infinite-DOF system, including wave-induced instability. Simulations conducted across different scenarios show that MPC is effective in mitigating the effect of both instability mechanisms, when tuning the controller parameters properly. However, when the vehicle-guideway interaction is taken into account, a lower tracking accuracy is achieved than in the 1.5-DOF system. This vehicle offset remains within a range of few millimetres and is thus considered acceptable. Compared to the PD controller, MPC exhibits stable behaviour over a broader range of supercritical velocities, indicating improved performance in dealing with wave-induced instability for the considered simulation cases and controller configuration.
The increased model dynamics of the continuous guideway model, comes at the cost of substantially higher computational effort, with solver runtimes reaching several hours. This is a major disadvantage of the MPC controller, as MPC must be solved within the sampling interval in order to provide timely control actions based on the latest information. When this delay happens the control performance may degrade.

MPC presents a promising control strategy for development teams working on the hyperloop system. This research is of practical importance for developers of the hyperloop or other concepts of Maglev trains.

7. Discussion

This study aimed to investigate the effect of MPC on a hyperloop system. The results show that MPC is a promising control method and could serve as an alternative to the commonly applied PD controller. This study does not cover all aspects needed for implementation in practice, and those limitations are discussed in this chapter.

Performance has so far been considered only for the nominal situation under perturbations. During the operation process of a maglev or Hyperloop vehicle, however, there are multiple sources of disturbance. In addition, model uncertainty and measurement noise are not considered. The controller should ensure stability and performance under these scenarios. These uncertainties and disturbances could be modelled in the simulation model, while the prediction model assumes the nominal dynamics. Track irregularity can be modelled using existing models, and Gaussian noise can be added into the states. It would be interesting to investigate the trade-off between robustness and tracking performance.

Furthermore, in these simulations, all states are assumed measurable. In reality, not all states can be measured directly. A state observer may then be used, and its effect on the closed-loop control performance should be studied.

Simulations are often performed in combination with experimental validation. In such case, it is important to check the accuracy of the prediction model used. As this often limits the performance of MPC. Specific methods can then be used to online update the model and its parameters.

It has been shown in this research that the computation time required to solve the MPC optimization problem exceed the sample time of the fast EMS dynamics. Therefore, until now, MPC is mainly applied to slow processes. Several methods exist that significantly improve the computation time. Therefore, suboptimal methods have been suggested as first way to address it. These methods break the optimization after a predefined number of iterations or within a selected time limit, regardless of whether the optimal solution has been found. In this thesis application, as in many other cases, this approach led to unstable behaviour. Another often mentioned approach is the explicit NMPC, which decreases online computation effort by solving the control law for all admissible of states and storing it as a lookup table or piecewise function. This approach requires large memory storage and a significant amount of offline computation to generate solutions for all possible scenarios.

The present study has provided insight into the relationship between controller parameters and closed-loop performance. This improved understanding can support a more informed selection of both the tuning parameters and the optimization method for the type of optimization problem. In particular, the observed discontinuities in the NMPC cost function appear to contribute to the non-intuitive observation of an increasing horizon length leading to less optimal performance. Future work could therefore investigate more global or adaptive tuning approaches, such as genetic algorithms, reinforcement learning based tuning, or other methods better suited to nonconvex parameter landscapes.

The present work does not include a Laplace domain eigenvalue analysis for the MPC controller, as was done by Faragau et al. (2023), this is because MPC does not yield an explicit control law but computes a control input through a discrete time optimization problem. Consequently, the stability and performance were evaluated through closed-loop simulations for a few scenarios. Future research could extend this work by establishing a formal stability analysis of the controller.

Bibliography

Allgöwer, F., Badgwell, T. A., Qin, J. S., Rawlings, J. B., & Wright, S. J. (1999). Nonlinear Predictive Control and Moving horizon Estimation — An introductory overview. In Springer eBooks (pp. 391–449). https://doi.org/10.1007/978-1-4471-0853-5_19

Angelo, J., Angelo, J., Monteiro, N., & Monteiro, N. (2018). A new concept of superelevation in magnetic levitation – prodynamic. Транспортные Системы И Технологии, 4(4), 77–111. https://doi.org/10.17816/transsyst20184477-111

Astrom, K. J., & Murray, R. M. (2008). Feedback systems: an introduction for scientists and engineers. Choice Reviews Online, 46(04), 46–2107. https://doi.org/10.5860/choice.46-2107

Bächle, T., Hentzelt, S., & Graichen, K. (2013). Nonlinear model predictive control of a magnetic levitation system. Control Engineering Practice, 21(9), 1250–1258. https://doi.org/10.1016/j.conengprac.2013.04.009

Bachtiar, V., Kerrigan, E. C., Moase, W. H., & Manzie, C. (2015). Continuity and monotonicity of the MPC value function with respect to sampling time and prediction horizon. Automatica, 63, 330–337. https://doi.org/10.1016/j.automatica.2015.10.042

Bithmead, R. P., Wertz, V., & Gerers, M. (1991). Adaptive Optimal Control: the Thinking Man's G.P.C. In Prentice Hall Professional Technical Reference eBooks. https://escholarship.org/content/qt01z3w6d7/qt01z3w6d7.pdf?t=qa7yla

Brown, J. W., & Churchill, R. V. (1996). Complex variables and applications. McGraw-Hill Science, Engineering & Mathematics.

Camacho, E. F., & Alba, C. B. (2013). Model Predictive control. Springer Science & Business Media.

Cannon, M. (2004). Efficient nonlinear model predictive control algorithms. Annual Reviews in Control, 28(2), 229–237. https://doi.org/10.1016/j.arcontrol.2004.05.001

Cavenago, F., Rivolta, A., Paolini, E., Sanfedino, F., Colagrossi, A., Silvestrini, S., & Pesce, V. (2023). Control. In Elsevier eBooks (pp. 543–630). https://doi.org/10.1016/b978-0-323-90916-7.00010-x

Chaidez, E., Bhattacharyya, S. P., & Karpetis, A. N. (2019). Levitation methods for use in the Hyperloop High-Speed transportation system. Energies, 12(21), 4190. https://doi.org/10.3390/en12214190

Daniel, R., Antonio, F., Francisco, B., Camilo, L., David, S., & Carlos, S. (2025). A qLPV-MPC Control Strategy for Fast Nonlinear Systems with Stability and Feasibility Conditions. Arabian Journal for Science and Engineering, 50(14), 11395–11407. https://doi.org/10.1007/s13369-024-09931-5

DeCarlo, R. A. (1989). Linear Systems: a state variable approach with numerical implementation. http://ci.nii.ac.jp/ncid/BA07339180

Denisov, G. G., Kugusheva, E., & Новиков, В. В. (1985). On the problem of the stability of one-dimensional unbounded elastic systems. Journal of Applied Mathematics and Mechanics, 49(4), 533–537. https://doi.org/10.1016/0021-8928(85)90065-6

Department of Engineering Structures, Delft University of Technology, Delft, the Netherlands, B. Faragau, A., Wang, R., V. Metrikine, A., & N. Van Dalen, K. (2023). The interplay between the electro-magnetic and wave-induced instability mechanisms in the hyperloop transportation system. NODYCON, 1a1ab7a4-c6bb-4f07-9803-c1e68482ebae.

Di Palma, F., & Magni, L. (2006). On optimality of nonlinear model predictive control. Systems & Control Letters, 56(1), 58–61. https://doi.org/10.1016/j.sysconle.2006.07.011

Diehl, M., Bock, H., Diedam, H., & Wieber, P. (2007). Fast direct multiple shooting algorithms for optimal robot control. In Springer eBooks (pp. 65–93). https://doi.org/10.1007/978-3-540-36119-0_4

Documentation — CVXOPT. (n.d.). https://cvxopt.org/documentation/index.html

Earnshaw, S. (1848). On the nature of the molecular forces which regulate the constitution of the luminiferous ether. Transactions of the Cambridge Philosophical Society, 7, 97. https://ui.adsabs.harvard.edu/abs/1848TCaPS. . .7. . .97E/abstract

Findeisen, R., Imsland, L., Allgower, F., & Foss, B. A. (2003). State and Output Feedback Nonlinear model Predictive Control: an overview. European Journal of Control, 9(2–3), 190–206. https://doi.org/10.3166/ejc.9.190-206

Garriga, J. L., & Soroush, M. (2008). Model Predictive controller tuning via Eigenvalue placement. 2008 American Control Conference. https://doi.org/10.1109/acc.2008.4586529

Garriga, J. L., & Soroush, M. (2010). Model Predictive Control Tuning Methods: a review. Industrial & Engineering Chemistry Research, 49(8), 3505–3515. https://doi.org/10.1021/ie900323c

Garriga, J. L., Soroush, M., & Soroush, H. M. (2010). On the Effects of Tunable Parameters of Model Predictive Control on the Locations of Closed-Loop Eigenvalues. Industrial & Engineering Chemistry Research, 49(17), 7951–7956. https://doi.org/10.1021/ie100030e
Gilson, F. B. J., & José, A. L. B. (2013). PID Control Design for a Maglev Train System. Applied Mechanics and Materials, 389, 425–429. https://doi.org/10.4028/www.scientific.net/amm.389.425
Gros, S., Zanon, M., Quirynen, R., Bemporad, A., & Diehl, M. (2016). From linear to nonlinear MPC: bridging the gap via the real-time iteration. International Journal of Control, 93(1), 62–80. https://doi.org/10.1080/00207179.2016.1222553
Haber, A. (2023, September 13). Model Predictive Control (MPC) Tutorial 1: Unconstrained Formulation, Derivation, and Implementation in Python from Scratch – Fusion of Engineering, Control, Coding, Machine Learning, and Science. https://aleksandarhaber.com/model-predictive-control-mpc-tutorial-1-unconstrained-formulation-derivation-and-implementation-in-python-from-scratch/#google_vignette
Han, H., & Kim, D. (2016). Magnetic levitation. In Springer tracts on transportation and traffic. https://doi.org/10.1007/978-94-017-7524-3
Hardt hyperloop. (n.d.). Hardt Hyperloop. https://www.hardt.global/
Hardt Hyperloop. (2025). Hyperloop Progress Paper. https://static1.squarespace.com/static/64b506533bfadb6b8b2dc2a8/t/64df70560a764c3c1c5fae7a/1692364899818/2023-08-11+Hyperloop+Progress+Paper+V1.1.pdf
Hu, W., Zhou, Y., Zhang, Z., & Fujita, H. (2021). Model predictive control for hybrid levitation systems of Maglev trains with state constraints. IEEE Transactions on Vehicular Technology, 70(10), 9972–9985. https://doi.org/10.1109/tvt.2021.3110133
J. Mas Soldevilla, J. M. (2022). Dynamic analysis and stability study of the electromagnetic suspension levitation system of the hyperloop. TU Delft.
Joshy, A. J., & Hwang, J. T. (2024). PySLSQP: A transparent Python package for the SLSQPoptimization algorithm modernized with utilities for visualization andpost-processing. The Journal of Open Source Software, 9(103), 7246. https://doi.org/10.21105/joss.07246
Köhler, J., Zeilinger, M. N., & Grüne, L. (2023). Stability and performance analysis of NMPC: Detectable stage costs and general terminal costs. IEEE Transactions on Automatic Control, 68(10), 6114–6129. https://doi.org/10.1109/tac.2023.3235244
Li, F., Sun, Y., Xu, J., He, Z., & Lin, G. (2023). Control methods for levitation system of EMS-Type Maglev Vehicles: An Overview. Energies (Basel), 16(7), 2995. https://doi.org/10.3390/en16072995
Ma, D., Song, M., Yu, P., & Li, J. (2020). Research of RBF-PID control in Maglev System. Symmetry (Basel), 12(11), 1780. https://doi.org/10.3390/sym12111780
Marafioti, G., Olaru, S., & Hovd, M. (2009). State estimation in nonlinear model predictive control, unscented Kalman filter advantages. In Lecture notes in control and information sciences (pp. 305–313). https://doi.org/10.1007/978-3-642-01094-1_25
Mayne, D. (2013). An apologia for stabilising terminal conditions in model predictive control. International Journal of Control, 86(11), 2090–2095. https://doi.org/10.1080/00207179.2013.813647
Meena, G. D., & Janardhanan, S. (2017). Taylor–Lie formulation based discretization of nonlinear systems. International Journal of Dynamics and Control, 6(2), 459–467. https://doi.org/10.1007/s40435-017-0317-7
Metrikine, A. V., & Popp, K. (1999). Instability of vibrations of an oscillator moving along a beam on an elastic half-space. European Journal of Mechanics, a, Solids (Print), 18(2), 331–349. https://doi.org/10.1016/s0997-7538(99)80020-5
Mitropoulos, L., Kortsari, A., Koliatos, A., & Ayfantopoulou, G. (2021). The Hyperloop System and Stakeholders: A review and future directions. Sustainability, 13(15), 8430. https://doi.org/10.3390/su13158430
Morari, M., & Lee, J. H. (1999). Model predictive control: past, present and future. Computers & Chemical Engineering, 23(4–5), 667–682. https://doi.org/10.1016/s0098-1354(98)00301-9
MPC and constrained systems | Maurice Heemels. (2013). https://heemels.tue.nl/research/mpc-and-constrained-systems
Noland, J. K. (2021). Prospects and Challenges of the Hyperloop Transportation System: A Systematic Technology review. IEEE Access, 9, 28439–28458. https://doi.org/10.1109/access.2021.3057788
None, N. (2021). Competitive potential of Hyperloop from a travellers' perspective. https://resolver.tudelft.nl/uuid:10364108-e5c9-4d36-9e4e-9d354d70a5b2

Oppeneiger, B., Lanza, L., Schell, M., Dennstädt, D., Schaller, M., Zamzow, B., Berger, T., & Worthmann, K. (2024). Model predictive control of a magnetic levitation system with prescribed output tracking performance. Control Engineering Practice, 151, 106018. https://doi.org/10.1016/j.conengprac.2024.106018

Özbek, R., & Çodur, M. Y. (2021). Comparison of hyperloop and existing transport vehicles in terms of security and costs. Modern Transportation Systems and Technologies, 7(3), 5–29. https://doi.org/10.17816/transsyst2021735-29

Quirynen, R., & Di Cairano, S. (2021). Sequential Quadratic Programming Algorithm for Real-Time Mixed-Integer Nonlinear MPC. 2021 60th IEEE Conference on Decision and Control (CDC), 993–999. https://doi.org/10.1109/cdc45484.2021.9683714

Riviera, M. (2018). High-speed trains comparison to Hyperloop: Energy, sustainability and safety analysis Hyperloop integrations to reach the NOAH concept. Politecnico Di Torino. https://webthesis.biblio.polito.it/9231/

Schmid, P., Eberhard, P., & Dignath, F. (2019). Nonlinear Model Predictive Control for a Maglev Vehicle regarding Magnetic Saturation and Guideway Irregularities. IFAC-PapersOnLine, 52(15), 145–150. https://doi.org/10.1016/j.ifacol.2019.11.665

Schwenzer, M., Ay, M., Bergs, T., & Abel, D. (2021). Review on model predictive control: an engineering perspective. □the □International Journal of Advanced Manufacturing Technology/International Journal, Advanced Manufacturing Technology, 117(5–6), 1327–1349. https://doi.org/10.1007/s00170-021-07682-3

Song, R. R., Wang, H., & Chen, Z. L. (2013). An Improved Expert Intelligent PID Control in Maglev Transportation System with Different Track Irregularities. Applied Mechanics and Materials, 409–410, 1141–1146. https://doi.org/10.4028/www.scientific.net/amm.409-410.1141

Tjandra, S., Kraus, S., Ishmam, S., Grube, T., Linßen, J., May, J. F., & Stolten, D. (2024). Model-based analysis of future global transport demand. Transportation Research Interdisciplinary Perspectives, 23, 101016. https://doi.org/10.1016/j.trip.2024.101016

Tramacere, E., Pakštys, M., Galluzzi, R., Amati, N., Tonoli, A., & Lembke, T. A. (2024). Modeling and experimental validation of electrodynamic maglev systems. Journal of Sound and Vibration, 568, 117950. https://doi.org/10.1016/j.jsv.2023.117950

Ulbig, A., Olaru, S., & Dumur, D. (2008). Explicit model predictive control for a magnetic levitation system. Mediterranean Conference on Control and Automation. https://doi.org/10.1109/med.2008.4602086

Ulbig, A., Olaru, S., Dumur, D., & Boucher, P. (2010). Explicit nonlinear predictive control for a magnetic levitation system. Asian Journal of Control, 12(3), 434–442. https://doi.org/10.1002/asjc.191

Van Den Boom, T. (2020). Model Predictive Control: Lecture notes for the course SC42001/EE4C04 [Delft University of Technology]. Delft Center for Systems and Control.

Van den Boom, T., & De Schutter, B. (2018). Optimization in systems and control: Lecture notes for the course SC42055. TU Delft.

Veritchev, S. (2002). Instability of a vehicle moving on an elastic structure. http://repository.tudelft.nl/assets/uuid:6b66f302-01c6-40e0-8f3d-1f1c4f3c178e/ceg_veritchev_20021126.pdf

Xu, J., Chen, C., Gao, D., Luo, S., & Qing-Quan, Q. (2017). Nonlinear dynamic analysis on maglev train system with flexible guideway and double time-delay feedback control. Journal of Vibroengineering, 19(8), 6346–6362. https://doi.org/10.21595/jve.2017.18970

Zhang, Z., Zhou, Y., & Tao, X. (2020). Model predictive control of a magnetic levitation system using two-level state feedback. Measurement + Control/Measurement and Control, 53(5–6), 962–970. https://doi.org/10.1177/0020294019900333

Zhu, Q., Wang, S., & Ni, Y. (2024). A review of levitation Control Methods for Low- and Medium-Speed MagLeV Systems. Buildings, 14(3), 837. https://doi.org/10.3390/buildings14030837

Zietkiewicz, J., & Owczarkowski, A. (2017). Direct nonlinear model predictive control and predictive control with feedback linearization. A comparison of the approaches. 2017 18th International Carpathian Control Conference (ICCC). https://doi.org/10.1109/carpathiancc.2017.7970442